Aus der Medizinischen Universitätsklinik und Poliklinik Tübingen
Abteilung für Innere Medizin VIII
Medizinische Onkologie und Pneumologie

Oncolytic Virotherapy of Neuroendocrine Neoplasms with the Vaccinia virus GLV-1h68 and the Herpes simplex virus T-VEC

Inaugural-Dissertation
zur Erlangung des Doktorgrades
der Medizin

der Medizinischen Fakultät
der Eberhard Karls Universität
zu Tübingen

Vorgelegt von
Kloker, Linus Daniel

2022

Dekan:	Professor Dr. B. Pichler
1. Berichterstatter:	Professor Dr. U. Lauer
2. Berichterstatterin:	Privatdozentin Dr. C. Schneidawind
3. Berichterstatterin:	Professorin Dr. Susanne Bailer
Datum der Disputation:	31.01.2022

TABLE OF CONTENTS

CHAPTER 1: INTRODUCTION

Neuroendocrine Neoplasms (NEN) are rare types of cancer that can arise at pleiotropic anatomical sites. The diagnosis encompasses a localized, surgically curable disease; aggressive, fast growing tumors and also asymptomatic, metastatic cancer. Both, the rareness and diversity of NEN challenge clinicians of different disciplines and call for a variety of adequate treatment options.

Oncolytic virotherapy might be a suitable one. The idea of treating tumors with viruses is nothing too new, first trials with cancer patients infected with viruses in therapeutic intention were reported in the middle of the 20th century. Observations of tumor patients undergoing oncological remission after incidental viral disease are even older. However, virotherapy has evolved as a relevant subject to oncology research and has become much safer, more efficient and precise in the past 20 years. This finally led to the first oncolytic virus (OV) being significantly effective in cancer therapy in a randomized controlled clinical trial. The Herpes simplex virus (HSV) T-VEC (Talimogene laherparepvec) was consequently approved by the United States (US) Food and Drug Administration (FDA) for treatment of advanced melanoma in 2015. Numerous other OVs, such as GLV-1h68, the second virus employed in this study, are in preclinical and clinical development.

This study seeks to verify the therapeutic potential of two oncolytic viruses in NEN. For this purpose, the Vaccinia virus (VACV) GLV-1h68 and the Herpes simplex virus T-VEC were employed. Both viruses are well characterized and have already been extensively tested in clinical settings. Cell lines from different NEN were collected and cultivated. Cytotoxicity of the viral agents was measured and compared with a current state-of-the-art treatment option. Also, replication kinetics were investigated and visualized by fluorescence and electron microscopy. Further, combinatorial treatment options including OVs and molecular targeted therapy (MTT) were studied.

During the work on this thesis, results and ideas have already been published in three separate publications in renowned scientific journals by our research group [1-3]. Two of them are original scientific papers containing the main results of this thesis [1, 2]. The other one is a literature review about research applying advanced cell culture systems to

the field of oncolytic virotherapy [3]. Several verbatim quotes referring to these publications are made in this work and are indicated as italic text with the respective reference attached.

In this chapter, the nature and classification of NEN is discussed and the role of Everolimus in treatment of those is summarized briefly (section 1 and 2). Next, the underlying mechanisms and challenges in oncolytic virotherapy are outlined (section 3). Then, previous trials and experiences with virotherapeutics in NEN are summarized (section 4) and both OVs employed in this study are introduced (section 5 and 6). Afterwards, the interaction between T-VEC and the virostatic drug Ganciclocvir (GCV) is illustrated (section 7). Finally, the fundamental questions this study aims to respond to are raised (section 8).

1. Neuroendocrine Neoplasms

NEN is a generic term, including neuroendocrine tumors (NETs) and neuroendocrine carcinomas (NECs). NETs were referred to as carcinoid tumors causing the clinical carcinoid syndrome until the new WHO classification in 2010. The common feature of all NEN is that they originate from neuroectodermal cells which are part of the endocrine system. These cells usually produce hormones or neurotransmitters. NETs and NECs can be distinguished with histological grading using the immunohistochemical Ki67 staining, a protein strictly correlated with cell proliferation [4]. Ki67 indexes ≤2 % indicate well differentiated G1 NETs, G2 NETs include Ki67 indices up to 20 %. Fast growing, aggressive NECs are classified as poorly differentiated G3 tumors with Ki67 >20 %. Recent research suggests that G3 NETs with a high proliferative index (Ki67 >20 %) but good histological differentiation should be separated from NECs [5, 6].

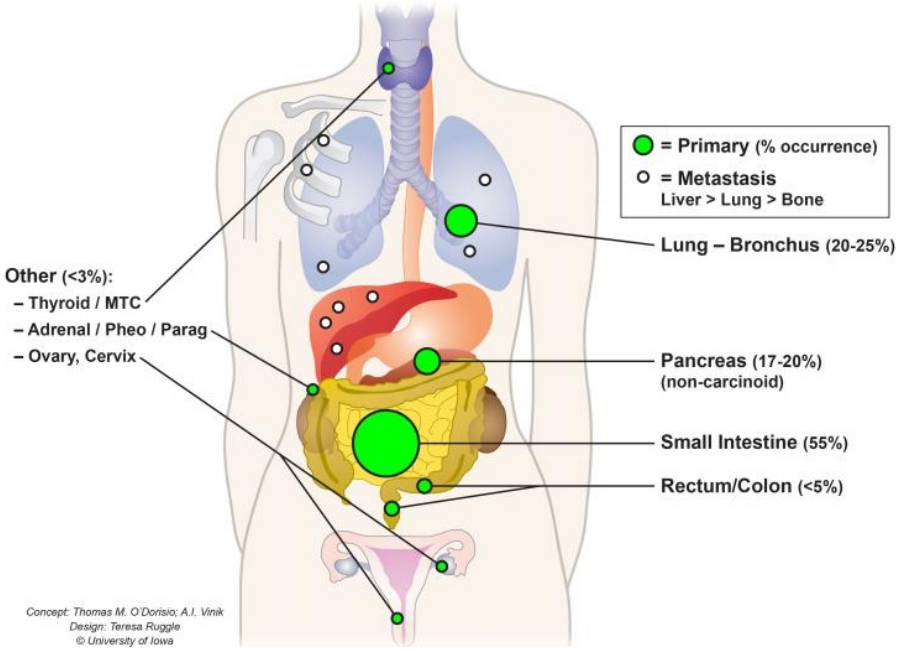

Figure 1: Anatomical and numeric distribution of NETs. Medullary thyroid carcinoma (MTC); Pheochromocytoma (Pheo); Paraganglioma (Parag). Taken from [7] with permission.

NETs can occur at various anatomical sites, such as the lung, thyroid, pituitary or gastro-enteropancreatic system (GEP-NETs). NETs of the lung are still named typical or atypical carcinoid, whereas GEP-NETs can be divided into gastric NETs (gNETs), pancreatic NETs (pNETs) or small intestinal (siNETs).

As visualized in Figure 1, NETs most frequently arise from the small intestine, lung, and pancreas. They often tend to metastasize in the liver, where functional NETs cause the characteristic carcinoid syndrome. In general, only 30 % of all NETs produce hormones and are therefore called functional, whereas the majority of NETs are non-functional [8]. Both, functional and non-functional NETs, often only become symptomatic with metastases and localization of the primary tumor can be difficult. That is why they are usually only diagnosed in late tumor stages, e.g. pNETs with already 22 % regional and 64 % distant metastases at diagnosis in the US [9]. Besides symptoms directly caused by the tumor mass, the production of vasoactive substances such as serotonin and kallikrein from liver metastases of functional NETs induces the carcinoid syndrome. Patients present with a typical triad of the symptoms flush, diarrhea and right-sided heart failure due to serotonin driven valvular fibrosis. The incidence of NETs is rising alarmingly in the US (Fig. 2); however, it remains unclear if this is an epidemiological phenomenon or due to more precise diagnosis and increasing clinical awareness of NETs [9].

For localized NETs, surgery is the therapy option of choice. Resection of the primary tumor, involved lymph nodes and liver metastases in curative intention is possible. First-line therapy for metastasized, inoperable NETs are somatostatin analogues (SSA), as the majority of NETs express somatostatin receptors. If NETs are somatostatin receptor negative, Interferon-α2b (IFN-α2b) constitutes an alternative to SSAs. Another therapy option is MTT employing the multikinase inhibitor Sunitinib for progredient pNETs or Everolimus as treatment for progredient pancreatic, intestinal and lung NETs (discussed in section 2 of this chapter) [10]. Peptide receptor radionuclide therapy (PRRT) using the somatostatin receptor as therapeutic target for radionuclides is another promising therapy option [11]. Traditional chemotherapy plays a minor role in NET therapy and is employed as a second- or third-line option after therapy failure or for high-grade or bulky NETs. Generally, streptozotocin or temozolomide based regimens are used, but evidence regarding progression free and overall survival is still weak [12]. Other palliative treatment possibilities for NETs are radiation or debulking surgery.

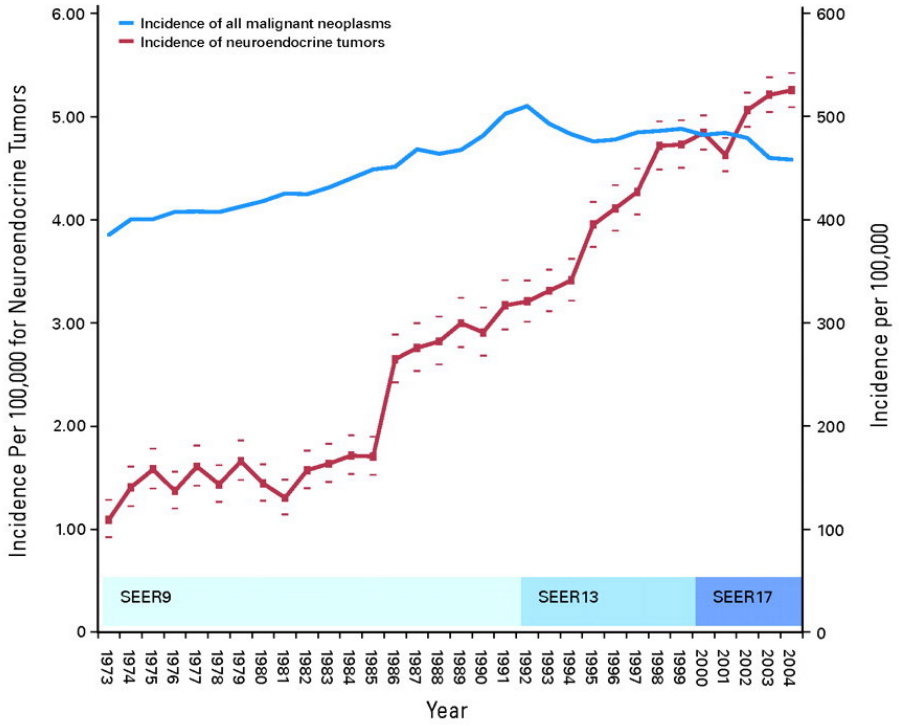

Figure 2: Incidence of NETs in the US from 1973 to 2004. The incidence of all malignant neoplasms is shown for comparison. Data are age-adjusted to the US population in 2000 and are from the Surveillance, Epidemiology, and End Results (SEER) database. 95 % confidence interval is shown. Reprinted with permission from [9]. © 2020 American Society of Clinical Oncology. All rights reserved.

NECs are far more aggressive tumors with a fast proliferation and early metastases. They are generally non-functional due to their poor differentiation. NECs can be histologically divided into large cell and small cell NECs, including small cell lung cancer (SCLC). 80 % of NECs are diagnosed in a metastasized stage, usually with involvement of the liver. The primary tumor is located in the lung in most cases, rarely in the colon. Therapy options are scarce, surgery with adjuvant chemotherapy is the only curative option. NECs are responsive to platinum-based chemotherapy, but still with a poor prognosis and fast relapse [13].

To resemble a broad spectrum of NEN, six cell lines were employed in this study and tested for their susceptibility to oncolytic virotherapy. Two cell lines were derived from pNETs, two from typical lung carcinoids and two from intestinal NECs (cf. Material and Methods, section 1.1).

2. Everolimus in treatment of neuroendocrine tumors

Everolimus (trade name Afinitor) is an inhibitor of the mammalian target of rapamycin (mTOR). The intracellular protein kinase mTOR mediates several signaling cascades involved in cell proliferation, apoptosis, angiogenesis, autophagy and cell metabolism. Phosphatidylinositol-3-kinase (PI3K)/Akt/mTOR signaling is mainly regulated by several growth factors, such as insulin and insulin like growth factors I and II. After binding to their respective receptor tyrosine kinase, insulin receptor substrate (IRS) is phosphorylated and binds the PI3K. The activated complex of IRS and PI3K activates an intracellular second messenger system by phosphorylating phosphatidylinositol-4,5-bisphosphate (PIP_2) into phosphatidylinositol-3,4,5-trisphosphate (PIP_3). The second messenger PIP_3 can be inactivated through dephosphorylation by the tumor suppressor gene product of the phosphatase and tensin homolog (PTEN). PIP_3 leads to the activation of the serine/threonine kinase Akt (proteinkinase B), which is able to phosphorylate pleiotropic downstream molecules and influences similar functions like mTOR, such as cell cycle progression, proliferation and suppression of apoptosis. MTOR itself, including mTORC1 and mTORC2, is one of the key integrators of metabolic cellular signaling. Both complexes have similar (DEPTOR, mLST8) and unique components. Akt is able to activate mTORC1 through disinhibition via the tuberos sclerosis proteins 1 and 2 (TSC1/2) and mTORC2 can be directly activated by PIP_3. The two main downstream effector proteins of mTORC1 are the P70S6 kinase and 4EBP1 [14]. The various downstream effectors of mTOR are reviewed in detail by Laplante and Sabantini [15]).

Several proteins involved in this signaling pathway are frequently altered in a variety of cancers [16] and also in NETs [17, 18] and are therefore thought to be crucial for tumor development and progression. Hyperactivation of the components of this pathway promotes cell cycle entry, inhibition of apoptosis and autophagy as well as angiogenesis.

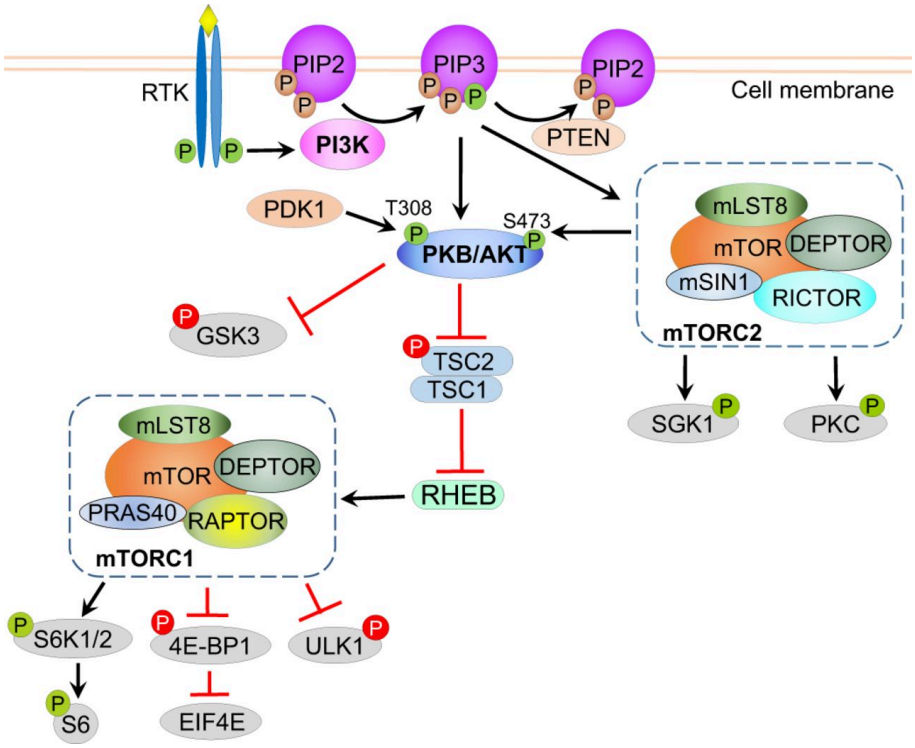

Figure 3: The PI3K/Akt/mTOR signaling pathway. Green Ps indicate activating phosphorylation, red Ps inactivating phosphorylation and brown Ps are not affected by this signaling pathway. Reproduced with permission from [14].

The mTOR inhibitor Everolimus has its main inhibitory effect on mTORC1, while having less interaction with mTORC2 [19]. Inhibition of mTORC1 has an inhibitory effect on cell growth, proliferation and angiogenesis. It has first been approved as immune-suppressive agent for renal transplant and organ transplant rejection. Later, anticancer activity has been discovered for renal cell carcinomas, NETs and breast cancer. Further, Everolimus has been approved for tuberous sclerosis associated conditions such as seizures or subependymal giant cell astrocytoma, where a mutation of TSC1/2 leads to an impaired regulation of mTOR [20].

The efficacy of Everolimus in the treatment of NETs was investigated in the RADIANT trials. The RADIANT-III study showed significantly longer progression free survival (PFS, 11 vs. 4.6 month with placebo) for progressive G1/G2 pNETs. Everolimus was the first therapy for 40 % of study patients, whereas around 60 % were pretreated with SSAs or chemotherapy [21]. In the RADIANT-IV trial, Everolimus was studied for its efficacy in advanced, progressive lung and intestinal G1/G2 NETs, again leading to a significantly longer PFS (11 vs. 3.9 month with placebo) [22]. RADIANT-III led to the FDA approval

of Everolimus for progressive pNETs in 2011 and RADIANT-IV succeeded in the FDA approval of Everolimus for nonfunctional, progressive lung and intestinal NETs in 2016.

In the current clinical setting, Everolimus is usually used as a second line option after tumor progression under SSA treatment, mainly because of a lower probability of side effects with SSA therapy. The expression of the somatostatin receptor and the accessibility of PRRT also play a role in clinical practice and usage of Everolimus. The selection of patients which would benefit from Everolimus as a first-line agent and its role in treatment of functional intestinal NETs remain unclear [23, 24].

In this study, Everolimus was investigated to be compared and combined with oncolytic virotherapy. It is approved for a broad spectrum of advanced NETs and the similar clinical situation and tumor stage would be a conceivable application for virotherapy in NETs.

3. Oncolytic Virotherapy

Virotherapy constitutes a novel alternative cancer treatment and special subtype of immunotherapy. The underlying strategy involves viruses, which selectively infect, replicate in and kill tumor cells. These viral agents are either natural virus strains selected by cell culture for their tropism for tumor cells or are specifically targeted to malignant cells by genetic engineering. The aim of virotherapy is that these viruses enter, replicate in and kill tumor cells, whereas healthy cells are left untouched. Mechanisms of tumor cell specificity can be divided into general mechanisms applying to most OVs and virus specific mechanisms.

All viruses take advantage of the hallmarks of cancer, which distinguish tumor cells from normal healthy cells [25]. The key features of tumors make tumor cells generally more susceptible to viral infection. Alterations in cellular metabolism and sustained proliferative signaling make it easier for viruses to hijack the cellular synthesis machinery without the need to activate it. The resistance to growth suppressors and defective apoptosis signaling in tumor cells make them often unable to evade and suppress viral infection. Immune evasion mechanisms give OVs an environment where they can initiate viral replication without being affected by the immune system. Further, tumor induced angiogenesis produces insufficient vessels, where intravenously (i.v.) delivered viruses easily get caught in the tumor bed and reach tumor cells. Moreover, most tumor cells fail to react to viral infection by activating innate immunity via a type I IFN response [26, 27]. Further, a deficiency of the stimulator of interferon genes (STING) in tumors was linked to high susceptibility to viral infection [28].

Besides these general mechanisms of viral tumor selectivity, there are OV specific features for tumor cell selectivity. These can include natural tropism of viruses for certain cell types, usage of specific entry receptors for viral infection (e.g. CD 46 for measles vaccine virus) or gene promoters of tumor expressed genes in the viral genome (e.g. chromogranin A promoter in the genome of the OV AdVince [29]). The identification of unique signaling pathways or molecules in tumor cells, which can be employed to target viral agents for an efficient and selective antitumor activity is crucial for the development of an OV.

As a result, OVs replicate in tumor cells and hence lyse them by their inherent cytotoxic mechanisms. These mechanisms can be augmented by certain gene deletions or insertions of cytotoxic transgenes.

This first part is called the direct oncolytic activity, which was thought to be the crucial one in the beginnings of virotherapy research. By tumor selective replication and cell killing, viruses were thought to lyse the tumor on their own, at best completely. But despite great research efforts, the success in clinical studies remained moderate. To improve antitumor activity, toxic transgenes were inserted. Enzymes which activate cytostatic drugs could be selectively delivered to tumor cells and transform cytostatic prodrugs like GCV or 5-Fluorocytosine to their active metabolites directly at the tumor site [30, 31]. These enzymes like thymidine kinase or cytosine deaminase further increased the cytotoxicity of viral agents, but no breakthrough was achieved with them.

In the past ten years, another mechanism was found to be crucial for the success of oncolytic virotherapy. It was observed that virus injections in a single tumor site also led to a response in distant metastases, despite no viral particles could be detected in the bloodstream [32, 33]. Instead, an infiltration of metastasis with immune effector cells was detected, indicating that a generalized immune activation against the tumor took place. This systemic antitumor response was recently shown to be the critical part of oncolytic virotherapy [34].

The first step of direct oncolytic cell killing leads to the release of so-called tumor specific neo-antigens into the extracellular space. Combined with the inflammatory viral environment, this is a strong signal for immunoactivation. Macrophages and dendritic cells are able to detect and process these antigens, generating an immune response against the tumor. Thus, oncolytic viruses were shown to increase the tumor infiltration of T-cells and NK-cells, as well as reduce the number of immunoregulatory cells like regulatory T-cells (T_{regs}) and myeloid derived suppressor cells (MDSCs) [34]. This secondary antitumor immune response can be augmented by arming oncolytic viruses with immune activating transgenes like IL-12, granulocyte-macrophage colony stimulating factor (GM-CSF) or chemokines. Further, OVs have been “armed” with genes expressing BiTE (bispecific T-cell engager) molecules, targeting T-cells to the tumor by binding CD3 on the T-cell surface as well as a tumor specific surface antigen [35].

Taken together, *"infections by OVs were found to turn immunosuppressive "cold" tumor microenvironments into "hot" ones by attracting a significant influx of immune cells. As a result, profound and long-lasting antitumoral immune responses can be induced."* **- [2]**

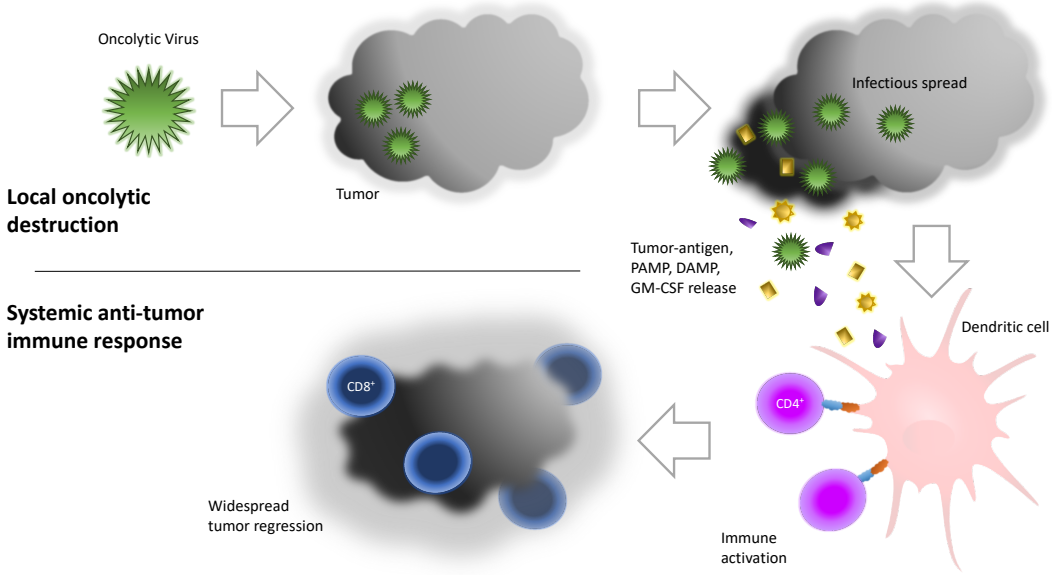

Figure 4: Mechanisms of oncolytic virotherapy. OVs infect the tumor and spread within it, leading to cell death with release of tumor-antigens, pathogen-associated molecular patterns (PAMPs), damage-associated molecular patterns (DAMPs) and immunostimulatory transgenes harboured by the OV, such as GM-CSF. Immune cells are attracted to the tumor, dendritic cells internalize tumor-antigens and subsequently activate the adaptive immune system. $CD4^+$ T-cells stimulate cytotoxic $CD8^+$ T-cells, which attack and infiltrate the primary tumor and metastases.

In recent studies, it could be found that the combination of OVs with immune checkpoint inhibitors (ICIs) such as anti-PD-1 (programmed death 1) and anti-CTLA-4 (cytotoxic T-lymphocyte-associated antigen 4) antibodies has a strong synergistic effect and can significantly increase response rates. After the combination of T-VEC with ipilimumab and pembrolizumab showed promising results for melanoma treatment [36, 37], several studies combining T-VEC, the Vaccinia virus Pexa-VEC (JX-594) and various adenoviruses with ICIs for a variety of cancers have been initiated. Recent clinical trials are listed in detail by Ylösmäki and Cerullo [38].

Another challenge in oncolytic virotherapy is the delivery of the virus. Intratumoral injection is the most practiced and easiest way to deliver OVs, but practicability depends on the localization and accessibility of the tumor.

Further, *"virus delivery pathways include intraperitoneal, intrapleural, and intravenous delivery. Notably, early virus clearance constitutes a problem, especially when OVs are applied systemically/intravenously*." **- [2].**

Neutralizing antibodies, binding viruses before reaching the tumor, can either pre-exist or be induced after a first virus dose. Therefore, viruses can be shielded against the immune system by modification of the viral surface or by encapsulating viruses to reduce immunogenicity [39, 40]. Another way of augmenting i.v. VACV therapy could be inhibition of PI3K, which was recently shown to not only improve virus delivery to the tumors but also enhance antitumor efficacy [41].

"As complement inhibition seems to play a crucial role in virus depletion following intravenous application [42], a new strategy is the application of an anti-C5-antibody (eculizumab) prior to virotherapy [NCT02714374]. Another recent approach to prevent intravascular virus clearance is to administer virus loaded cells as a carrier system for viral particles [43]. Reasonable options for NENs constitute intravenous administrations as well as direct virus injections into the hepatic artery in case of liver involvement (NCT02749331) [29]. Further, intratumoral virus administrations or surgically guided administrations into the resection beds can be considered." - **[2].**

Until now, there is only one single approved oncolytic virus in Germany. In Latvia, an oncolytic, unmodified ECHO-7 virus (Rigvir) was approved for melanoma patients in 2004. China approved an oncolytic adenovirus, H101 (Oncorine), as a treatment for advanced head and neck cancer in 2005. However, both viruses lack appropriate phase III study data.

The only oncolytic virus which has proved efficacy in randomized, controlled trials which met FDA and European Medicines Agency (EMA) standards is T-VEC. Therefore, the genetically modified herpes simplex virus is approved for treatment of late stage melanoma in Europe, the US and Australia since 2015 [44]. This virus is using a GM-CSF transgene to improve its immune stimulatory activity and was also incorporated in this study.

The two OVs investigated here are introduced in section 1.5 and 1.6, respectively.

4. Virotherapy of Neuroendocrine Neoplasms

"So far, there are only 2 clinical studies using virotherapeutics to treat neuroendocrine cancer. One phase I trial was conducted with intravenous administration of Seneca Valley virus (SVV-001) for patients with SCLC and NETs, but it only showed promising results for SCLC [45]. In another ongoing clinical phase I/II study (NCT02749331), a genetically engineered adenovirus (AdVince) is injected in the hepatic artery to treat NETs exhibiting liver metastases. AdVince has been specifically targeted to NET cells by putting the viral E1A gene, which is crucial for viral replication, under the human chromogranin A promoter [29]. Further virotherapeutic approaches with adenoviruses for NETs are in preclinical testing [46], but no other OVs than SVV-001 and adenoviruses have been evaluated for their efficacy in NETs yet." - **[1]**

With virotherapy in NEN, virus delivery is one of the crucial aspects, as tumors and metastases might be difficult to access for intratumoral injection (e.g. the pancreas). In this study, the two different viruses pursue different ways of delivery. T-VEC is injected in the local tumor, which is primarily possible for liver metastases. Endoscopic injection might be feasible for lung or gastrointestinal NEN. GLV-1h68 can also be directly injected but has been tested in clinical settings for intravenous delivery as well. Both ways would be suitable for NEN, as well as injection in the hepatic artery.

5. The Vaccinia Virus GLV-1h68

"The [first] *oncolytic virus employed in this study is a genetically modified DNA virus which has already been tested intensively in clinical settings. GLV-1h68 (proprietary name GL-ONC1) carries three separate transgenic expression cassettes (encoding β-glucuronidase, β-galactosidase, as well as the Ruc-GFP marker gene) inserted into a vaccinia virus (VACV) backbone derived from the Lister strain which has demonstrated its safety throughout years serving as a major smallpox vaccine. These triple insertions reduce the replication of GLV-1h68 in healthy cells and favor its replication in tumor cells [47, 48]; beyond they also allow the monitoring of virus activities in cancer patients [49]."* **- [2]**

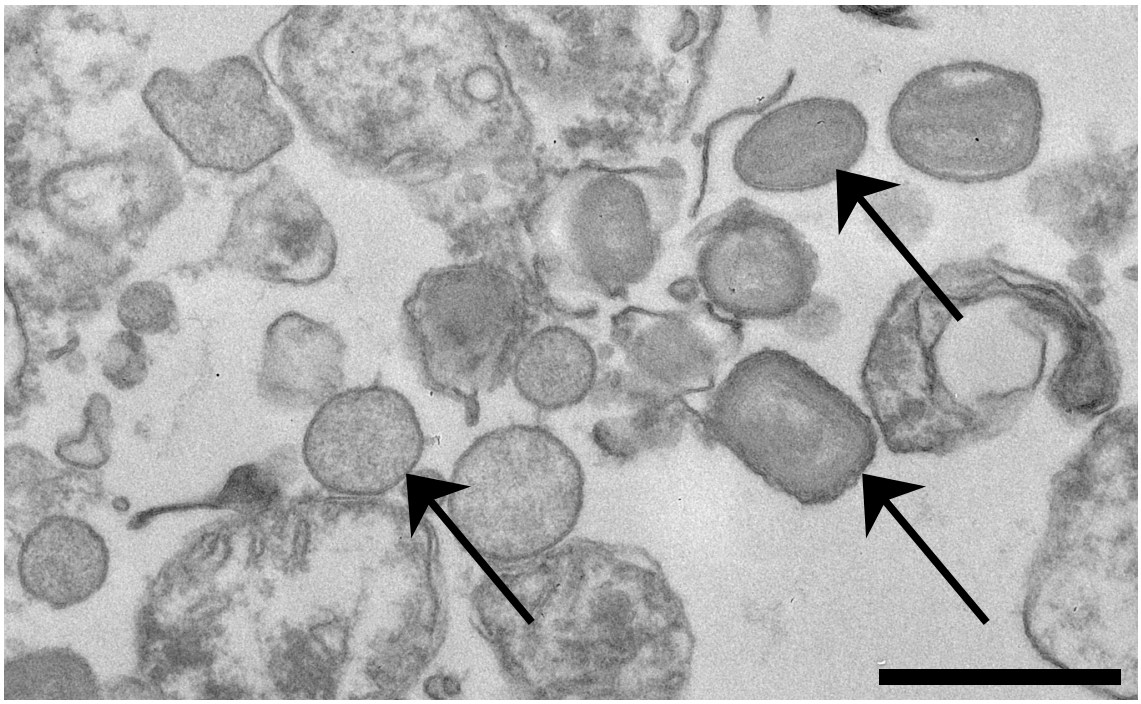

Figure 5: Enveloped GLV-1h68 virions. Vaccinia virus virions (arrows) reach up to 300 nm and usually have a typical, brick-shaped form like the one in the middle. The biconcave core consisting of proteins harbours the viral DNA. The least developed form (immature virion) can be observed on the left, the membrane wrapped brick-shaped virion (lower right) is an intracellular enveloped virion (IEV), whereas an intracellular mature virion (IMV) can be seen on the upper right. Scale bar indicates 500 nm. Taken from [50].

VACVs produce distinct forms of virions, intracellular mature virions (IMV) develop to intracellular enveloped virions (IEV), which are an intermediate form between IMVs and

extracellular enveloped virions (EEV) (Fig. 5). The more resistant EEVs carry a second enveloping membrane derived from the ER of the host cell, protecting the virion from the host's immune and complement system [51, 52]). The EEV is therefore thought to be responsible for the viral spread within the host. However, IMVs constitute the vast majority of released virions and are released through cell lysis, whereas EEVs egress the cells prior to lysis and are only the minority of viral progeny [53, 54] Pharmaceutically produced VACV only include IMVs and no EEV, however GLV-1h68 is able to produce EEVs after viral replication and thus might be able to spread to other tumor sites within the patient.

"As this oncolytic virus is not targeted to a specific type of tumor, oncolytic activity has already been detected in a broad spectrum of tumor entities in preclinical models as well as in several clinical trials [49, 55, 56]. Moreover, combinatorial approaches with chemotherapy, radiation or targeted therapies have displayed synergistic antitumor activities [57-61].

Currently, there are three active clinical studies (NCT02759588, NCT02714374, NCT01766739) which employ GLV-1h68/GL-ONC1." **- [2]**

In these studies, GLV-1h68 is applied intraperitoneally for ovarian cancer and peritoneal carcinomatosis (NCT02759588), intrapleurally to treat pleural malignancies (NCT01766739) or intravenously prior to surgery for several solid organ cancers (NCT02714374).

6. The Herpes Simplex Virus T-VEC

"T-VEC, the [second] *virotherapeutic agent employed in this study, is the only EMA/FDA-approved OV. T-VEC is a genetically modified herpes simplex virus (HSV) type 1 where a viral gene responsible for virulence has been deleted to ensure tumor-specific replication (ICP 34.5) and another gene normally reducing viral immunogenicity (ICP 47) has been deleted as well.*" - **[1]**

ICP 47 deletion additionally leads to an earlier expression of the viral US11 gene, which enhances the ability of viral replication of ICP 34.5 deleted HSVs [62].

"Instead, a GM-CSF transgene has been inserted to enhance the stimulation of the immune system [63]." - **[1]**

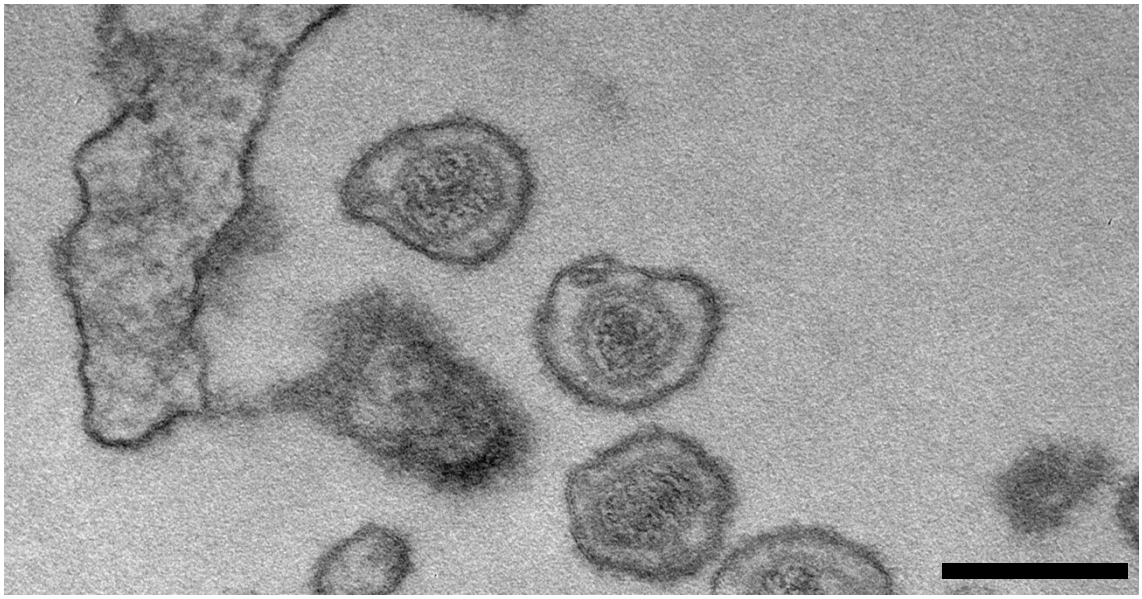

Figure 6: Viral T-VEC particles. Visualized with transmission electron microscopy, scale bar indicates 200 nm. Viral nucleocapsid, tegument protein and envelope become visible (cf. Results, section 4.2).

"The first clinical trial for this OV was conducted in 2006 [64], and it has been approved in 2015 as a second line treatment for late-stage melanoma [44]. For melanoma treatment, it is injected intralesionally and leads to a response in injected as well as noninjected lesions, taking the advantage of both direct tumor cell lysis and systemic antitumoral immune activity [65]. The duration of response and response rate were shown to be augmented in combination with checkpoint inhibitors such as anti- PD-1

(programmed death 1) and anti-CTLA-4 (cytotoxic T-lymphocyte-associated antigen 4) antibodies [36, 37].” - **[1]**

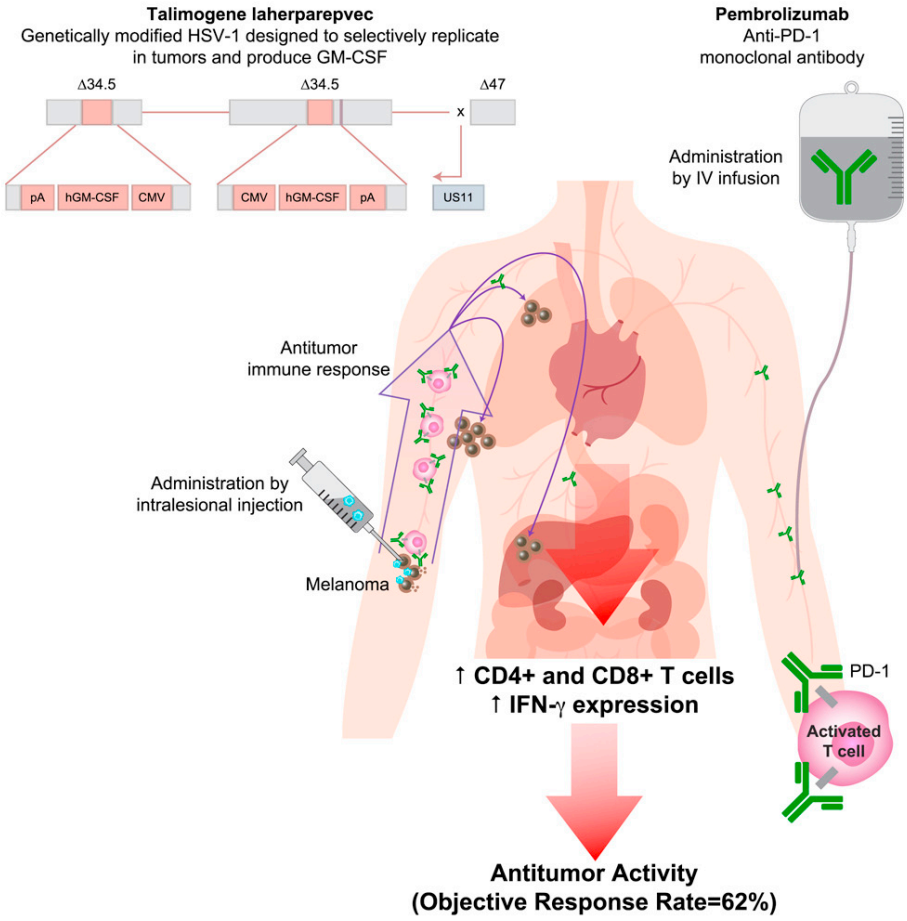

Figure 7: Combining T-VEC with the anti-PD-1 antibody Pembrolizumab. Genetic alterations of T-VEC are shown in the upper left corner, ICP 34.5 and 47 have been deleted and US11 is expressed immediate-early. GM-CSF transgenes under control of a CMV (Cytomegalovirus) promoter have been inserted. Pembrolizumab (upper right corner) is infused, blocking PD-1 on activated T-cells. In combination with the oncolytic activity of T-VEC in injected lesions, T-cells infiltrate the tumor and distant metastases, leading to increased IFNγ expression and higher objective response rates than either drug alone. Reprinted from [37] with permission from Elsevier.

“Therefore, T-VEC is currently studied in several clinical studies for combinatorial treatment regimens to expand approval also for other malignancies. Besides melanoma, T-VEC is under clinical investigation for diverse tumor entities such as liver tumors (NCT02509507), pancreatic cancer (NCT03086642), breast cancer (NCT02658812), or sarcoma (NCT03069378). But, until now, it has not been investigated for its efficacy in neuroendocrine malignancies neither in a clinical nor a preclinical setting.” - **[1]**

In this study, the combination of T-VEC with the mTOR inhibitor Everolimus was investigated. Everolimus strongly inhibits mTORC1, which regulates Akt via a negative feedback loop. Akt is therefore overactivated during mTOR inhibition with Everolimus. As Akt activity constitutes one of the key features for HSV cell entry and correlates with viral infection and replication, synergistic effects of T-VEC and Everolimus are conceivable [66]. It has already been shown that the mTOR inhibitor rapamycin is able to augment the oncolytic activity of an ICP 34.5 deleted HSV in cell lines resistant to OV alone [67]. Further, mTORC1 is also involved in the cellular type I IFN response. Its inhibition can enhance cellular susceptibility to viral infection of both Vaccinia and Herpes viruses [68, 69].

7. The thymidine kinase/ganciclovir system

Thymidine kinase (TK) is an enzyme occurring in almost all bacterial and eukaryotic cells. It acts in cellular nucleotide metabolism by transferring phosphate from ATP (adenosine triphosphate) to deoxythymidine, resulting in thymidine monophosphate (TMP). TMP can be further phosphorylated by other cellular kinases to TTP (thymidine triphosphate), a major substrate for DNA synthesis. This pathway constitutes a salvage pathway to reuse thymidine in cellular nucleotide metabolism.

The HSV-TK, encoded by HSVs, is a subtype of this enzyme having a broader substrate specificity and also being able to phosphorylate deoxycytidine and several nucleoside analogues, such as Acyclovir (ACV) and GCV. HSV-TK itself is not essential for viral replication but has a significant impact on virulence [70]. HSV-TK seems to be important for viral replication in non-dividing cells with a low nucleotide metabolism and especially in latency of herpes virus infection [71]. As TK does only play a minor role for viral replication in cancer cells, deleting the TK gene in Herpes viruses is one strategy to attenuate HSVs for a more cancer specific virus replication in oncolytic virotherapy.

The properties of the HSV-TK are used in antiviral therapy with ACV or GCV. Since only the HSV-TK is able to phosphorylate these nucleoside analogues, they are only phosphorylated in virus infected cells. The resulting monophosphates are subsequently phosphorylated to triphosphates by cellular kinases and serve as nucleotide analogues which terminate DNA synthesis. ACV terminates DNA synthesis due to a lack of a hydroxyl group at the 3’ end, which blocks further elongation of the DNA strand. GCV is incorporated into DNA instead of adenosine, but because of its molecular structure, no phosphodiester bridges can be built up between both strands what subsequently destabilizes DNA. In summary, both agents inhibit viral DNA synthesis and act as potent virostatic drugs.

GCV-triphosphate not only inhibits viral, but also cellular DNA synthesis and induces apoptosis [72]. After transferring an HSV-TK gene into tumor cells, only tumor cells activating GCV and their neighboring cells are sensitive to GCV mediated cytotoxicity. This so called TK/GCV suicide gene system has been intensively studied and used in gene therapy [73].

As T-VEC is an HSV-TK positive OV, the combinatorial use of GCV is possible in both intentions. GCV can be (I) applied to limit viral replication exhibiting a safety feature in the case of an uncontrolled viral replication or (II) applied to further enhance cytotoxicity in tumor cells expressing HSV-TK after viral infection with T-VEC. In this work, GCV was added to T-VEC infected tumor cells at an early stage of viral infection to investigate its properties as a virostatic drug as well as at a late stage of viral infection to analyze its ability to enhance oncolytic effects.

8. Fundamental questions

The aim of this dissertation was to verify if oncolytic virotherapy using GLV-1h68 and T-VEC could be a suitable treatment option for neuroendocrine cancer. Two clinically well-characterized viruses were picked to assess which virus holds the greatest oncolytic activity against cells derived from NETs and NECs. In addition, combinatorial treatments with virotherapy were studied. It was verified whether or not a combinatorial treatment of both OVs with Everolimus could be a therapeutic option, as the clinical indications for Everolimus treatment match the pursued clinical indications for virotherapy. In combination with T-VEC treatment, GCV was investigated for its ability to limit T-VEC replication in neuroendocrine cancer cells as well as for a possible augmenting effect on cytotoxicity.

In this purpose, (I) cytotoxicity of both OVs was measured in vitro, (II) viral replication kinetics were studied and (III) quantified as well as (IV) viral transgene expression was proven via fluorescence microscopy and ELISA. Moreover, (V) electron microscopic images were taken to comprehend the replication cycle and envelopment of T-VEC. Facing a combinatorial treatment, (VI) interaction of both OVs with the mTOR inhibitor Everolimus, which is approved for advanced metastatic NETs, was analyzed. Further, (VII) the effect of the virostatic drug GCV on T-VEC replication in NET cells was studied. Finally, (VIII) both the envelopment as well as the cell egress of T-VEC were studied using transmission electron microscopy (TEM).

So far, to our knowledge this is the first study employing GLV-1h68 or T-VEC in neuroendocrine cancer cells. Also, T-VEC replication and egress were visualized the first time using TEM.

CHAPTER 2: MATERIALS AND METHODS

All procedures were performed under sterile conditions and under a laminar air flow hood, except specified otherwise. Media and cell culture material were also used in sterile form. Dulbecco´s modified Eagle´s Medium (DMEM, Sigma-Aldrich St. Louis, MO, USA) was used with 4.5 g Glucose/L and with L-Glutamine. RPMI-1640 medium (Gibco, Waltham, MA, USA) was employed containing GlutaMAX. Standard cell culture was performed without antibiotics. Culture media, phosphate buffered saline (DPBS w/o calcium chloride and magnesium chloride, Sigma-Aldrich) and substances in contact with cells were pre-warmed in a 37 °C water bath before use and were stored in a 4 °C fridge. Everolimus, GCV and viral agents were stored in aliquots in a -80 °C freezer.

1. Cell culture

1.1. Cell characteristics

A panel of 6 different cell lines originating from a variety of neuroendocrine neoplasia was collected. H727 and UMC-11 cell lines are both derived from typical lung carcinoids with a low Ki67 Index [74, 75]. BON-1 and QGP-1 cells are both originating from pancreatic NETs. BON-1 are serotonin producing tumor cells and were established from a peripancreatic metastatic lymph node [76]. QGP-1 cells were derived from somatostatin and carcinoembryonic antigen (CEA) producing pancreatic NET [77]. Further, two NEC cell lines were employed in this study. HROC-57 cells are high grade tumor cells from a large colon ascendens NEC [78]. NEC-DUE1 cells originate from a liver metastasis of a Cisplatin/Etoposide pre-treated patient whose primary tumor was a large cell NEC at the gastroesophageal junction [79]. All tumor cell lines were shown to express the neuroendocrine markers Synaptophysin, Chromogranin A and CD56 previously.

1.2. Cell passage and medium exchange

Cell line	Culture medium	Standard passage ratio	Cells seeded in 6-well plates	Cells seeded in 24-well plates	Trypsin	Cell strainer	Source
NCI-H727	RPMI 1640 with 10 % FCS (Biochrom)	1:4	$4*10^5$/well	$6*10^4$/well	0,25 % (Sigma-Aldrich)		ATCC (American Type Culture Collection)
UMC-11	RPMI 1640 with 10 % FCS	1:4		$8*10^4$/well	0,05 % (Gibco)	100 µm (Falcon)	ATCC
BON-1	DMEM with 10 % FCS	1:6	$3*10^5$/well	$4*10^4$/well	0,05 %		Dr. Ulrich Renner, MPI Psychiatry, Munich, Germany
QGP-1	RPMI 1640 with 10 % FCS	1:3	$6*10^5$/well	$8*10^4$/well	0,05 %	100 µm (Falcon)	JCRB (Japanese Collection of Research Bioresources Cell Bank)
HROC-57	DMEM/F12 (Gibco) with 10 % FCS	1:3		$6*10^4$/well	0,05 %		Dr. Michael Linnebacher, University Hospital Rostock, Germany

NEC-DUE1	RPMI 1640 with 10 % FCS	1:4	10^6/well	$2*10^5$/well	0,25 %		Dr. Andreas Krieg, University Hospital Duesseldorf, Germany
Vero	DMEM with 10 % FCS	1:10		$5*10^4$/well	0,25 %		German Collection of Microorganisms and Cell Cultures DSMZ, Braunschweig, Germany
CV-1	DMEM with 10 % FCS	1:10		10^5/well	0,25 %		ATCC

Table 1: Culture conditions of the cell lines employed in this study.

Cells were maintained as monolayer cell culture in 75 cm^2 cell culture flasks (Greiner Bio One, Kremsmünster, Österreich) with 15 ml medium in the incubator at 37 °C and 5% CO_2 in a humid atmosphere. The media utilized for the cultured cell lines are specified in Table 1. No antibiotics were used in monolayer cell culture. 10 % FCS (Biochrom, Berlin, Germany) was added to every cell culture medium. Medium was exchanged every three days when cells were not passaged. Therefore, medium was discarded and 15 ml of fresh medium were added. Cells were passaged when confluent, in average every 4 days. For cell passage, medium was removed and cells were washed once with 10 ml of PBS (Sigma-Aldrich, DPBS w/o calcium chloride and magnesium chloride) to discard residual medium and serum. Afterwards, 2 ml of trypsin solution (0,25% or 0,05%, Table 1) were added to detach the cells from the culture flask. For this, cells were incubated for about 4 min in the incubator until they detached. Then, 10 ml of medium were added to inactivate trypsin. After that, cell suspension was transferred to a 15-ml tube (Falcon, Corning, NY, USA) and centrifuged for 4 min at 1000 rpm. Supernatant was discarded and cells were resuspended in 4 to 10 ml (dependent on the size of the cell pellet) of medium. For cell passage, the desired amount of cell suspension (depending on passage ratio) was transferred to the culture bottle and medium was added to a total volume of 15 ml. At the end, the cell culture flask was put in the incubator again. Cell line specificities for cell culture maintenance are outlined in Table 1.

1.3. Freezing and thawing cells

For freezing, cells were usually cultivated in a 150 cm^2 flask (Greiner Bio One) with 25 ml of the respective culture medium to expand the cell count. When confluent, instructions for cell passage were followed. After centrifuging, the cell pellet was taken up in 4 ml cell freezing medium, consisting of 70% cell culture medium, 20 % FCS and 10 % DMSO (AppliChem, Darmstadt, Germany). 1.5 ml cryovials were filled each with 1ml of cell suspension, then put in a freezing container (Mr. Frosty, Thermo Fisher, Waltham, MA, USA) and frozen in an -80 °C freezer. The next day, cryovials were moved to a -150 °C freezer.

To thaw cells, cryovials were put quickly in a 37 °C bath. When thawed, the cell suspension was transferred to a 15 ml tube, 5 ml of the respective cell culture medium was added by resuspending and then the cell suspension was centrifuged for 4 min at 1000 rpm to remove freezing medium. Afterwards, supernatant was discarded and cell pellet was gently resuspended in 5 ml of cell culture medium. Regularly, thawed cells were first cultivated in a 25 cm^2 culture flask and transferred to a 75 cm^2 culture flask when confluent.

1.4. Determination of cell count

To determine cell count, an improved Neubauer haemocytometer was employed. Instructions for cell passage were followed and the cell pellet was taken up in an appropriate amount (3 to 10 ml) of culture medium. For some cell lines, it was necessary to filter cells through a cell strainer (Table 1). Then, 10 µl of the cell suspension were mixed with 90 µl of trypan blue solution (0.4 %, Sigma-Aldrich) in a 1.5 ml Eppendorf cup (dilution 1:10) to stain dead cells in dark blue. After short vortexing, 10 µl of the suspension were pipetted into the counting chamber. Cells were counted in each of the four large counting squares under the bright field microscope with magnification x10. The average cell count per square was determined to calculate the suspension´s cell concentration with the following formula:

$$\frac{cells}{ml} = 10^4 * dilution * \frac{cells}{square}$$

1.5. Seeding cells

To plate a defined number of cells, cell count had to be determined at first. Then, the needed amount of cell suspension was calculated. Cells were seeded in 6-well plates (Falcon) in a volume of 2 ml/well, in 24-well plates (TPP, Trasadingen, Switzerland) in a volume of 500 µl/well or in 96-well plates (E-Plate 96, Roche Applied Science, Mannheim, Germany) in a volume of 150 µl/well.

2. Microscopy

2.1. Bright field and phase contrast microscopy

Cells maintained in cell culture flasks as well as treated cells in culture plates were observed daily under the Olympus (Hamburg, Germany) CK 40 bright field microscope with a 4-fold magnification. Cells were counted in the Neubauer haemocytometer under the same microscope with a 10-fold magnification.

The Olympus IX 50 microscope was employed for microscopic pictures using an F-View II Soft Imaging System (Olympus) and the associated analySIS software. This microscope was used for Phase contrast microscopy as well by choosing the PhL filter.

2.2. Fluorescence microscopy

For fluorescence microscopy, an Olympus U-RFL-T fluorescence system and the Olympus IX 50 microscope were employed. The respective filter was used to make the fluorescent protein GFP visible. Images were taken using the F-View Soft Imaging System. Subsequently, colorization was conducted with the analySIS software. To create overlaid images without software editing, the microscope lamp was dimmed and exposure time was extended so that fluorescent as well as non-fluorescent cells became visible. For colored overlay pictures, bright field pictures and fluorescent pictures were overlaid after microscopy using the Apple Preview 10.0 software.

2.3. Transmission electron microscopy (TEM)

To visualize the infection and replication of the Herpes simplex virus T-VEC, infected samples were investigated under a transmission electron microscope. For this purpose, the pancreatic NET cell line QGP-1 was employed. Cells were seeded in five 60 cm^2 petri dishes (8.7 cm in diameter, TPP) with 10 ml of cell culture medium and $2*10^6$ cells per petri dish. The day after seeding, four dishes were infected with T-VEC at MOI 0.01 and one dish was mock infected. This MOI was chosen because it led to approximately 50 % cell mass reduction after 96 h. For microscopy, cells were harvested and fixed 24, 48, 72 and 96 hours post infection (hpi), mock infected cells were fixed at 96 hpi as well. For harvesting, cells were trypsinized and centrifuged as described. The cell pellet was taken

up in 1.3 ml of Karnovsky's fixative and incubated for 1 hour at room temperature. Then, samples were stored at 4°C until further processing for TEM.

"For electron microscopic analyses, the cell pellets were embedded in 3.5% agarose at 37° C, coagulated at room temperature, and fixed again in Karnovsky's solution. Postfixation was based on 1.0% osmium tetroxide containing 1.5% K-ferrocyanide in 0.1 M cacodylate buffer for 2 h. Samples were rinsed with distilled water, block-stained with uranyl acetate (2% in distilled water), dehydrated in alcohol (stepwise 30–96%), immersed in propylenoxide, embedded in glycide ether (polymerized 48 h at 60 ° C, Serva, Heidelberg), and cut using an ultramicrotome (Ultracut, Reichert, Vienna, Austria). Ultrathin sections (30 nm) were mounted on copper grids and analyzed using a Zeiss LIBRA 120 transmission electron microscope (Carl Zeiss, Oberkochen, Germany) operating at 120 kV." - **[1]**

3. Treatment of cultures

3.1. Infection of seeded cells

Two OVs were employed in this study. Vaccinia virus GLV-1h68 (stock titer $3*10^8$ PFU/ml, LIVP strain) and with the herpes simplex virus Talimogene Laherparepvec (T-VEC, stock titer $2*10^7$ PFU/ml) were kindly provided by Genelux Corporation (San Diego, CA, USA) and Amgen Inc. (Thousand Oaks, CA, USA), respectively. 24 h prior to virus infection, cells were seeded in 96-, 24- or 6-well plates. Shortly after thawing, vials with viruses were sonicated in a 4 °C water bath for 30 seconds and subsequently put on ice. For 6-well plates, 1 ml infection medium was needed; for 24-well plates 250 µl and for 96-well plates 50 µl were prepared. Virus was diluted in DMEM with 2 % FCS for Vaccinia virus and serum-free DMEM for T-VEC for the respective number of wells and multiplicity of infection (MOI). MOI means viral particles per cell, i. e. MOI 1 means one infectious particle per cell. After preparing the infection medium, cells were washed once with PBS. Afterwards, infection medium was added and plates were put in the incubator again for one hour to allow virus infection. During the hour of infection, plates were swayed gently every 15 min. Then the inoculum was removed and replaced by the respective cell culture medium. In general, 4 wells of a 24-well plate were infected with the same MOI and 4 wells were treated as controls with virus free infection medium (mock infected).

3.2. Everolimus and Ganciclovir treatment

Single agent treatment with Everolimus (stock concentration 10 mM, Selleckchem, Munich, Germany) was performed in a 24-well plate. 24 h after seeding, cell culture medium was replaced with medium containing different concentrations of Everolimus. Therefore, Everolimus was diluted in the respective cell culture medium to the desired concentrations (generally 10-fold dilutions from 10 µM to 10 pM). Generally, 3 wells were treated with the same concentration and 3 wells were left untreated. Plates were analyzed 72 and 96 hours post treatment (hpt) by sulforhodamine B assay. For combinatorial treatment with oncolytic viruses, the virus infection medium was replaced after allowing 1 hour of virus infection with cell culture medium containing Everolimus in the respective concentration.

GCV (stock concentration 10 mM, Selleckchem) was diluted in cell culture medium to concentrations of 1 to 50 µM. 24 h after seeding, cell culture medium was replaced with medium containing different concentrations of GCV (0, 1, 10, 50 µM) for single agent GCV treatment. For GCV addition to virus infected cells at 1 hpi, infection medium was replaced with cell culture medium containing GCV. For addition to virus infected cells at 72 hpi, 55 µl of cell culture medium per well were prepared with a 10-fold higher GCV concentration than the final concentration and added to the 500 µl of cell culture medium in each well to a final volume of 555 µl.

3.3. Viral growth curves

For viral growth curves, cells were seeded in a 6-well plate. All 6 wells were infected with the same MOI as described previously. Therefore, the MOI which led to approx. 50% cell mass reduction after 96 h was chosen to allow viral replication without extensive cell killing. After removing the infection medium, each well was washed three times with 1 ml of PBS to remove all free viral particles so that only viral particles which had already entered the cells stayed in the plate. Then, 1 ml of the respective culture medium was added. For growth curves in the presence of Everolimus, Everolimus was diluted in cell culture medium to a final concentration of 1 nM before. This concentration was chosen because it was the lowest concentration which led to a measurable effect on cell mass. For growth curves in the presence of GCV, it was diluted in the respective cell culture medium to replace infection medium 1 hpi. The concentrations 10 µM for H727 cells and 1 µM for QGP-1 and NEC-DUE1 cells were employed.

Cells and supernatants were harvested every 24 h from one well for virus quantification. Therefore, cells were scraped in medium using a cell lifter (Corning). Then, the cell suspension was harvested by pipetting up and down for a few times, transferred to an Eppendorf cup and put in the -80 °C freezer. Empty wells were filled with 1 ml PBS to avoid drying out of the cell cultures and the plate was put in the incubator again.

4. Analysis of treated cultures

4.1. Sulforhodamine B assay

Sulforhodamine B (SRB) assay is a cell viability assay where proteins in adherent cells are unspecifically stained whereas dead, non-adherent cells are washed out [80]. It was carried out either 72 h or 96 h post infection/treatment in 24-well plates. First, cells were washed once with 500 µl 4 °C cold PBS. Afterwards, 250 µl of 10 % trichloroacetic acid (TCA, Carl Roth, Karlsruhe, Germany) were added to each well and the plate was put in a 4 °C fridge for at least 30 min for fixation of adherent cells. Then, TCA was pipetted in the hazardous waste, and the plate was washed three times with water. For infected plates, water was pipetted in the wells under the laminar flow hood, whereas plates without virus could be washed under unsterile conditions in a beaker. Plates were put in a 40 °C incubator to dry for at least 3 h or overnight.

From here, the procedure was no longer performed under sterile conditions. After incubation, the fixed cells were stained using SRB staining solution (0.4 % in 1 % acetic acid, Sigma-Aldrich). For this, 250 µl SRB solution were pipetted in each well and plates were allowed to dye for at least 10 min. Subsequently, plates were rinsed with 1 % acetic acid (VWR Radnor, PA, USA) until the washing solution became colorless. For drying, plates were put in the 40 °C incubator again for at least 3 h or overnight.

When dried, 250 µl to 2 ml of TRIS base (10 mM, pH 10,5, Carl Roth) were added and plates were put on a horizontal shaker for at least 10 min to solve SRB. The amount of TRIS base was dependent on staining intensity, if staining was too intense more TRIS base had to be used, but always the same amount of TRIS had to be used for each well of one plate. When SRB was solved, 80 µl solution of one well of the 24-well plate was pipetted in one well of a 96-well plate for photometric analysis. Samples were analyzed in duplicates, so that one 96-well plate was sufficient for analysis of two 24-well plates. The extinction of each well of the 96-well plate was measured at a wavelength of 564 nm in a Tecan Genios Plus Microplate Reader (Männedorf, Switzerland). The extinction is proportional to the cell mass of fixed adherent cells. In graphics, the extinction of the samples was based on mock extinction which was calibrated as 100 % cell mass.

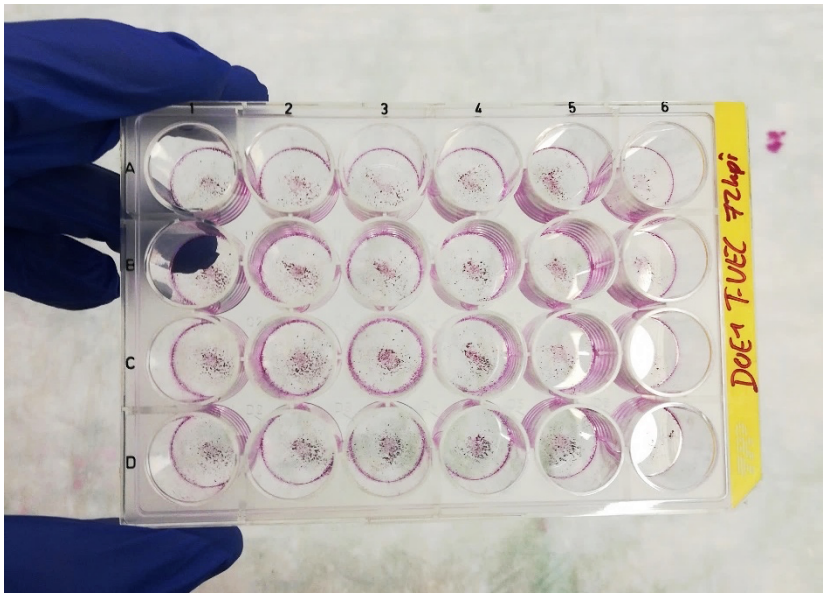

Figure 8: Stained SRB assay. Dried, SRB stained NEC-DUE1 cells in a 24-well plate before solving SRB with TRIS.

4.2. Real-time cell monitoring

For Real-time cell monitoring conducted with the xCELLigence RTCA SP system (Roche Applied Science, Mannheim, Germany), tumor cells had to be seeded in 96-well E-plates. $2*10^4$ H727 cells were employed in each well. 24 h after seeding, cells were either infected with OV in the respective MOIs (0.001 and 0.0001 for T-VEC; 0.25 and 0.1 for GLV-1h68) or treated with Everolimus or Triton X-100 0.1 %. Mock wells were treated like virus infection with virus free infection medium. For combination of OV and Everolimus, virus infection medium was replaced with the respective cell culture medium containing Everolimus after 1 h of viral infection. The impedance of the cellular layer was monitored every 30 min over a period of 120 h in total. The Cell index was determined by the RTCA Software (1.0.0.0805).

4.3. Virus quantification

To determine the number of viral particles and thus viral replication, samples were diluted and viral plaques were counted. For this purpose, indicator cell lines which are highly susceptible for viral infection were employed. CV-1 cells were used for GLV-1h68 and Vero cells for T-VEC, respectively. Cells were seeded in 24-well plates 24 h prior to titration. One 24-well plate was sufficient for two samples. Moreover, 5 Eppendorf cups per sample with 900 µl of the respective infection media (DMEM with 2 % FCS for

Vaccinia and DMEM without FCS for T-VEC) were prepared. Then, samples were quickly thawed, so that the cells were lysed and intracellular viral particles were released. After short vortexing, thawed samples were sonicated in a 4 °C water bath for 30 seconds and subsequently put on ice. For titration, the samples were diluted in a 10-fold dilution series by pipetting 100 µl from the sample to the first prepared Eppendorf cup. After subsequent vortexing, 100 µl were pipetted again to the next Eppendorf cup. That procedure was repeated 5 times for each sample, resulting in dilutions from 10^{-1} to 10^{-5}. After two samples were diluted like this, one 24-well plate with the respective indicator cells was taken out of the incubator. Culture medium was discarded and 250 µl of each dilution was pipetted in duplicates in the wells by using the following scheme:

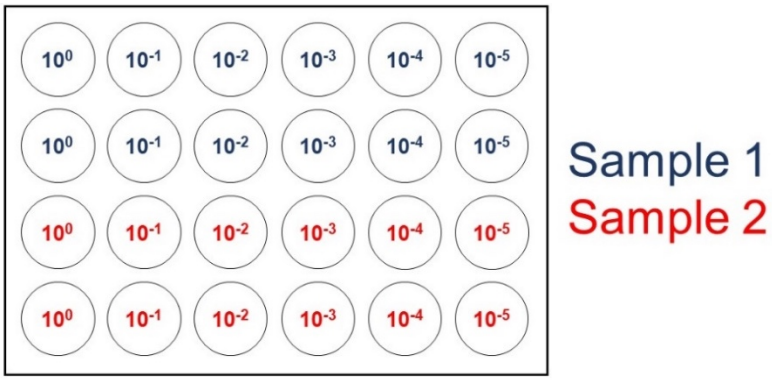

Figure 9: Dilution scheme for viral plaque assay.

Afterwards, the plate was put in the incubator for 1 hour and moved every 15 min to allow viral infection. Then, 1 ml of DMEM with 5 % FCS, 1 % Pen/Strep and 1.5 % carboxymethylcellulose (CMC, Sigma-Aldrich) was added to each well. CMC prevents viral distribution through the culture medium so that viral infection can only spread to adjacent cells and thus, plaques become visible in the confluent cell layer. 48 hpi for titration of Vaccinia viruses or 96 hpi for titration of T-VEC, 0.25 ml of 0.1 % crystal violet solution (Fluka Chemie AG, Buchs, Switzerland, in ddH_2O with 5 % ethanol and 10 % formaldehyde) was added to each well for staining. After 3 h or overnight, the plates were emptied and washed twice with water. Now, plaques should be visible in at least one dilution. Plaques were counted in wells with a plaque count from 8 to 80 and the mean of the duplicates was used for calculation of plaque forming units per ml (PFU/ml). PFU/ml were calculated with the following formula:

$$\frac{PFU}{ml} = Plaque\ count * \frac{1\ ml}{250\ \mu l} * Dilution^{-1}$$

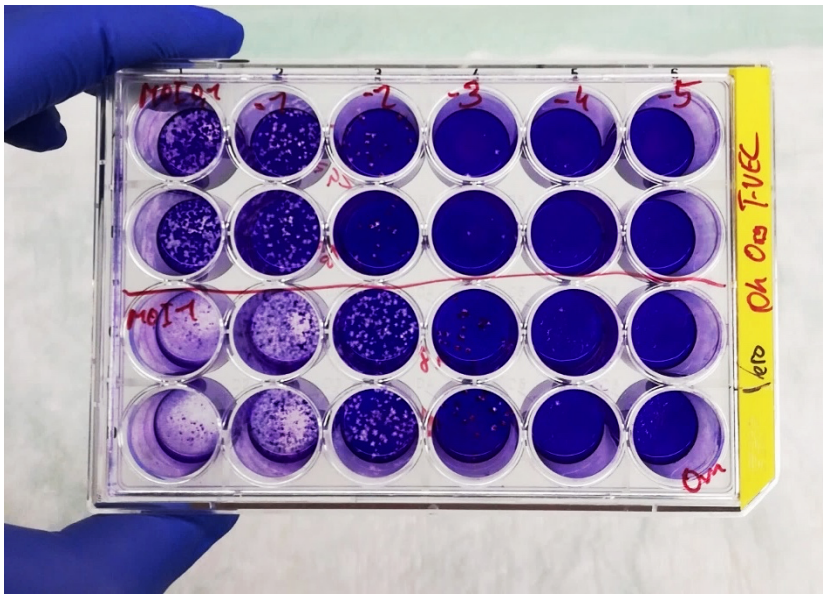

Figure 10: Stained viral plaque assay. Crystal violet stained Vero cells, plaques became visible in dilutions of both samples (MOI 0.1 and MOI 1), plaques were counted in the 10^{-2} dilution of the upper sample and in the 10^{-3} dilution of the lower sample

4.4. Human GM-CSF ELISA

As the genetically engineered HSV T-VEC holds a GM-CSF transgene and no fluorescent transgene, the GM-CSF expression of infected cells was measured. For this purpose, supernatants were harvested from cell culture or organoid culture at the respective time points and pipetted into 2 ml Eppendorf cups. To remove cells, the Eppendorf cups were centrifuged for 5 min at 4500 RPM and supernatant was transferred to other Eppendorf cups and subsequently frozen at -80°C. When enough samples were collected, they were thawed in the 37°C water bath and GM-CSF concentrations were analyzed with the BioLegend (San Diego, CA, USA) Human GM-CSF ELISA Max Kit according to the manufacturer's instructions. The ELISA plates were analyzed with a Tecan Genios Plus Microplate Reader at a wavelength of 450 nm.

4.5. Statistical analysis

If not specified otherwise, mean and standard deviation (SD) are shown in the figures. An unpaired, two-tailored t-test for in inhomogeneous variations was carried out in cases were further statistical evidence was necessary. Therefore, Microsoft Excel version 16.34 was used. P values ≤ 0.05 were considered to be statistically significant.

CHAPTER 3: RESULTS

In this chapter, the results of this study are described. Both OVs were investigated in a single agent treatment setting as well as in combination with Everolimus. T-VEC was also combined with GCV. In section 1, Everolimus was used to treat the panel of NET/NEC cell lines in order to assess the appropriate concentrations for combinatorial therapy and to compare results with those from both OVs. In the second section, GLV-1h68 was studied, first as a monotherapy agent (section 2.1) and afterwards in combination with Everolimus (section 2.2). The same was done with T-VEC in the sections 3.1 and 3.2, respectively. GCV was combined with T-VEC in section 3.3. In the last section of this chapter, TEM images of QGP-1 cells infected with T-VEC were provided to visualize T-VEC virions and their cellular egress and envelopment in NET cells. Further details can also be found in [1] and [2].

1. Efficacy of Everolimus monotherapy

First of all, the panel of six NET/NEC cell lines was treated with Everolimus. In this purpose, the respective concentration of Everolimus was added to the cell culture medium. As a consequence, cells were exposed to Everolimus over the whole time period of the experiment.

1.1. Everolimus has limited effects on cell viability

To assess cell viability, SRB viability assays were carried out using Everolimus in concentrations from 10 pM to 10 µM in logarithmic steps (Fig. 11). Only for UMC-11 lung NET cells, which already showed quite extensive reduction of tumor cell count with 1 nM in the first experiments, a concentration of 500 pM was added while 10 µM were left out in the following runs (Fig. 11 B). An arbitrary threshold of 60 % cells compared to mock treatment was set for all SRB viability assays in this study. Results showing a tumor cell reduction below 60 % can be seen as highly relevant for further studies, being likely to exhibit a profound, relevant antitumor effect. In this experiment, cellular susceptibility to Everolimus treatment was classified in three categories: cells already reaching the threshold with 1 nM Everolimus 96 hpt were classified (I) highly sensitive,

cells only reaching the threshold with higher concentrations (>1 nM) 96 hpt were ranked (II) sensitive, and cells not meeting the threshold at all were classified (III) resistant.

As a result, Everolimus could reduce the tumor cell count in all six NET/NEC cell lines tested in a dose dependent manner. The reduction was found to be higher after 96 than 72 h in all cell lines except QGP-1 and HROC-57, were the reduction in tumor cell count 96 hpt was similar or slightly smaller than 72 hpt. All tumor cell lines showed a characteristic pattern of response. With concentrations between 500 pm and 10 nM, a significant reduction of tumor cell count could be achieved in all cell lines. Lower concentrations did not lead to relevant effects, whereas higher concentrations reduced the cell count only slightly further. This characteristic effect resulted in a plateau which was reached with concentrations around 1 nM. Therefore, a concentration of 1 nM was selected to be employed in further experiments combining Everolimus with viral agents to investigate its effects on viral replication. For SRB viability assays combining virotherapy and Everolimus, 1 nM was chosen for H727 cells whereas 0.25 nM was picked for NEC-DUE1 cells, being more susceptible to Everolimus treatment.

According to the three categories introduced above, H727, UMC-1 and NEC-DUE1 cells were classified as highly sensitive to Everolimus (Fig. 11 A, B and F). BON-1, QGP-1 and HROC-57 cells were categorized sensitive, meeting the threshold with concentrations >1 nM (Fig. 11 C, D and E). No cell line was found to be resistant to Everolimus treatment. Breaking the results down to the anatomical origin of the cell lines, both lung NET cell lines were found to be highly sensitive, whereas both pNET cell lines were “only” classified to be sensitive. Anyway, even though high Everolimus concentrations were employed, no complete tumor cell reduction (≤10 %) could be accomplished in any tumor cell line. This was rather indicative for antiproliferative than cytotoxic effects. As the SRB viability assay is generally not capable to discriminate cytotoxic and antiproliferative effects, real-time cell monitoring was employed.

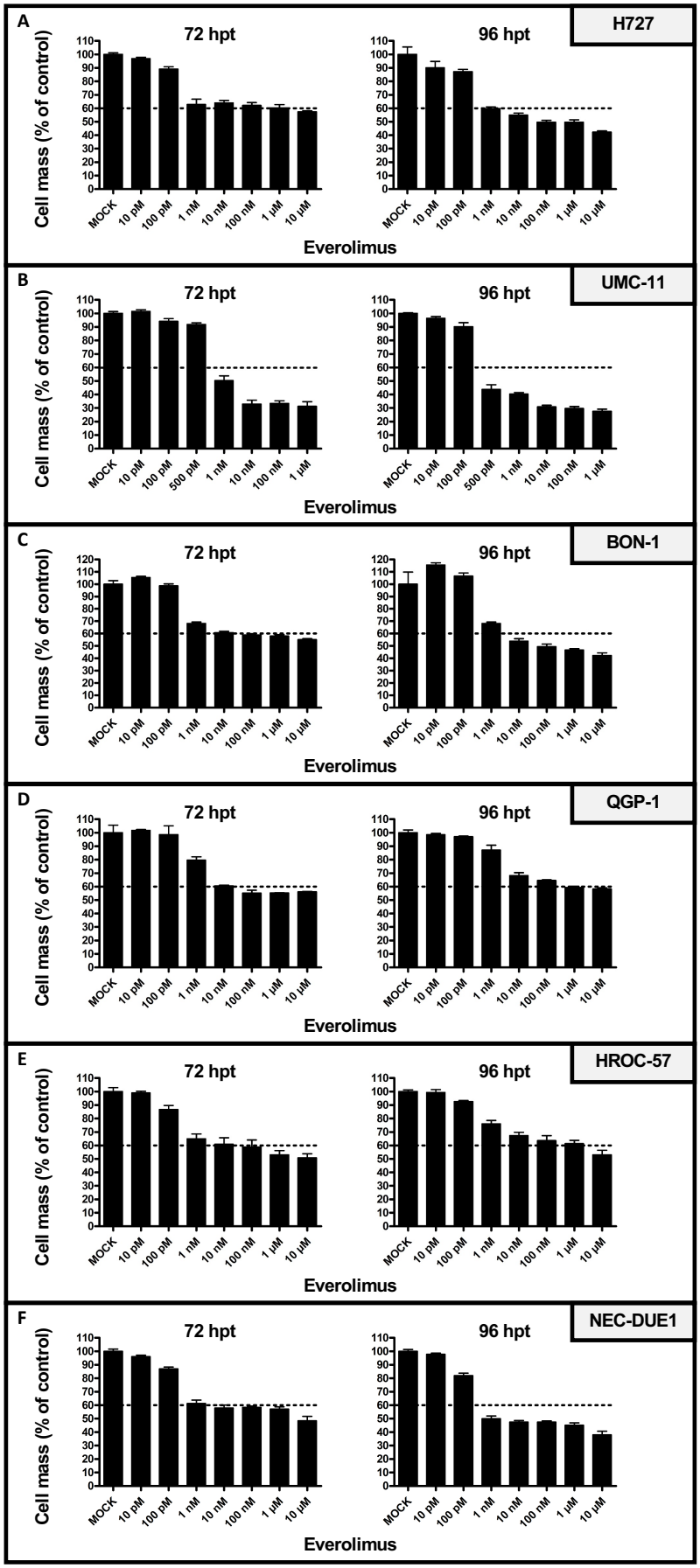

Figure 11: SRB viability assay with Everolimus treated NET/NEC cell lines. Analysis performed at 72 and at 96 hpt; mean and SD of 2 independent experiments carried out in triplicates are shown. "*At 1 nM Everolimus, a significant reduction of tumor cell numbers was observed for all NET/NEC human cell lines; however, even when using high concentrations (up to 10 µM), no complete tumor cell reduction could be achieved with Everolimus monotherapy.*" Reprinted from [1].

1.2. Everolimus exhibits antiproliferative effects

The xCELLigence® Real Time Cell Analyzer (RTCA) system was employed for real-time cell monitoring to measure impedance of the cell layer over 120 h (Fig. 12). The Cell Index, which can be seen as a surrogate for cell viability, was subsequently calculated. The representative lung NET cell line H727 was employed and treatment with concentrations of 1, 10 and 100 nM Everolimus was conducted at 24 h after seeding.

Triton as a control treatment for complete cell lysis resulted in immediate cell death, represented as an immediate drop of the cell index (Fig. 12, green line). Treatment with Everolimus did not significantly alter cell proliferation compared to mock treatment. Only higher concentrations of 10 and 100 nM led to a slightly lower gradient of the curve (Fig.12, blue line). This is suggestive for a slower cell proliferation with Everolimus treatment, indicating an antiproliferative effect of Everolimus. As no drop of the Everolimus curves could be detected, no cytotoxicity could be proved. For following real-time monitoring experiments in combination with virotherapy, an Everolimus concentration of 100 nM was chosen as Everolimus only exhibited little effects in this method.

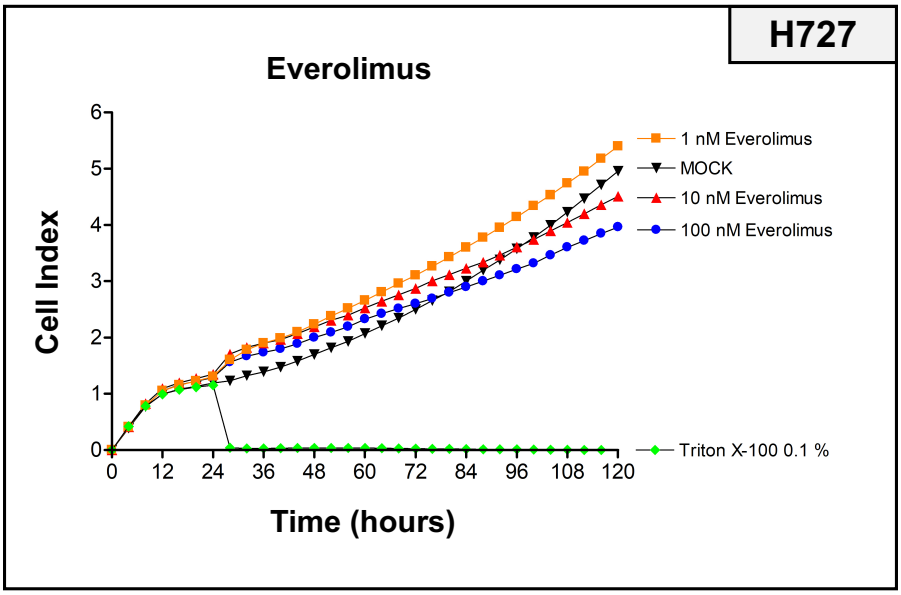

Figure 12: Real-time cell monitoring of Everolimus treated H727 cells. The experiment was carried out in quadruplicates, symbols show mean. SD is not shown for clarity; however, no statistical significance could be found between Everolimus and mock curves. Cells were treated with different concentrations of Everolimus or Triton at 24 h. Rising concentrations led to a slightly lower gradient of the curve, but even with 100 nM, only antiproliferative effects but no cytotoxicity could be detected. Reproduced from [1].

2. GLV-1h68 mediated virotherapy of NEN

The first OV tested was the VACV vector GLV-1h68. Both the effects of GLV-1h68 alone (section 2.1) and in combination with Everolimus (section 2.2) on all of the six NET/NEC cell lines were assessed. For viral infection of cell lines, tumor cells were incubated one hour with an infection medium containing viral particles. Afterwards, the inoculum was removed and only virions which already had already infected the tumor cells could subsequently replicate and kill tumor cells.

2.1. GLV-1h68 monotherapy is effective in NET/NEC cell lines

To study the effects of GLV-1h68 treatment in detail, SRB viability assays were conducted to assess cytotoxicity and the kinetics of cytotoxic effects were investigated using real-time cell monitoring (Fig. 13 and 14). Further, viral titers were determined sequentially to create viral growth curves (Fig. 15) and the expression of viral GFP transgene was proved by fluorescence microscopy (Fig. 15-16).

2.1.1. GLV-1h68 reduces cell viability dose dependently

SRB viability assays of GLV-1h68 infected NET/NEC cells were carried out using MOIs of 0.001, 0.01, 0.1, 0.5 and 1. For the most sensitive BON-1 cells, adjusted MOIs of 0.01, 0.025, 0.05, 0.1 and 1 (Fig. 13 C) were used. The 60 % threshold for SRB viability assays was applied again.

"Three categories to classify cellular response to GLV-1h68 virotherapy were introduced: (I) highly permissive cell lines, meeting the 60 % threshold with MOI 0.1 or less after 96 h; (II) permissive cell lines requiring MOI 0.5 to meet the threshold at 96 hpi, and (III) resistant cell lines which required more than MOI 0.5 to meet the threshold at 96 hpi." **- [2]**

In summary, all NET/NEC cell lines were susceptible to viral infection with GLV-1h68. The cytotoxicity of GLV-1h68 was found to be strictly time and dose dependent. Higher MOIs always led to lower remnant tumor cell masses, and longer infection periods with the same concentration also always resulted in lower remnant tumor cell counts.

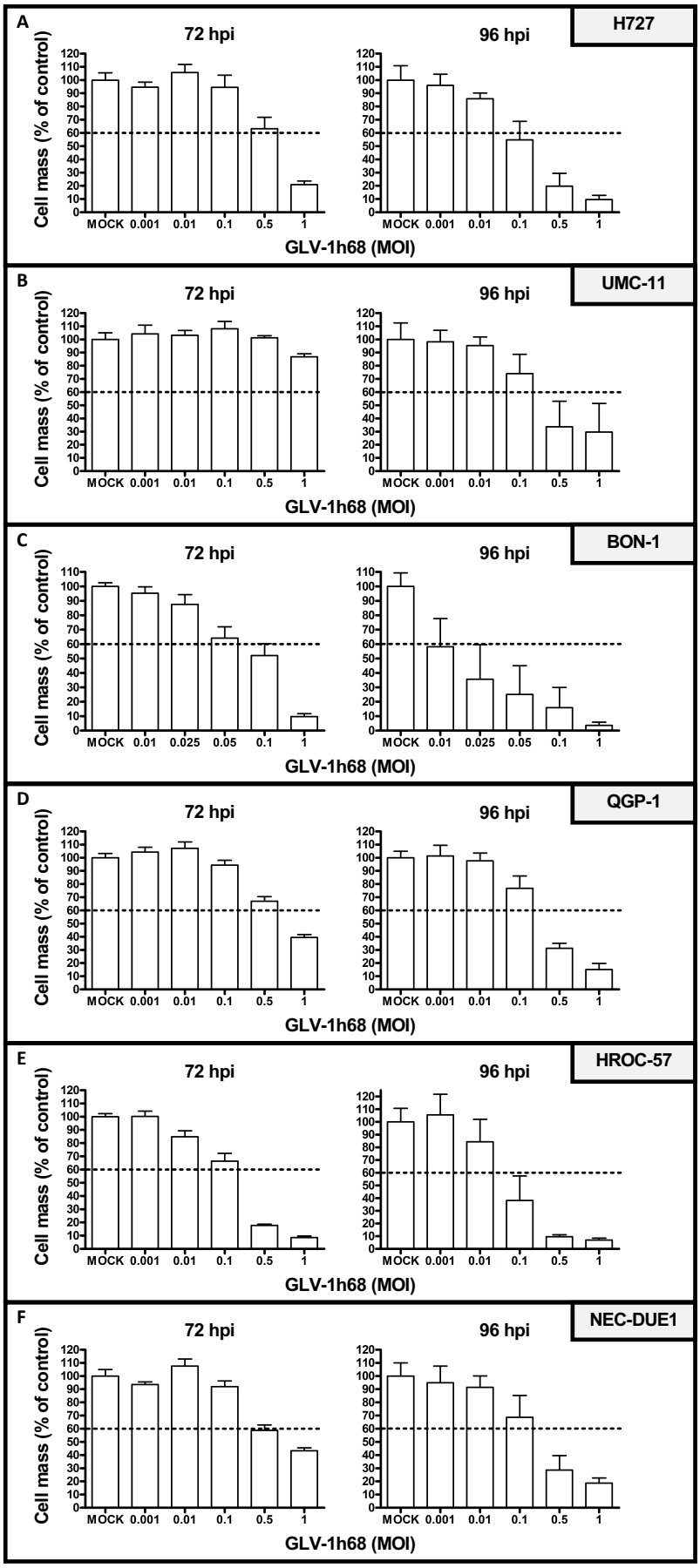

Figure 13: SRB viability assay with GLV-1h68 infected NET/NEC cell lines. Analysis performed at 72 hpi and at 96 hpi; two independent experiments (four for 96 hpi, six for 96 hpi UMC-11 cells) were carried out in quadruplicates; bars show mean and SD. All cell lines were found to be susceptible to GLV-1h68 mediated oncolysis. "*H727, BON-1 and HROC-57 cells were found to be highly permissive; UMC-11, QGP-1, and NEC-DUE1 cells were classified as permissive. BON-1 cells exhibited a quite strong response, requiring only MOI 0.01 to reach the threshold of 60% remaining tumor cells.*" Partially reprinted from [2].

Three cell lines could be classified as highly permissive to GLV-1h68. H727, BON-1 and HROC-57 cells only required MOI 0.1 to meet the threshold after 96 h (Fig. 13 A, C and E). Higher MOIs resulted in further reduction of tumor cell count, achieving a complete reduction of tumor cells in all three cell lines.

UMC-11, QGP-1 and NEC-DUE1 cells reached the threshold only with MOI 0.5 after 96 h, classifying them as permissive (Fig. 13 A, D and F). However, no complete reduction of tumor cell count could be identified in the three permissive cell lines. No cell line was classified as resistant.

Taken together, all cell lines met the 60 % threshold using the highest MOI, suggesting a broad antitumor activity of GLV-1h68. In three out of six cell lines, a complete reduction of tumor cell mass could be achieved. In contrast, a complete reduction of tumor cell count was not observed with Everolimus treatment under any condition (Fig. 11). Three cell lines were classified as highly permissive, among them one cell line from each anatomical origin (lung NET, pNET, NEC). Three cell lines were classified permissive, whereas no cell line met the criteria for resistance.

The extremely low tumor cell counts resulting after infection with high MOIs indicated cytotoxic effects of GLV-1h68, but real-time cell monitoring had to be carried out for demonstration of such.

2.1.2. GLV-1h68 exhibits cytotoxic effects

The lung NET cell line H727 was employed for real-time cell monitoring over 120 h, viral infection, mock or Triton treatment was conducted at 24 h after seeding of cells. H727 cells were chosen because of their highly permissive response in SRB viability assay. For infection, MOIs which resulted in remaining tumor cell counts of around 50 % in the previous experiment were picked (MOI 0.1 and 0.25).

Mock treatment resulted in a constant cell proliferation (Fig. 14 A, black line), and Triton lysis control led to an immediate cell death (Fig. 14 A, green line). Virus infected cells grew similar to mock treated cells until their viability curves reached their peaks. The curve for infection with MOI 0.25 peaked at 52 h (Fig. 14 A, grey line) and the curve for infection with MOI 0.1 at 60 h (Fig. 14 A, red line), respectively. Afterwards, cell index

decreased constantly, being lower with the higher virus dose applied (Fig. 14 A, grey line). After 120 h, MOI 0.25 resulted in a cell index of 0.5, whereas MOI 0.1 resulted in a cell index of 1.

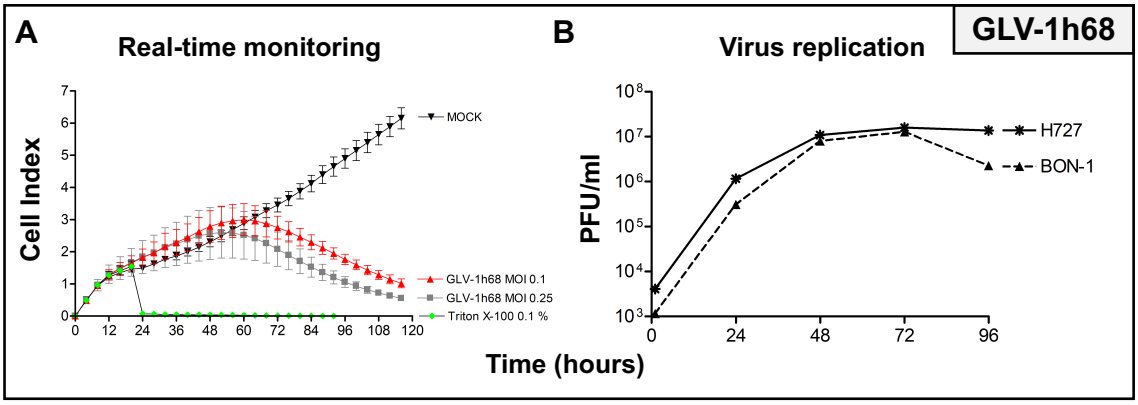

Figure 14: Replication and cytotoxicity kinetics of GLV-1h68. (A) H727 cells were employed for real-time cell monitoring and infected with MOIs 0.1 and 0.25. The experiment was carried out in quadruplicates, mean and SD are shown. Dose dependent tumor cell cytotoxicity of GLV-1h68 could be proved. Reprinted from [2]. **(B)** For virus growth curves, H727 cells were infected with MOI 0.25 and BON-1 cells with MOI 0.025. Two independent runs were carried out and samples were analyzed every 24 h in duplicates, one representative result is shown. Efficient viral replication was found in both cell lines reaching virus titers higher than 10^7 PFU/ml. Reproduced from [2]

This experiment confirmed dose and time dependency discovered with SRB viability assays. According to the well-known and fast replication characteristics of this VACV, a decline in cell viability starting between 28 and 36 hpi could be observed. In the end, the higher MOI reduced cell viability more efficiently, confirming the results from SRB viability assays. In summary, the cytotoxic effect of GLV-1h68 presumed in the SRB assays could be confirmed.

2.1.3. Efficient virus replication of GLV-1h68

In order to prove viral replication and the production of viral progeny, viral growth curves were generated by determination of the viral titer every 24 h. The highly permissive pNET cell line BON-1 and the lung NET cell line H727 were chosen for this experiment. For infection, MOI 0.25 was employed for H727 cells and MOI 0.025 for BON-1 cells, because these MOIs caused a tumor cell reduction of approximately 50 % in SRB viability assays. All free viral particles were removed after infection. Consequently, only viral particles which had already entered the tumor cells as well as viral progeny were detected.

In both cell lines, a strong virus replication reaching virus titers higher than 10^7 PFU/ml could be observed (Fig. 14 B). Values at 1 h correlate with the MOI used for viral infection and are consequently higher in H727 cells, because no viral progeny could already be produced at this early point of time. Virus titers were peaking at 72 hpi with $1.6*10^7$ PFU/ml for H727 cells and with $1.28*10^7$ PFU/ml for BON-1 cells. A decrease in virus titer could be observed between 72 and 96 h in particular with highly permissive BON-1 cells (Fig. 14 B, dotted line). This was most likely due to an oncolytic reduction of host cells for viral replication. This phenomenon could also be observed with H727 cells, but to a lesser degree as they were not as permissive as BON-1 cells to GLV-1h68 infection.

Taken together, strong viral replication could be observed, being a prerequisite for an efficient viral spread throughout the tumor.

2.1.4. Intense expression of viral GFP transgene

To confirm viral gene expression, the GFP transgene of GLV-1h68 was visualized employing fluorescence microscopy. Pictures were taken 72 hpi (Fig. 15) and 96 hpi (Fig. 16) before SRB viability assays were conducted with the same cells. Photos were taken first using a phase contrast and then a fluorescence filter, both pictures were digitally overlaid.

GFP was found in all NET/NEC cell lines infected with higher MOIs. With the lowest MOIs, only the highly permissive BON-1 and HROC-57 showed GFP expression 96 hpi (Fig. 16). No mock infected samples displayed any GFP signal. As proved by the SRB assays, cell layer density decreased with increasing MOIs in all cell lines.

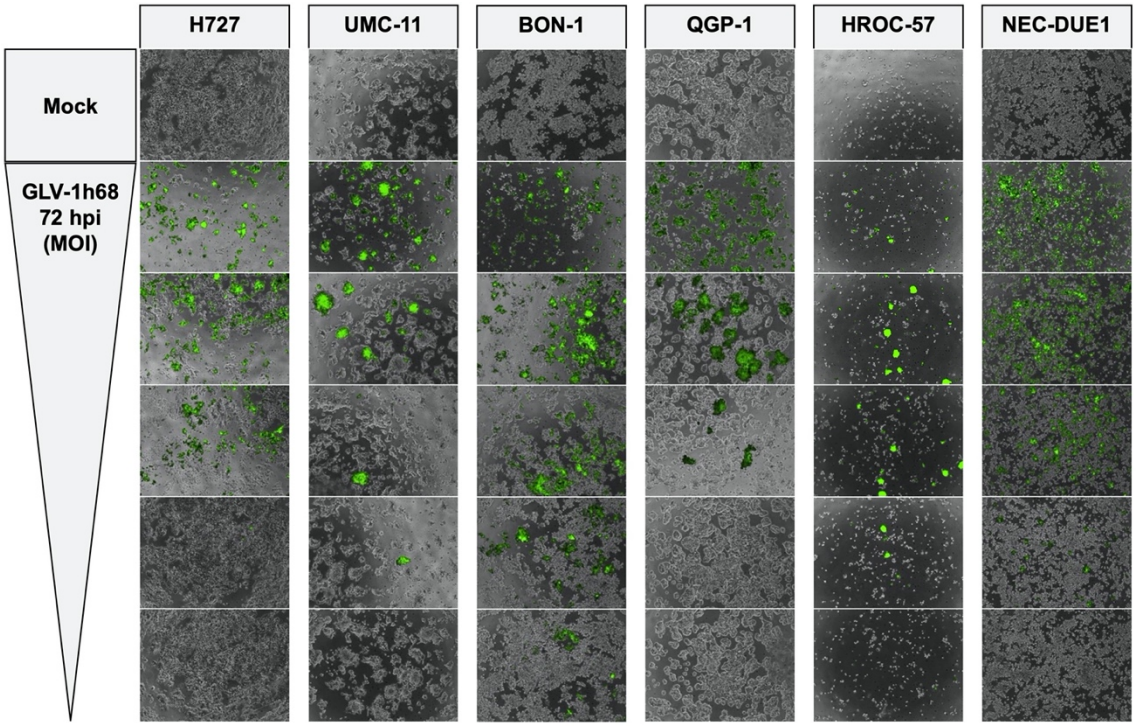

Figure 15: Microscopy of the NET/NEC cells infected with GLV-1h68 72 hpi. "*Fluorescence microscopy of the NET/NEC panel infected with oncolytic vaccinia virus vector GLV-1h68. Phase contrast and fluorescence pictures were taken at 72 hpi and overlaid. From top to bottom, MOIs decrease and match the MOIs used in the respective SRB viability assays (Fig. 13). When using higher MOIs, infected cells displayed higher transgene expression. […] No viral transgene expression could be observed in mock samples."* Cell layer density decreases with higher MOIs employed. Reprinted from [2].

At 96 hpi, similar effects to the viral growth curves (Fig. 14 B) could be visualized. When using high MOIs in highly permissive cell lines such as BON-1, transgene expression decreased 96 hpi due to a lower number of host cells being accessible for virus replication (Fig. 16).

In summary, microscopy proved sufficient viral infection and subsequent take-over of the cellular protein synthesis, resulting in viral transgene expression.

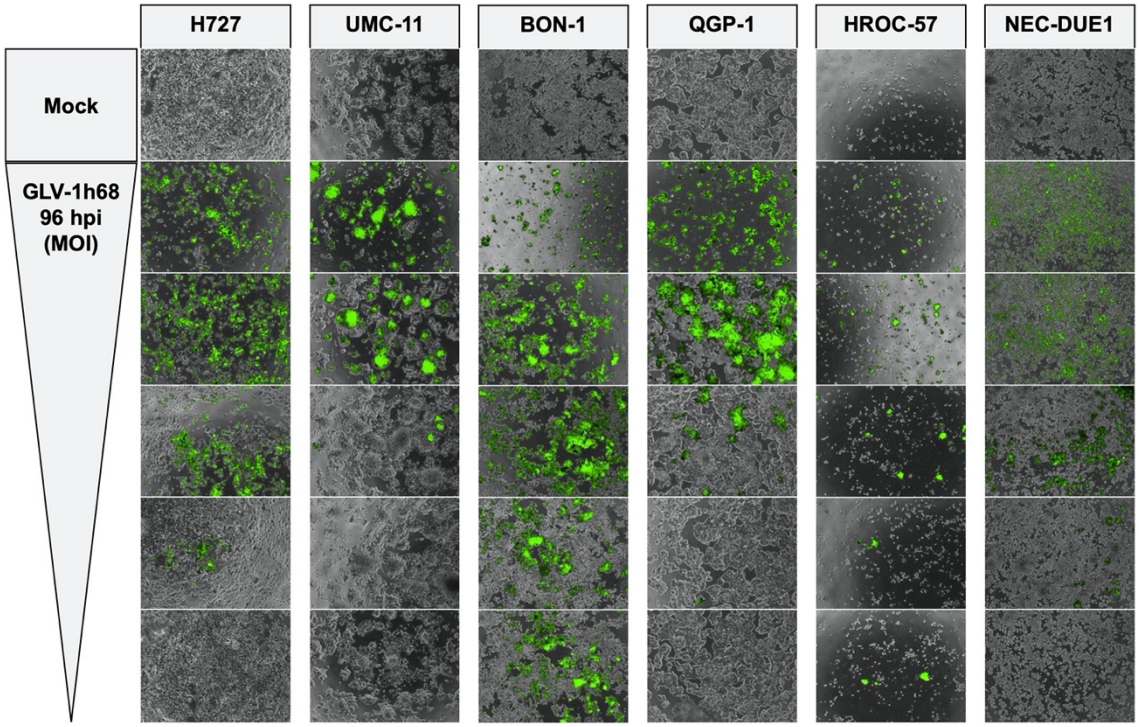

Figure 16: Microscopy of the NET/NEC cells infected with GLV-1h68 96 hpi. "*Phase contrast and fluorescence pictures were taken at 96 hpi and overlaid. […] In BON-1, HROC-57, and QGP-1 cells, being highly permissive or permissive to GLV-1h68 mediated oncolysis, tumor cell killing already had been accomplished at 96 hpi resulting in lower GFP signals using high MOIs*." Reprinted from [2].

2.2. Combinatorial therapy with GLV-1h68 and Everolimus

Next, Everolimus and GLV-1h68 were combined to figure out whether there are any additional or synergistic effects of both. To this end, SRB viability assays and real-time cell monitoring were conducted and viral growth curves were generated.

2.2.1. Combinatorial therapy has limited effects on cell viability

For SRB viability assays, the lung NET cell lines H727 and the NEC cell line NEC-DUE1 were used. The Everolimus concentrations determined earlier (Fig. 11) were 1 nM for H727 cells and 0.25 nM for NEC-DUE1 cells. Further, MOIs resulting in tumor cell reductions around 50 % (MOI 0.1 and 0.25 for H727; MOI 0.25 and 0.5 for NEC-DUE1) were employed and combined with Everolimus.

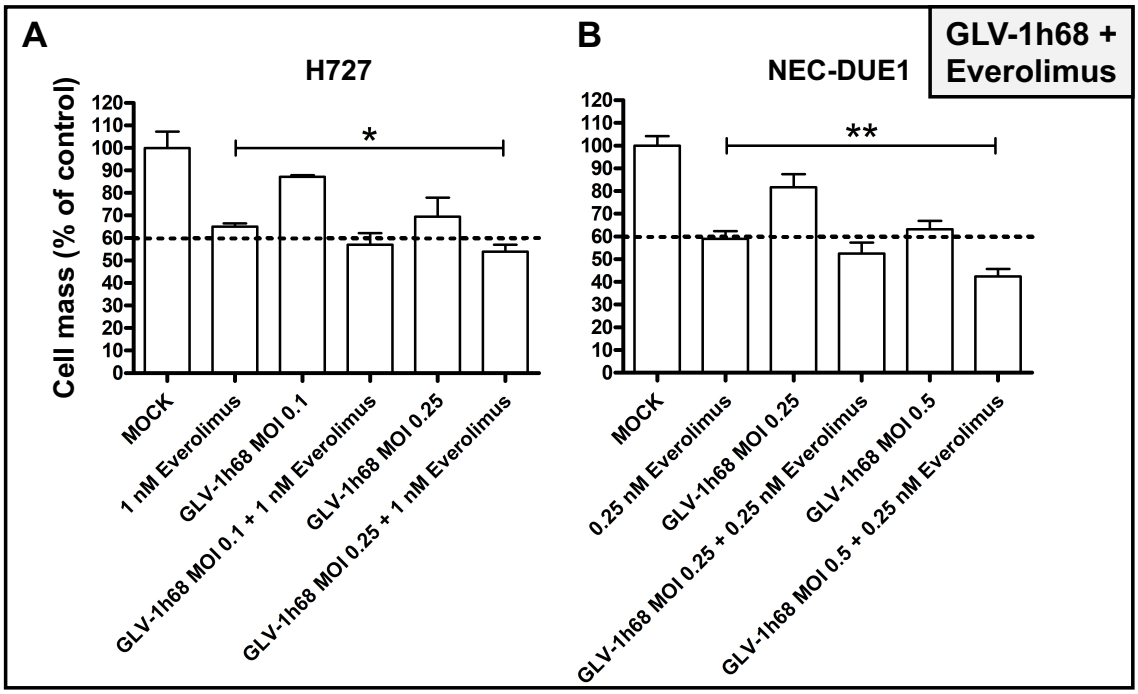

Figure 17: SRB viability assay of NET/NEC cell lines cotreated with GLV-1h68 and Everolimus. "*H727 cells originating from a lung NET and the NEC-derived NEC-DUE1 cell line were employed and analysis was performed at 96 hpi. Experiments were carried out in quadruplicates; bars show mean and SD. With both cell lines, combinatorial treatment with Everolimus was found to be slightly more effective than single agent treatment with either Everolimus or GLV-1h68 alone. In both cell lines and for both MOIs tested, the addition of Everolimus to GLV-1h68 further reduced the remaining tumor cell count. * = $p < 0.01$; ** = $p < 0.001$."* Reprinted from [2].

Monotherapy results were similar to the results described above (sections 1.1 and 2.1.1). For H727 cells, combinatorial therapy resulted in little increase of tumor cell killing. The addition of OV to Everolimus further decreased the remaining tumor cell count by 8 % (MOI 0.1) and 11 % (MOI 0.25) (Fig. 17 A). In NEC-DUE1 cells, the effect was slightly stronger with a decrease of 6 % (MOI 0.25) and 17 % (MOI 0.5) (Fig. 17 B). With both cell lines tested, the addition of the higher MOI to sole Everolimus was found to be statistically significant.

Taken together, the effect on cytotoxicity of the combinatorial treatment with Everolimus on cytotoxicity was neither synergistic nor additive and only small. Nevertheless, the combination was found to be slightly but significantly more efficient than monotherapy in either setting. Both agents did not seem to affect each other in a negative way. Again, GLV-1h68 appeared to be little more efficient in NEC cells.

2.2.2. Real-time cell monitoring shows differences between combination and monotherapy

To assess the development of H727 NET cell viability over time, real-time cell monitoring was carried out with the combinatorial therapy. H727 cells were infected with MOI 0.1 and 100 nM Everolimus were employed, as lower concentrations had only shown minimal effects in cell-monitoring of Everolimus monotherapy.

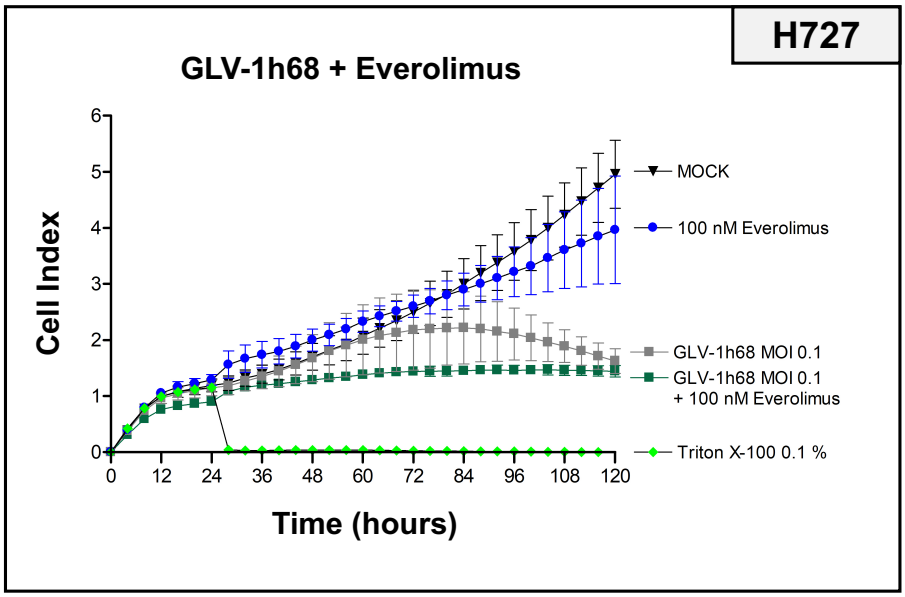

Figure 18: Real-time cell monitoring of H727 cotreated with GLV-1h68 and Everolimus. Lung NET cells H727 were employed for real time cell monitoring. The experiment was carried out in quadruplicates, mean and SD are shown. MOI 0.1 alone showed similar results to the previous experiments (Fig. 14 A). Combinatorial treatment with both GLV-1h68 and a high concentration of Everolimus kept cellular impedance low during the whole time, suggesting the most effective treatment option. However, after 120 h, single agent treatment with GLV-1h68 almost reached the same Cell Index as the combinatorial treatment option.

The results of either monotherapy were similar to those described above (sections 1.2 and 2.1.2). Combinatorial therapy kept the cell viability low over the whole period of time (Fig. 18, dark green line), only reaching a peak cell index of approx. 1.5 compared to a peak of 2.2 with GLV-1h68 monotherapy (Fig. 18, grey line). But also, combinatorial treatment did not exhibit a relevant decrease in cell index, resulting in a cell index of approx. 1.4 96 hpi, comparing to 1.6 with GLV-1h68 alone 96 hpi. This slight difference was also detected in SRB assays at 96 hpi (Fig. 17 A), whereas the difference during the time period of treatment could not be detected in SRB assays because they were only carried out as late as 72 and 96 hpi.

The small size of the combinatorial effect raised the question whether or not Everolimus restricts viral replication in any way.

2.2.3. Everolimus does not restrict GLV-1h68 replication

To evaluate the effects of Everolimus on GLV-1h68 replication, viral growth curves were created in the presence of Everolimus. Experiments were carried out as for the virus quantification with GLV-1h68 monotherapy, and the same cell lines (H727 and BON-1) and MOIs (0.25 for H727 and 0.025 for BON-1) were used to compare results to virus replication with GLV-1h68 alone. 1 nM Everolimus was added at 1 hpi.

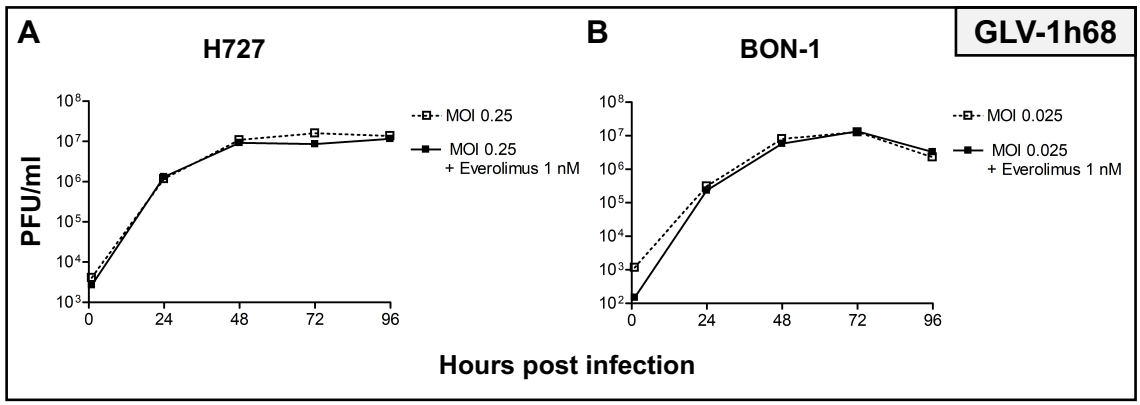

Figure 19: Virus growth curves of GLV-1h68 and Everolimus cotreated NET cells. "*Virus titer growth curves were performed with H727 and BON-1 tumor cells under the same conditions in presence of Everolimus (added at 1 hpi). Plaque forming units (PFU) were determined every 24 h; samples were analyzed in duplicates; experiments were performed twice; one representative result is shown. Previous results from monotherapy (Fig. 14 B) are shown (dotted lines). Interestingly, Everolimus did not alter viral replication in any significant way (solid lines)."* Reproduced from [2].

With both cell lines, virus titers were not significantly changed by the addition of Everolimus (Fig. 19, solid lines). This supported the assumption made in section 2.2.1, that both agents do not interfere in a negative way.

3. T-VEC virotherapy of NEN

In accordance with the experiments done with GLV-1h68, the oncolytic HSV T-VEC was tested in the same way. T-VEC monotherapy is outlined in section 3.1 and its combination with Everolimus in section 3.2. Further, T-VEC was combined with GCV (section 3.3).

3.1. Single agent T-VEC treatment is highly effective in NET/NEC cells

SRB viability assays were performed to assess cytotoxicity (Fig. 20). Real-time cell monitoring and viral growth curves were carried out (Fig. 21). Infected cell layers were visualized using phase contrast microscopy (Fig. 23 and 24). No fluorescence microscopy was done because T-VEC holds no fluorescent marker transgene, instead, a GM-CSF ELISA of the supernatant of infected cell was conducted to prove viral transgene expression (Fig. 22).

3.1.1. T-VEC kills NET/NEC cells with low MOIs

SRB viability assays were carried out and the panel of NET/NEC cell lines was infected with T-VEC using the MOIs 0.0001, 0.0005, 0.001, 0.005 and 0.01. After the first preliminary experiments, all MOIs were adjusted to be log 1 higher for QGP-1 and NEC-DUE1 cells, being relatively resistant to T-VEC mediated oncolysis (Fig. 20).

The three response categories highly permissive, permissive and resistant were defined different to GLV-1h68, as lower MOIs were used with T-VEC. Cell lines displaying less than 60 % remaining tumor cells with MOI 0.01 at 96 hpi were classified (I) highly permissive, cell lines requiring MOI 0.1 to meet the threshold at 96 hpi were classified (II) permissive, and cell lines not reaching the threshold with this MOI were classified (III) resistant.

Again, a dose and time dependent response to virotherapy could be detected in all infected NET/NEC cell lines. Higher MOIs and longer infection time almost always resulted in lower remaining tumor cell count. Four cell lines were classified as highly permissive, namely H727, UMC-11, BON-1 and HROC-57 (Fig. 20). QGP-1 cells were classified as permissive and NEC-DUE1 cells were classified as resistant, not reaching the threshold at all.

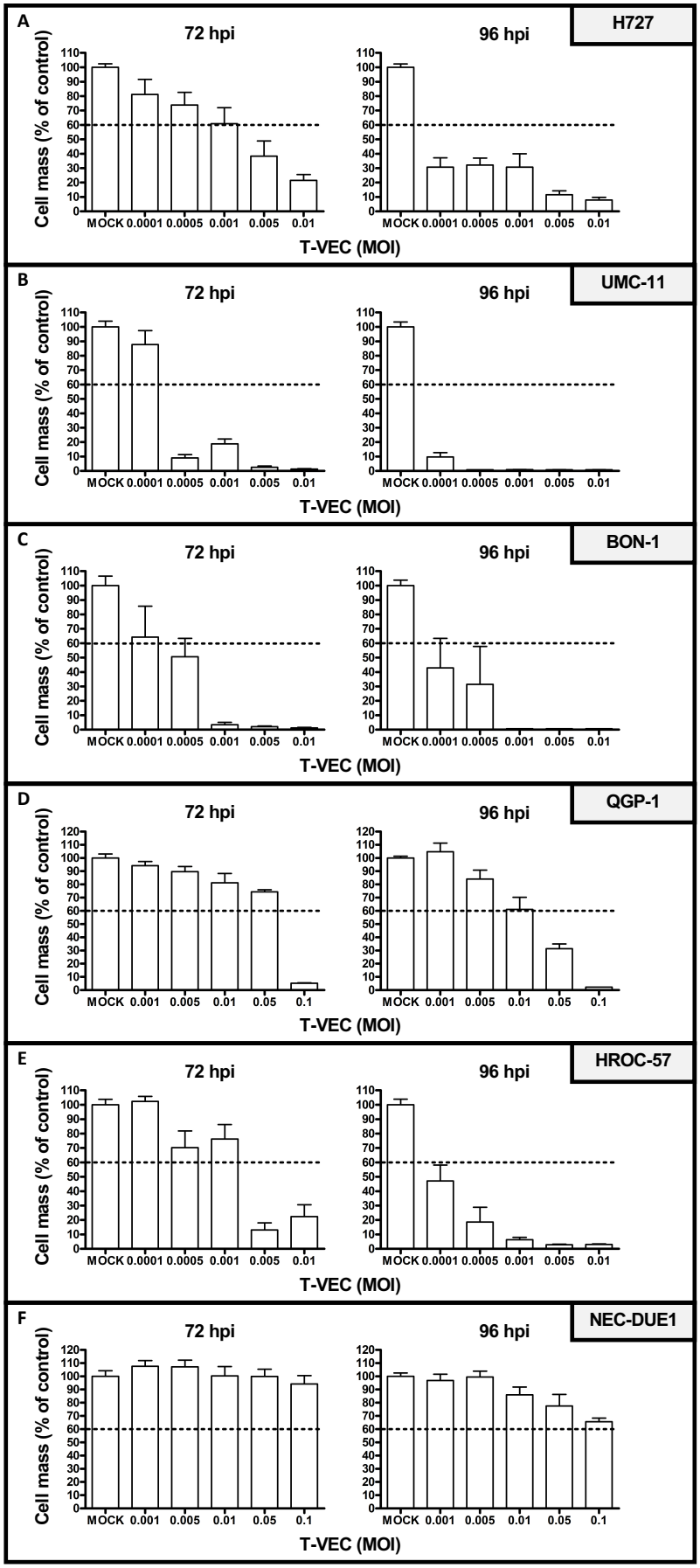

Figure 20: SRB viability assay with T-VEC infected NET/NEC cell lines. **"***Analysis performed at 72 and 96 hpi; mean and SD of 2 independent experiments carried out in quadruplicates are shown. T-VEC showed a highly effective cytoreduction already at extremely low MOIs; only in NEC-DUE1 cells, a relevant oncolytic effect could be observed only at 96 hpi when using much higher MOIs (up to 0.1)".* Reprinted from [1].

T-VEC achieved a complete tumor cell reduction in three out of six cell lines 72 hpi and in five out six cell lines 96 hpi, of note with extremely low MOIs compared to GLV-1h68. Four cell lines were ranked highly permissive, including both lung NET cell lines. With QGP-1 cells, a complete tumor cell reduction could be reached using MOI 0.1 (Fig. 20 D), classifying them as permissive. Only one cell line was classified as resistant. NEC-DUE1 cells possessed the highest degree of resistance, not even reaching the 60 % threshold with the highest MOI employed (Fig. 20 F).

This experiment underlined a high oncolytic potency of T-VEC in a wide spectrum of NET/NEC cell lines. Both lung NET cell lines were classified highly permissive. Low remaining tumor cell counts were reached with outstandingly low MOIs.

3.1.2. T-VEC exhibits strong cytotoxicity

For real-time cell monitoring, cellular impedance was measured continuously to reveal the development of tumor cell viability over time with after T-VEC infection. Therefore, H727 lung NET cells were infected with MOIs 0.0001 and 0.001 at the time point 24 h after seeding.

Again, a dose and time dependent effect of T-VEC could be observed (Fig. 21 A). Also, cytoreductive effects could be proved. After infection, viability curves of T-VEC infected cells grew similar to the mock curve until they reached their peaks, whereas the mock curve grew continuously until the end of the experiment. After 48 h, the curve of infection with MOI 0.001 reached its peak followed by a quick decrease of cell viability (Fig. 21 A, grey line). The MOI 0.0001 viability curve reached its peak as late as 64 h, again followed by a significant loss of cell viability (Fig. 21 A, red line). After 120 h, the MOI 0.001 resulted in a lower cell index of approx. 0.4, were MOI 0.0001 achieved cell index 0.8.

Comparing the results to the same experiment carried out with GLV-1h68, the first effects of T-VEC could be observed a little later after viral infection; however, this could be attributed to higher MOIs used with GLV-1h68. The higher negative gradient of the T-VEC curves after their peak indicated a faster loss of cell viability with T-VEC and therefore a stronger cytotoxic effect. Finally, the cell indices reached after 120 h were almost equal with both OVs.

3.1.3. High T-VEC virus titers in NET/NEC cells

Employing one cell line from each anatomical origin, viral titers were measured sequentially to confirm efficient virus replication. Viral titers were determined every 24 h, and MOIs resulting in approx. 50 % remaining tumor cells 96 hpi in SRB assays were chosen. For QGP-1 and NEC-DUE1 cells, MOI 0.01 was picked. H727 were infected with MOI 0.0001, the lowest MOI employed in the previous SRB assays.

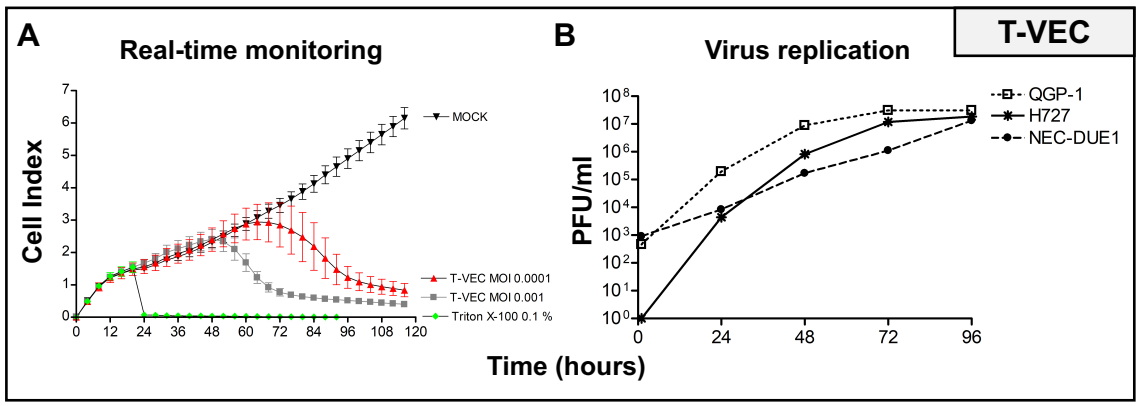

Figure 21: Replication and cytotoxicity kinetics of T-VEC. (A) H727 cells were employed for real-time cell monitoring and infected with MOIs 0.0001 and 0.001. The experiment was carried out in quadruplicates, mean and SD are shown. T-VEC infection resulted in a dose dependent reduction of cellular impedance, indicating cytoreductive effects. Reprinted from [1]. **(B)** For virus growth curves, H727 were infected with MOI 0.0001, QGP-1 and NEC-DUE1 cells with MOI 0.01. Two independent runs were carried out and samples were analyzed every 24 h in duplicates, one representative result is shown. Efficient viral replication was found in all three cell lines reaching virus titers higher than 10^7 PFU/ml. Reproduced from [1].

Resulting virus titers at 1 h correlated with the MOI applied for infection and were not connected to viral replication.

"Constantly growing virus titers were detected in all 3 cell lines and titers over 10^7 PFU/mL were reached (Fig. 21 B). The stagnation in virus titer growth after 72 h was explained by the efficient oncolytic depletion of tumor cells, resulting in significantly lower numbers of host cells being available for further rounds of infection and viral replication. This effect could be observed especially in H727 and QGP-1 cells (Fig.21 B) since both cell lines were found to be susceptible to oncolytic cell killing.

In NEC-DUE1 cells, slower but albeit still substantial replication kinetics of T-VEC were observed compared to the other cell lines, consistent with the results from the SRB

viability assay, where NEC-DUE1 were identified to be the most resistant cell line. Nevertheless, T-VEC produced high virus titers also in NEC-DUE1 cells, indicating slow but sufficient virus replication and therefore a relative resistance to oncolysis." **- [1]**

3.1.4. T-VEC encoded immunoactivating GM-CSF transgene is strongly expressed

In contrast to GLV-1h68, T-VEC holds no fluorescent transgene which could be detected microscopically. Hence, the amount of transgene protein was measured in the cell culture supernatant.

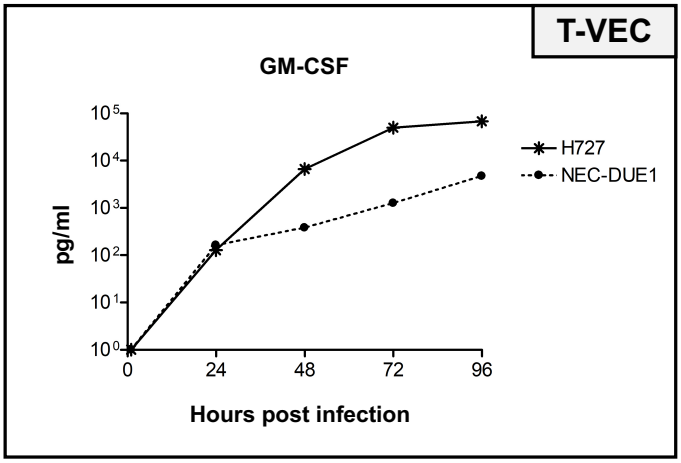

Figure 22: GM-CSF ELISA of supernatant of T-VEC infected NET/NEC cells. "*Expression of the T-VEC encoded GM-CSF cytokine gene could be detected with an ELISA first at 24 hpi, reaching its highest level at 96 hpi in both cell lines. Of note, GM-CSF concentration increased more slowly in NEC-DUE1 cells, this can be explained by the limited replication of T-VEC in this cell line."* Reprinted from [1].

"To prove expression of the T-VEC encoded GM-CSF transgene, an ELISA detecting human GM-CSF was employed. Two representative cell lines (H727 and NEC- DUE1) were first infected with T-VEC using MOI 0.0001 and MOI 0.1. Then supernatants were collected and analyzed every 24 h.

At 1 hpi, no GM-CSF protein could be detected at all (Fig. 22). However, at 24 hpi, a low GM-CSF concentration of 128 pg/mL became detectable in H727 cell line, whereas in NEC-DUE1 a slightly higher concentration of 163 pg/mL was measured. Then, GM-CSF concentrations were found to increase constantly over time in both cell lines, finally reaching their maxima of 68 ng/mL at 96 hpi in H727 cells and of 4.7 ng/mL in NEC-DUE1 cells. Taken together, strong transgene expression could be proved in particular in H727 cells, again indicating a highly significant infection and replication of T-VEC in H727 tumor cells. Lower transgene expression was found in NEC-DUE1 cells indicating a correlation between virus replication and transgene expression, as T-VEC replication was shown to be limited in NEC-DUE1 cells (Fig. 21 B)*."* - **[1]**

3.1.5. T-VEC thins out NET/NEC cell layers

Microscopic phase contrast images were taken shortly before conducting SRB viability assays with T-VEC infected NET/NEC cells 72 and 96 hpi (Fig. 23 and 24). Therefore, MOIs are similar to those in SRB assays.

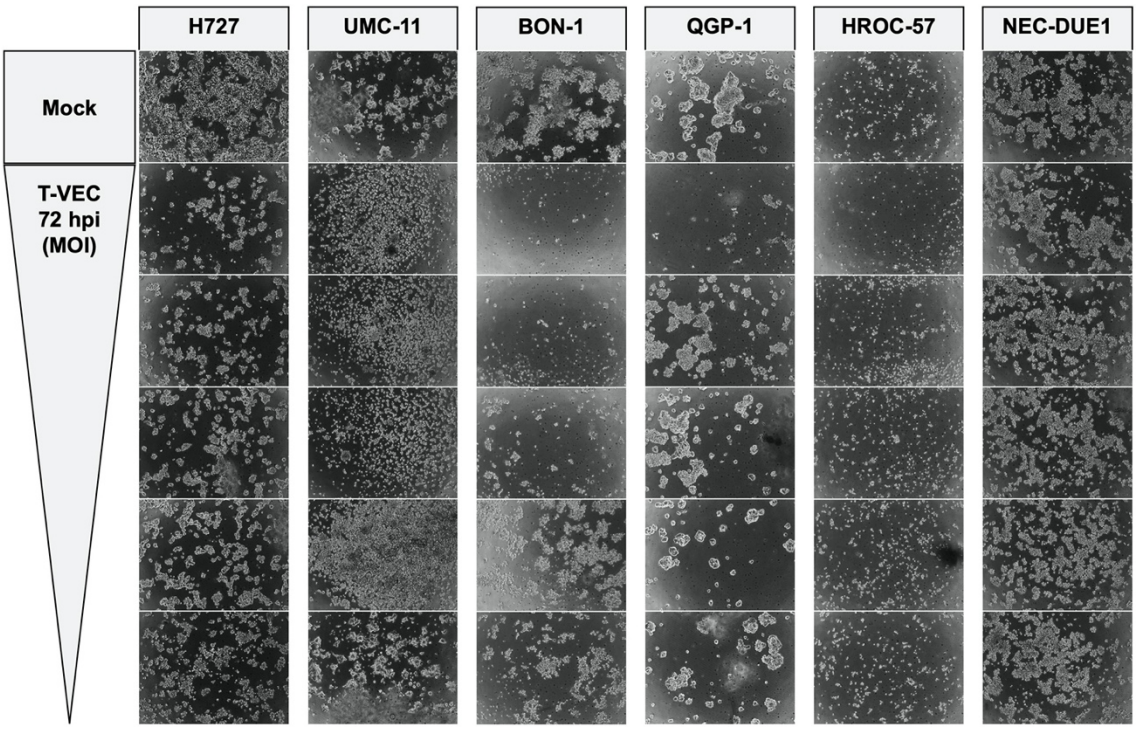

Figure 23: Microscopy of the NET/NEC cells infected with T-VEC 72 hpi. Representative microscopic pictures of the NET/NEC panel infected with recombinant oncolytic herpes simplex virus vector T-VEC. Phase contrast pictures (magnification x4) were taken at 72 hpi. From top to bottom, MOIs decrease and match the MOIs used in the respective SRB viability assays. Mock treated cells (pictures on top) show the highest confluence, whereas confluence of the cell layer decreases with higher MOIs. Many non-adherent/dead cells can be seen in the UMC-11 tumor cell line at high MOIs. Only little changes in confluence could be observed in NEC-DUE1 cells, which were shown to be relatively resistant to T-VEC in the SRB viability assay. Reprinted from [1].

Cell layer density was found to be highest with mock treatment. Consistent with the results from SRB assays, higher MOIs and longer infection period resulted in lower density of the cellular layer. Low impact of viral infection on the cell layer of NEC-DUE1 cells confirmed their resistance to T-VEC oncolysis. In cell lines infected with high MOIs, where a complete cytoreduction was detected with SRB assays, some cells were still detectable in microscopy. These cells were not adherent anymore and most likely to be

dead and therefore not detected in SRB assays (Fig. 23, UMC-11, BON-1 and QGP-1, highest MOI).

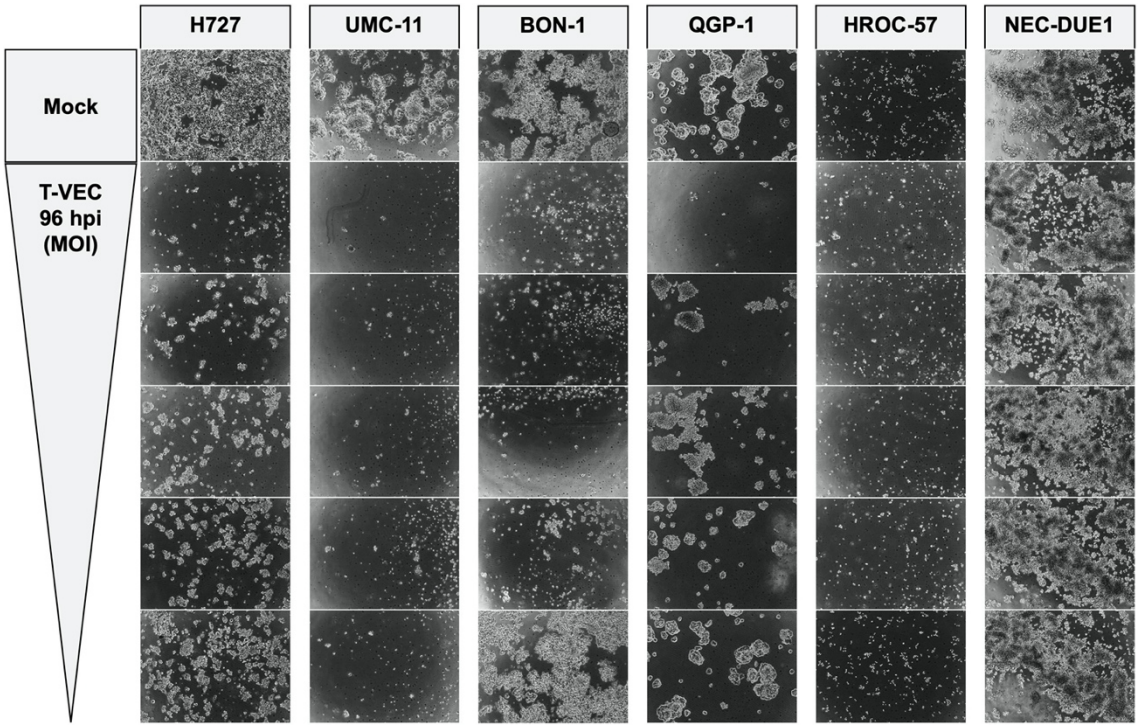

Figure 24: Microscopy of the NET/NEC cells infected with T-VEC 96 hpi. Representative phase contrast pictures (magnification x4) of the NET/NEC panel infected with T-VEC taken at 96 hpi. When comparing with the pictures taken at 72 hpi, confluence further decreased significantly; in UMC-11 cells, a total cytoreduction could be observed at all MOIs; only little effects on confluence were visible in NEC-DUE1 cells. Reprinted from [1].

3.2. Combination of T-VEC with Everolimus only shows minimal benefits

A combinatorial therapy using the virotherapeutic T-VEC and the mTOR inhibitor Everolimus was evaluated in this section. In this purpose, SRB assays employing the lung NET cell line H727 as well as the NEC cell line NEC-DUE1 were conducted to discover potential additional or synergistic cytotoxicity. Further, real-time cell monitoring was carried out and the impact of Everolimus on T-VEC replication in NET/NEC cells was studied.

3.2.1. Combinatorial therapy has hardly effects on cell viability

For SRB viability assays, H727 cells were infected with T-VEC at MOI 0.00005 and MOI 0.1 was used for NEC-DUE1 cells. Everolimus was employed in a concentration of 1 nM and 0.25 nM, respectively. The assay was carried out 96 hpi.

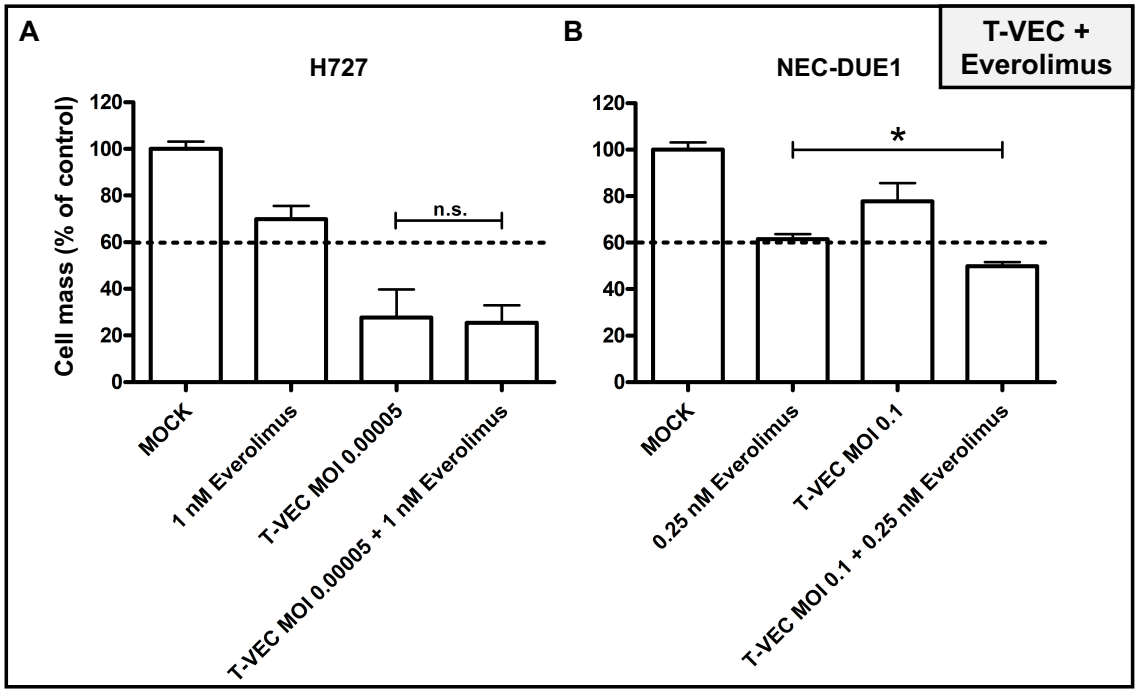

Figure 25: SRB viability assay of NET/NEC cell lines cotreated with T-VEC and Everolimus. Analysis performed at 96 hpi/hpt; experiments were carried out in quadruplicates; bars show mean and SD. H727 and NEC-DUE1 cells were treated with Everolimus, T-VEC and the combination of both. Although both agents exhibit significant effects in monotherapy, the combination therapy showed no relevant additive or synergistic effects. N. s. = not significant ($p > 0.05$); * = $p < 0.001$. Reprinted from [1].

Monotherapy results were similar to those described in the previous sections (1.1 and 3.1.1). The combination of both did not show any significant additive effect in H727 lung

NET cells. The reduction in tumor cell count was similar to the reduction with T-VEC alone (Fig. 25 A). With NEC-DUE1 cells, the combinatorial treatment resulted in approx. 50 % remaining tumor cells, whereas Everolimus or OV alone led to 60 % and 80 % remnant tumor cells, respectively (Fig 25 B). No statistical significance could be found with the combination in H727 cells, whereas the combination of T-VEC and Everolimus was significantly more efficient than Everolimus alone in NEC-DUE1 cells.

Again, the effect was not even additive and only visible in one of two cell lines. However, combinatorial therapy was not found to be worse than any monotherapy. The combination might only be beneficial in cell lines which are resistant to T-VEC virotherapy, like NEC-DUE1 cells.

3.2.2. Real-time cell monitoring shows slight advantages of combinatorial therapy

The combinatorial therapy was investigated using again H727 cells for real-time cell monitoring. They were infected with MOI 0.0001, which is the lowest MOI applicable in the 96-well plates necessary for this assay. Because the resulting tumor cell count was already shown to be very low with virotherapy using this MOI, Everolimus was added only in a concentration of 1 nM.

Like described above, 1 nM Everolimus alone did not lead to a significantly different viability curve than mock treatment (Fig 26 A, orange line). Cells infected with T-VEC at MOI 0.0001 displayed the same development of cell viability as outlined in section 3.1.2 (Fig. 26 A, red line). The combination of both did not relevantly alter the curve, running slightly but not significantly lower than the curve of OV alone (Fig. 26 A, blue line). The difference was only visible between 64 and 96 h, whereas both curves finally reached a cell index of 0.8 after 120 h. This is consistent with the result from previous SRB assays, where no difference in cytotoxicity could be detected 96 hpi (being 120 h in this experiment, Fig. 25 A).

3.2.3. Everolimus has no particular impact on T-VEC replication

To study whether Everolimus has a direct effect on virus replication, viral titers were determined sequentially. The cell lines for which viral growth curves were generated with

T-VEC monotherapy were used. H727 cells were infected with MOI 0.0001 and for QGP-1 and NEC-DUE1 cells, MOI 0.01 was used. 1 nM Everolimus was added 1 hpi.

The results from T-VEC monotherapy are shown to compare (Fig. 26 B-D, dotted lines). Everolimus did not have any relevant impact on virus replication in H727 and QGP-1 cells (Fig. 26 B and D, solid lines). In NEC-DUE1 cells, viral titers were found to be lower with Everolimus cotreatment (Fig 26 C, solid line). The difference could be explained by the sensitivity of NEC-DUE1 cells to sole Everolimus treatment and the resulting lower number of cells accessible for viral replication.

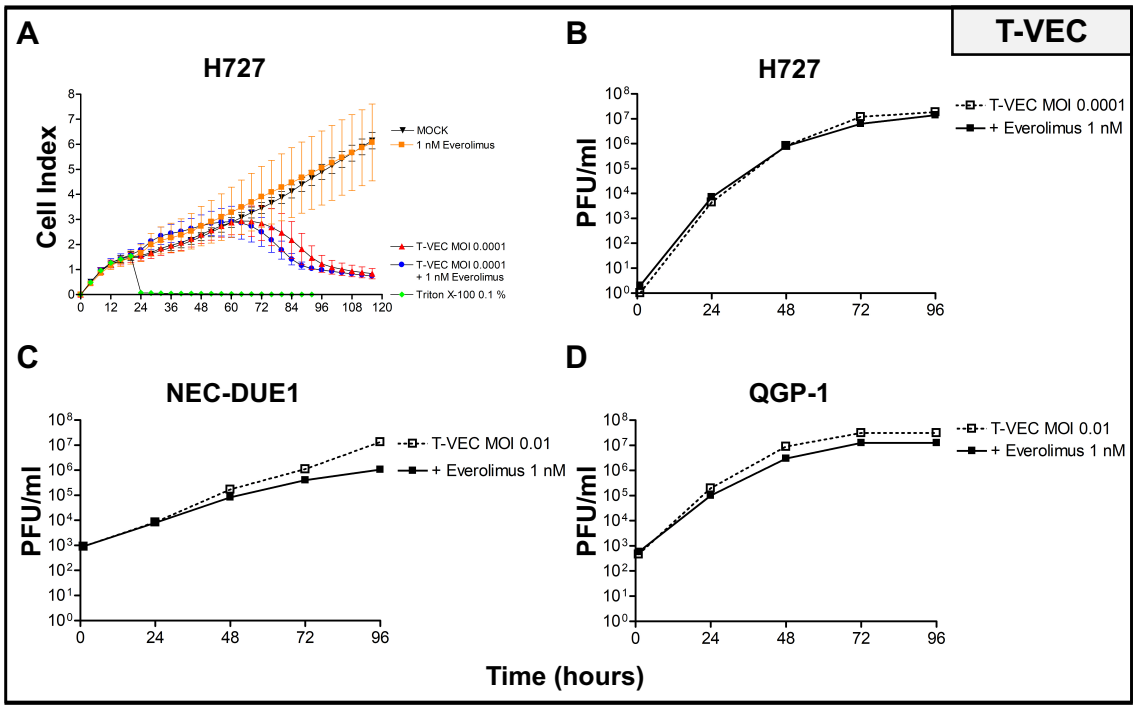

Figure 26: Replication and cytotoxicity kinetics of NET/NEC cell lines cotreated with T-VEC and Everolimus. (A) H727 cells were infected with MOI 0.0001 and cotreated with 1 nM Everolimus. The experiment was carried out in quadruplicates, mean and SD are shown. The combinatorial therapy resulted in a minimally lower cellular impedance than T-VEC alone, being only visible between 64 and 96 h (blue line). **(B-D)** One cell line from each anatomical origin was cotreated with T-VEC and 1 nM Everolimus. Two independent experiments were carried out and samples were analyzed every 24 h in duplicates, one representative result is shown. Everolimus did not affect viral replication in a relevant manner (solid lines). Reproduced from [1].

Taken together, no specific effect of Everolimus on T-VEC replication could be found. The efficacy of combinatorial therapy was definitely not worse than monotherapy with

each agent but could also not be proven to be superior to monotherapy in this experimental setting.

3.3. Addition of Ganciclovir to T-VEC infected NET/NEC cells

GCV is activated in T-VEC infected cells by the HSV TK. Theoretically, both a restrictive effect on virus replication and an augmenting effect on viral cytotoxicity were considered (Introduction, section 7). To study the nature of the combinatorial effect of GCV and T-VEC in NEC/NET cells, one cell line from each anatomical origin was picked. QGP-1 and NEC-DUE1 were chosen as they were not highly permissive to T-VEC treatment alone, requiring a possible combinatorial therapy. Cells were infected with T-VEC and cotreated with GCV at an early and a late point of viral infection (1 and 72 hpi). The effect was analyzed with SRB viability assays and virus quantification.

3.3.1. Ganciclovir prevents viral cell killing

The three cell lines were treated with GCV using the concentrations 1, 10 and 50 µM. GCV was either added directly after viral infection (1 hpi) or 72 hpi. For viral infection, T-VEC was used with MOI 0.0001 for H727 cells, MOI 0.05 for NEC-DUE1 cells and MOI 0.01 for QGP-1 cells. SRB viability assays were carried out 96 hpi.

"When GCV was added at 1 hpi without virus, no toxicity could be observed in H727 cells, whereas little toxicity was detected in QGP-1 and NEC-DUE1 cells with 50 µM GCV (Fig. 27 A–C, bars in black)*. When the cells were infected with T-VEC using the respective MOIs, the results from the SRB viability assay were confirmed when no GCV was added* (Fig. 27 A–C, bars in white and 0 µM GCV). *Using GCV and T-VEC together, a complete inhibition of viral cytotoxicity could be observed with 10 µM GCV in H727 cells and with only 1 µM GCV in QGP-1 and NEC-DUE1 cells (Fig.27 A–C, bars in white). With 50 µM GCV, the reduction of remnant tumor cell numbers was only due to the inherent cytotoxicity of GCV because presence/absence of T-VEC made no difference.*" **- [1]**

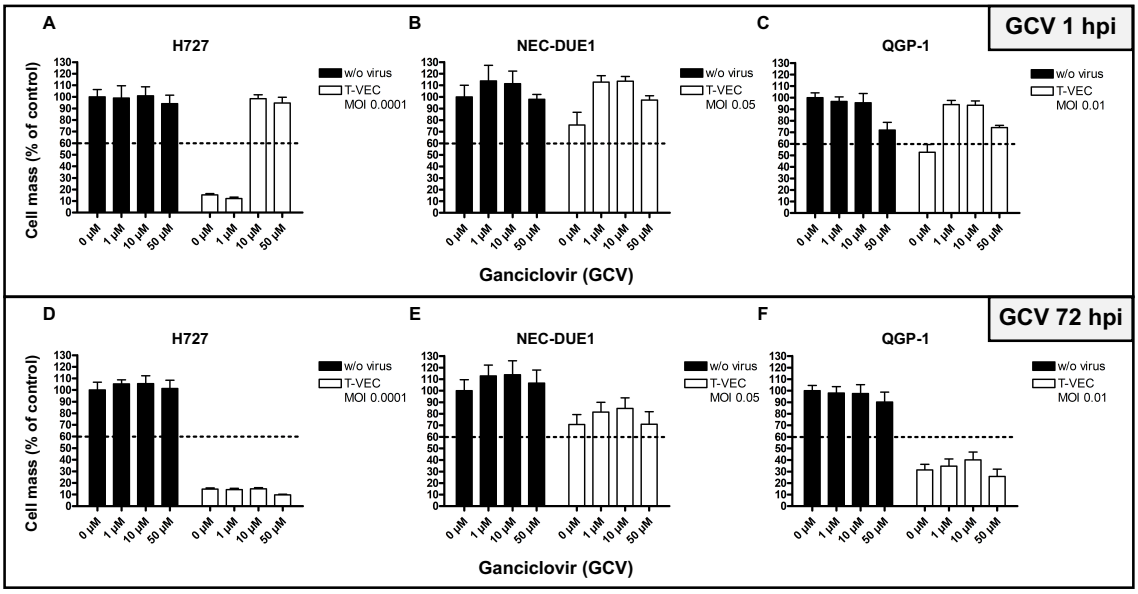

Figure 27: SRB viability assays of GCV treated and T-VEC infected NET/NEC cells. "*Assays were performed at 96 hpi; mean and SD of 3 independent experiments carried out in triplicates are shown.* ***(A-C)*** *When GCV was added at 1 hpi, 10 µM GCV were required to prevent T-VEC- mediated tumor cell killing in H727 cells (A); in contrast, 1 µM GCV was found to be sufficient in QGP-1 and NEC-DUE1 cells (B, C). Slight reductions in tumor cell counts obtained at 50 µM GCV are caused by the inherent cytotoxicity of GCV as they are similar in the T-VEC and mock treatment groups.* ***(D-F)*** *When GCV was added as late as at 72 hpi, T-VEC-mediated tumor cell killing could not be completely ablated any longer; tumor cells already had been oncolysed to a large degree, thereby preventing expression of relevant amounts of HSV-TK being required for GCV's virostatic effects. With 50 µM GCV added at 72 hpi, again a small increase in cytotoxicity could be observed."* Reprinted from [1].

With GCV addition 72 hpi, no relevant toxicity could be detected (Fig 27 D-F, black bars). Also, no augmenting effect on T-VEC cytotoxicity was found. Instead, 1 and 10 µM of GCV raised the remaining tumor cell count by 10-15 % in NEC-DUE1 and QGP-1 cells (Fig. 27 E and F, white bars). As H727 are highly permissive to T-VEC, tumor cell killing had already been accomplished when adding GCV 72 hpi, resulting in little effects (Fig. 27 D). With 50 µM GCV, again a reduction of tumor cell count could be observed with all three cell lines (Fig 27 D-F, white bars). If this effect is due to the inherent cytotoxicity of GCV or cytotoxicity of GCV activated by the HSV TK/GCV suicide gene system remains unclear. However, this augmenting effect with 50 µM GCV only canceled out the effects of smaller GCV concentrations and resulted in similar remaining tumor cell counts like T-VEC alone.

In summary, GCV demonstrated usability as virostatic drug in this setting, acting as a safety compound for T-VEC virotherapy. When added 1 hpi, it was able to completely abolish T-VEC cytotoxicity. Even when it was added 72 hpi, it still managed to increase the surviving cell population in two out of three cell lines.

Moreover, it could be shown that an enhancing effect on viral toxicity mediated via the TK/GCV suicide gene system does not play a relevant role in this setting.

3.3.2. Viral replication is limited by Ganciclovir

After the function of GCV as a virostatic agent was clarified, its limiting effect on T-VEC replication was investigated. In this purpose, the same three cell lines employed previously were infected with T-VEC and treated with GCV 1 hpi. For H727 cells, MOI 0.0001 was used, and MOI 0.01 was employed for NEC-DUE1 and QGP-1 cells. GCV was added in concentrations of 1 and 10 µM. For H727, 1 µM was left out because it had not shown any effects in SRB assay (Fig. 27, A). Viral titers were determined every 24 h.

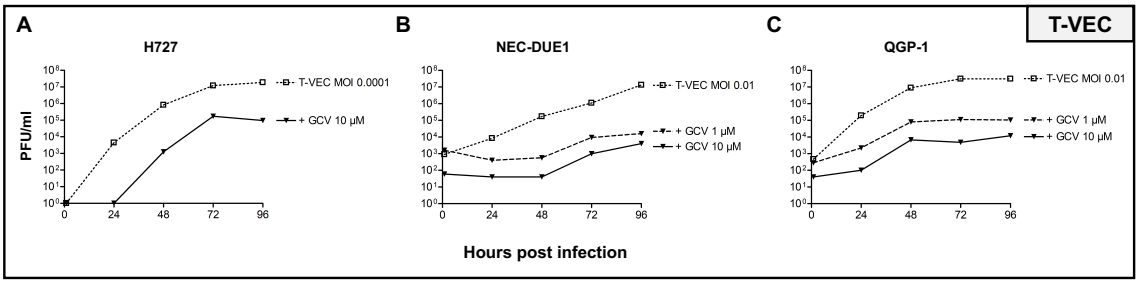

Figure 28: Virus growth curves of NET/NEC cell lines cotreated with T-VEC and GCV. Cells were infected with T-VEC and GCV concentrations of 1 and 10 µM were employed. Samples were analyzed every 24 h in duplicates. Results from T-VEC replication without GCV are shown to compare (dotted lines). GCV restricts viral replication in a dose dependent way. Reproduced from [1].

GCV was found to attenuate virus replication in a dose dependent manner in all three cell lines. 10 µM reduced virus titers by log 2 PFU/ml in H727 cells, by approximately log 4 PFU/ml in NEC-DUE1 and log 3 PFU/ml in QGP-1 cells (Fig. 28, solid lines). 1 µM resulted in approx. 1 log stage less reduction of virus titers. In H727 cells treated with 10 µM GCV, it took 48 h to detect the first viral progeny. As the virus titer still reached 10^5 PFU/ml in these highly susceptible cells (Fig. 28 A), GCV was found to be more effective in cells being more resistant to T-VEC oncolysis.

Although virus replication was detectable after GCV treatment, the virostatic was still able to prevent viral cell killing as proved by SRB viability assay (Fig. 27). These results highlight the effectivity of GCV as a safety compound in NEC/NET virotherapy with T-VEC.

4. Transmission electron microscopy of NET cells

The replication cycle of wildtype HSVs is well known. T-VEC carries genetic alterations which might alter virus egress or cellular response to virus infection. Also, replication of HSVs has never been visualized in pNET cells so far. In this section, QGP-1 cells were infected with T-VEC and fixed for TEM at different points of time of viral infection. TEM images are provided to retrace the replication cycle, viral egress and envelopment of T-VEC as well as changes in cellular morphology after T-VEC infection.

4.1. Native pancreatic NET cells

First, non-infected QGP-1 cells were processed for TEM 120 h after seeding to be compared to T-VEC infected cells (Fig. 29).

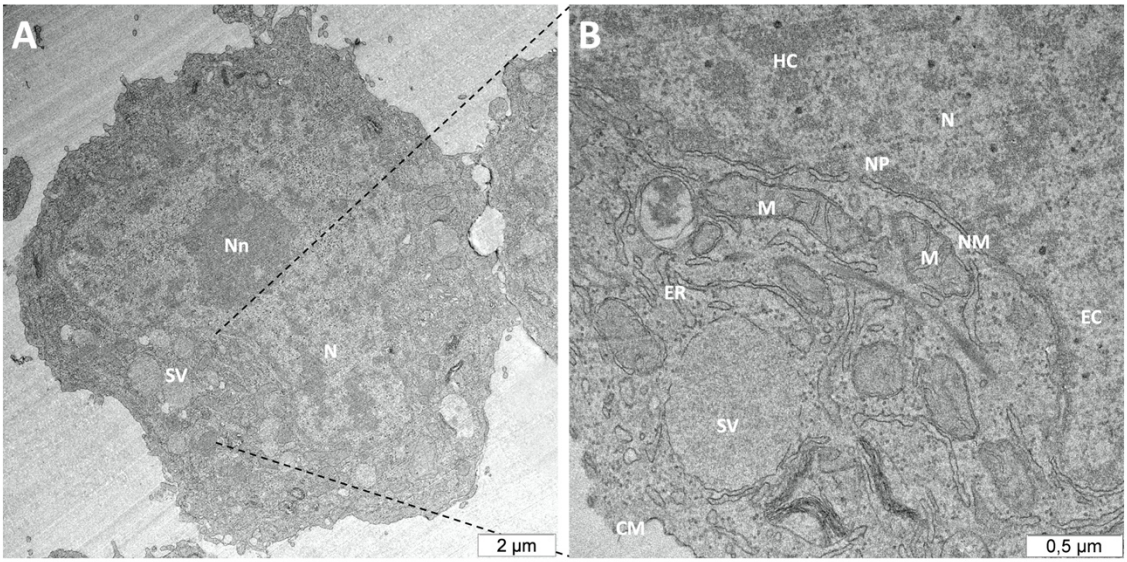

Figure 29: Native QGP-1 cells 120 h after seeding. (A) Pancreatic NET cell with approx. 12 µm in diameter*; "a big nucleus (N) with a large amount of euchromatin due to tumor cell characteristic synthesis and proliferative activity; electron dense nucleolus (Nn); secretory vesicles (SV) are visible as QGP-1 cells secrete somatostatin, 5-HT and carcinoembryonic antigen."* Reproduced from [1]. **(B)** Heterochromatin (HC); euchromatin (EC); nuclear pore (NP); nuclear membrane (NM); mitochondria (M); endoplasmatic reticulum (ER), cell membrane (CM).

4.2. TEM pictures of T-VEC infected pancreatic NET cells and T-VEC virions

QGP-1 pNET cells were infected with T-VEC using MOI 0.0001. Cells were then fixed and processed for TEM at 24, 48, 72 and 96 hpi.

24 and 48 hpi, no viral particles could be detected yet. Many cells displayed morphological changes, like enlarged nuclei, mitochondria and endoplasmatic reticulum (ER). Further, the nuclei changed to almost exclusively contain euchromatin (EC) which is essential for viral DNA synthesis (Fig. 30). All other changes could also be attributed to viral infection and subsequent massive synthesis of viral components. Not all cells displayed these characteristics (Fig 30 A). Disintegration of cells following viral cell lysis could already be found 24 hpi (Fig. 30).

Interestingly, several cells undergoing autophagy could be observed as of 48 hpi (Fig. 31). Wildtype HSVs are able to suppress autophagy with the ICP 34.5 gene. Autophagy only becomes visible to this extent because T-VEC is an ICP 34.5 deleted HSV and hence permits autophagy. This has already been shown for other ICP 34.5 deleted HSV, but not for T-VEC [81].

72 hpi, first viral capsids and virions could be detected (Fig. 32). Previous experiments suggest that viral particles are present much earlier, but the probability of cutting them in TEM sections is correlates with the virus titer, which was found to be much higher 72 hpi (Fig. 21). Also, cell fusion resulting in a cell with two nuclei could be observed, however, HSV-1 infection is rarely associated with the formation of syncytia in cell culture [82].

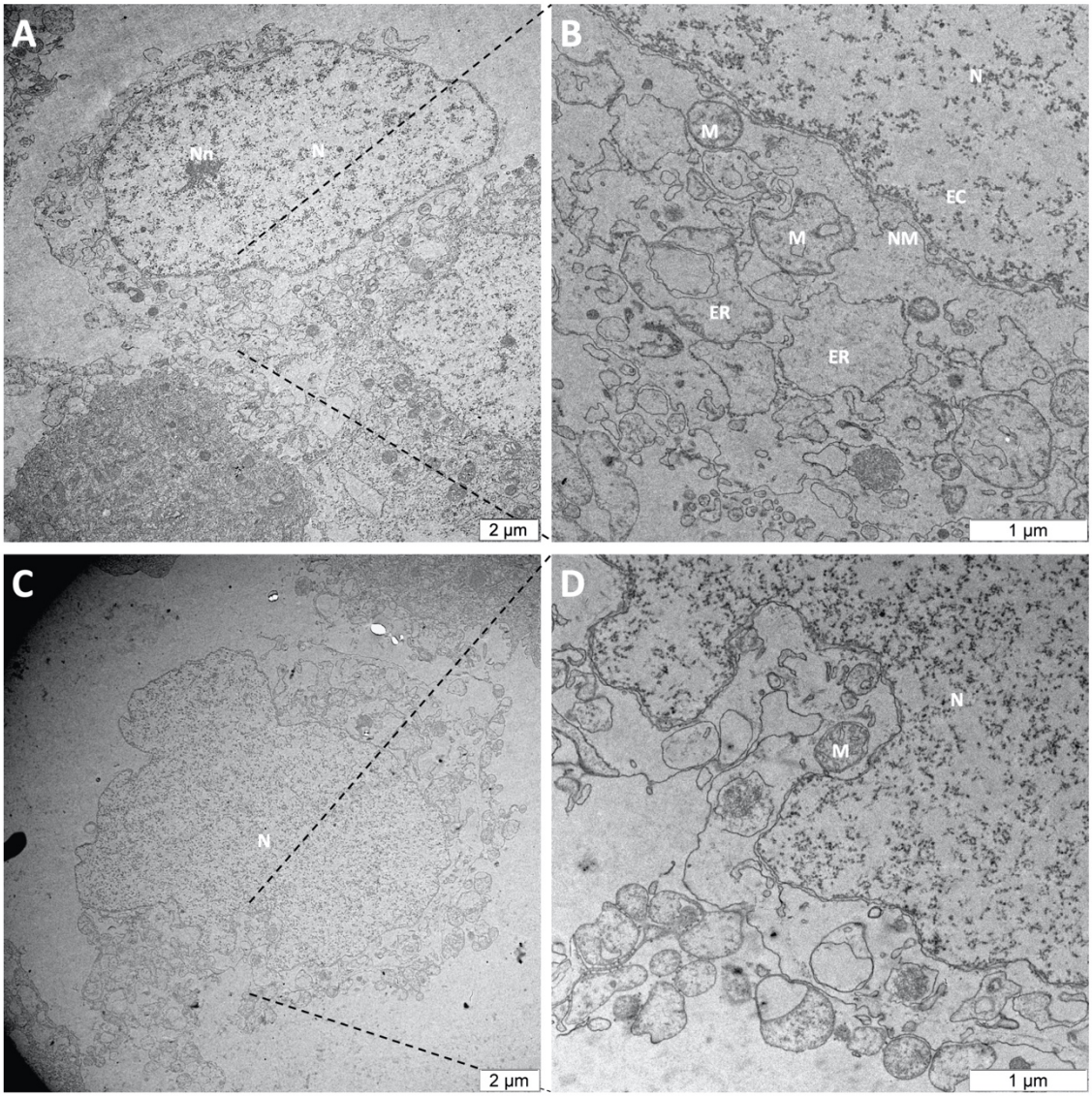

Figure 30: QGP-1 cells 24 and 48 hpi with T-VEC. (A) QGP-1 cell 24 h after T-VEC infection with MOI 0.0001. Infected cell with an enlarged nucleus (N) containing almost only euchromatin (EC) because of massive synthesis activity after T-VEC has occupied the anabolic cell mechanisms for production of huge amounts of viral particles. The cytoplasm is already disintegrated after 24 h. Reproduced from [1]. **(B)** Zoomed in from (A). Altered structure of the nucleus (N) and bloated endoplasmatic reticulum (ER) due to protein and virus synthesis, pathologically enlarged mitochondria. At this time point, no viral particles but only morphological consequences of the virus infection could be detected in TEM pictures, this might be due to low virus titers and therefore a small chance to cut viral particles at this early time point. **(C)** T-VEC mediated tumor cell lysis; the cytoplasm has lost its structure and the cell membrane is not detectable anymore. **(D)** Zoomed in from the cell shown in (C). The cell has undergone the same morphological changes mentioned in (A) and (B). No organized membrane structures are visible any more in the cytoplasm. Like in the 24 h samples, no viral structures were detected after 48 h.

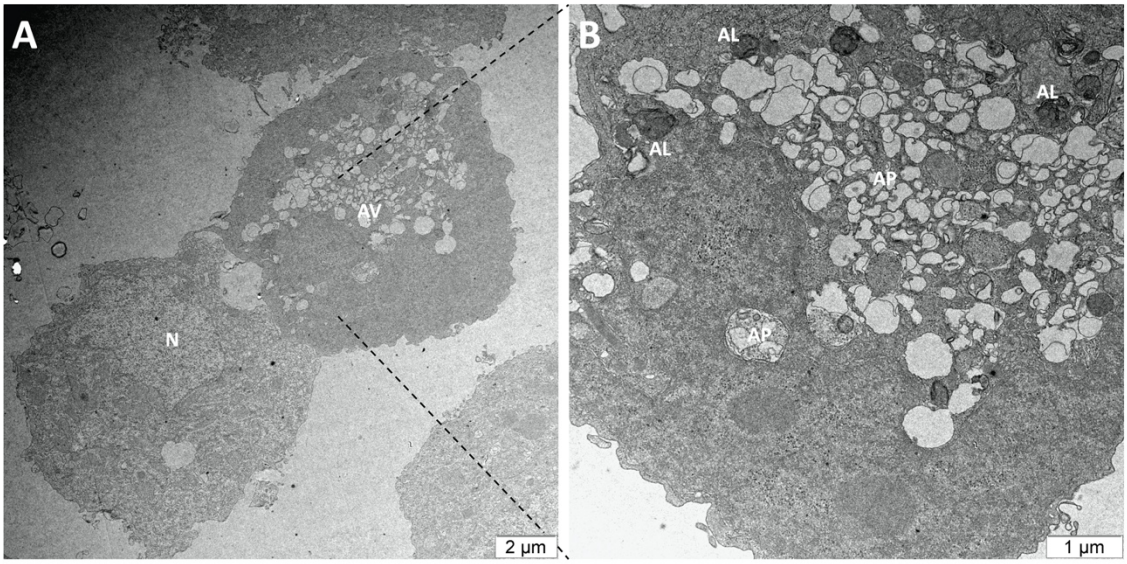

Figure 31: Autophagy after T-VEC infection. (A) Two QGP-1 cells 48 h after T-VEC infection. The lower cell does not show any morphological changes compared to non-infected tumor cells. The upper cell is undergoing extensive autophagy, showing autophagic vacuoles (AV). Reproduced from [1]. **(B)** Zoomed in from the autophagic cell shown left. Autolysosomes (AL) and autophagosomes (AP) become visible with larger magnification. Interestingly, the wildtype HSV was found earlier to suppress autophagy as a mechanism of immune evasion [81]. The ICP 34.5 gene plays a crucial role in this process and ICP 34.5 deleted Herpes simplex viruses like T-VEC were shown to permit autophagy as a response to viral infection [83].

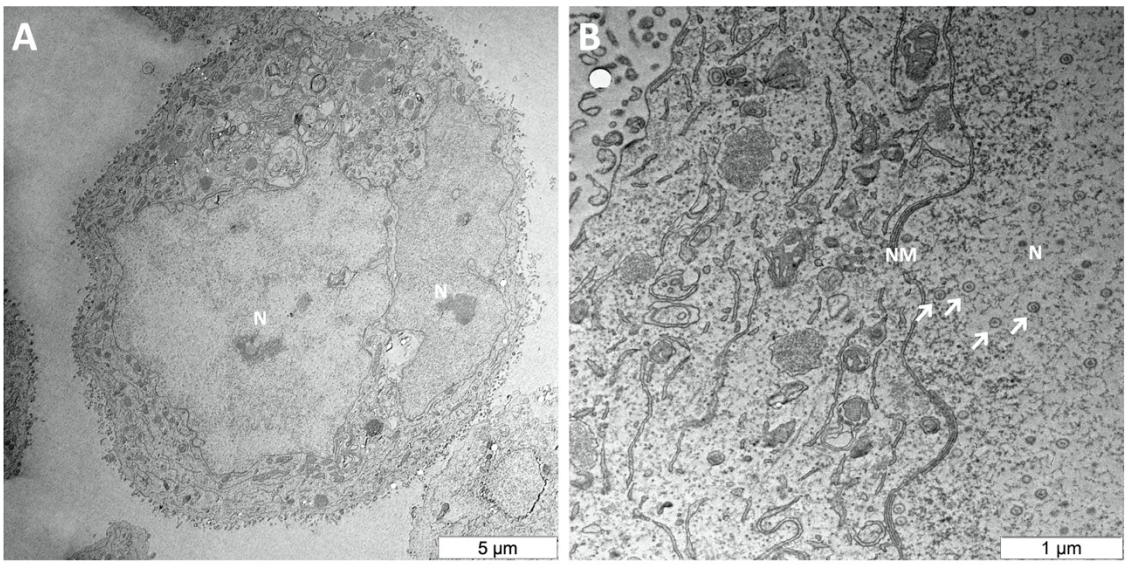

Figure 32: QGP-1 cells 72 hpi with T-VEC. (A) Virus infected cell harbouring two nuclei with different chromatin density. **(B)** Zoomed in from the cell shown left. Many virus capsids (arrows) become visible inside the nucleus (N) 72 on their way to the inner nuclear membrane for budding 72 hpi. Nuclear membrane (NM).

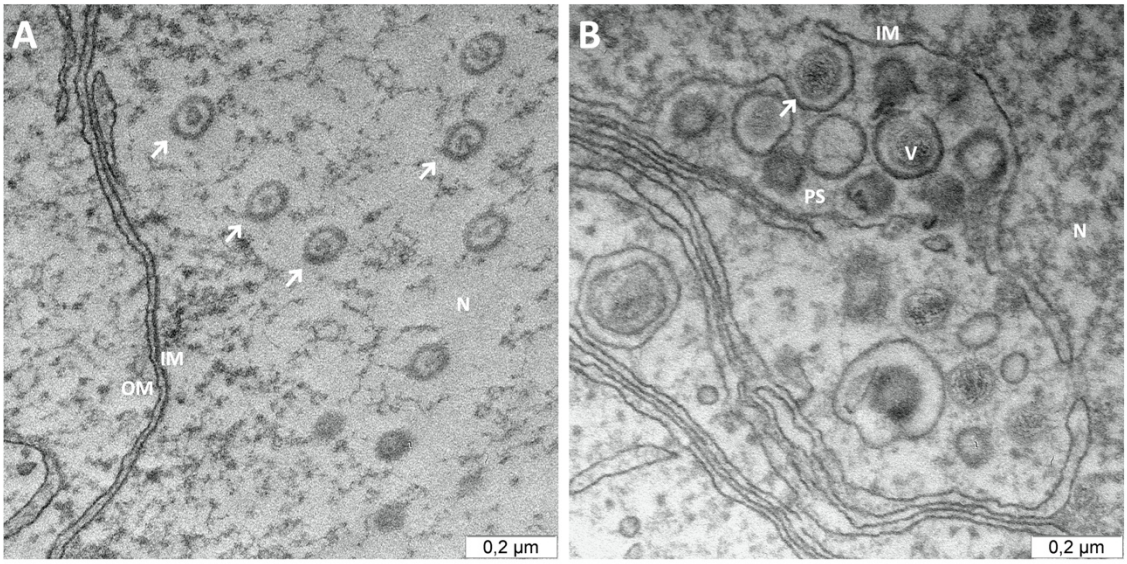

Figure 33: Herpes virus capsids. Reproduced from [1]. (A) Viral capsids (arrows) inside the nucleus (N) with a diameter of approx. 100 nm; the inner (IM) and outer nuclear membrane (OM) become visible with this magnification. (B) Viral capsid budding at the inner nuclear membrane (arrow). Enveloped capsids are detectable as complete virions (V) in the perinuclear space (PS).

Viral capsids are produced within the nucleus (Fig. 33 A). Viral structural proteins are translated in cytoplasmatic ribosomes, then structural proteins travel to the nucleus where viral capsids are assembled and packaged with viral DNA. Capsids then bud at the inner nuclear membrane becoming enveloped virions (Fig. 33 B).

Several different pathways of subsequent virus egress and envelopment are described [84]) and shown in Fig. 34.

"Briefly, viral capsids are produced in the nucleus (Fig. 33 A), then bud at the inner nuclear membrane (IM) into the perinuclear space (Fig. 33 B), or leave the nucleus via altered nuclear pores to bud at the outer nuclear membrane (OM), the endoplasmic reticulum or the Golgi network. Completed virions then get packaged into transport vacuoles to leave the cell and are released in the extracellular space by exocytosis (Fig.34). A third pathway of envelopment, including budding at the IM, deenvelopment at the OM, and secondary envelopment at cytosolic compartments, is described [85] but could not be retraced in this study." - **[1]**

Completed T-VEC virions are shown in Fig. 35 and were found to be phenotypically equal to HSV wildtype virions.

96 hpi, a complete disintegration of cells and nuclei could be observed. Further, numerous free viral particles could be seen around the cells (Fig.36).

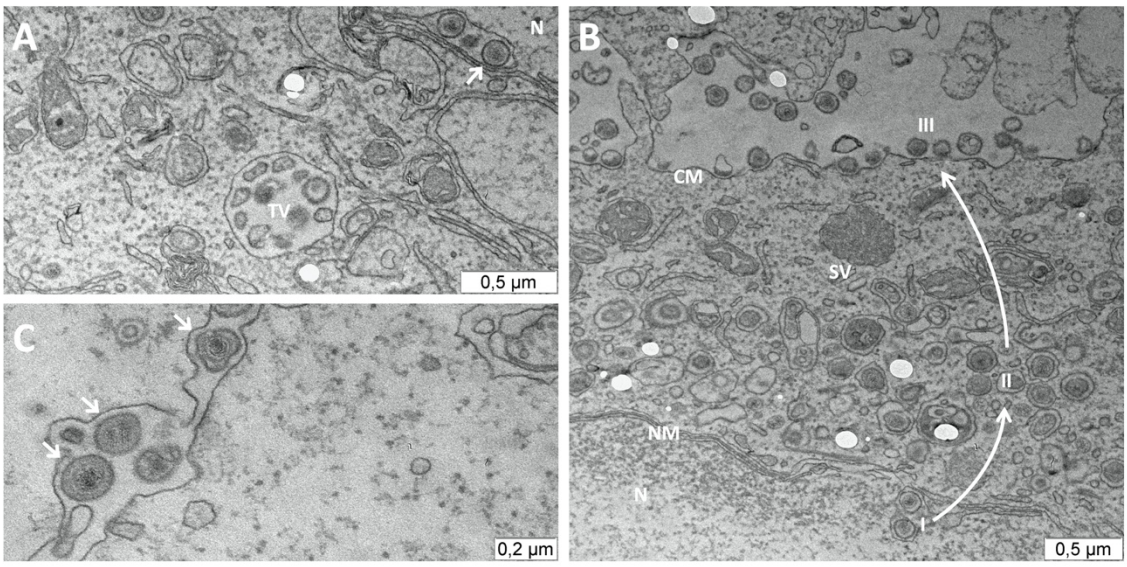

Figure 34: Pathways of T-VEC envelopment. Reproduced from [1]. **(A)** Transport vacuole (TV) containing multiple virions before exocytosis. Two virions are located in the perinuclear space (arrow). After budding at the inner nuclear membrane into the perinuclear space, virions are transported through the endoplasmatic reticulum (ER) to the Golgi complex, where they get packaged into transport vacuoles for exocytosis. A second pathway of HSV-1 envelopment includes capsids escaping the nucleus through altered nuclear pores, and budding at the outer nuclear membrane, the ER or at the Golgi network [84]. **(B)** Virions are visible in the perinuclear space shortly after budding (I), in the cytoplasm in transport vacuoles containing single virions (II) and in the extracellular space after exocytosis (III). Nucleus (N); nuclear membrane (NM); cell membrane (CM); secretory vesicle (SV). **(C)** Complete Herpes simplex virus virions (arrows) consisting of capsid, tegument and envelope reach a size up to 200 nm in diameter.

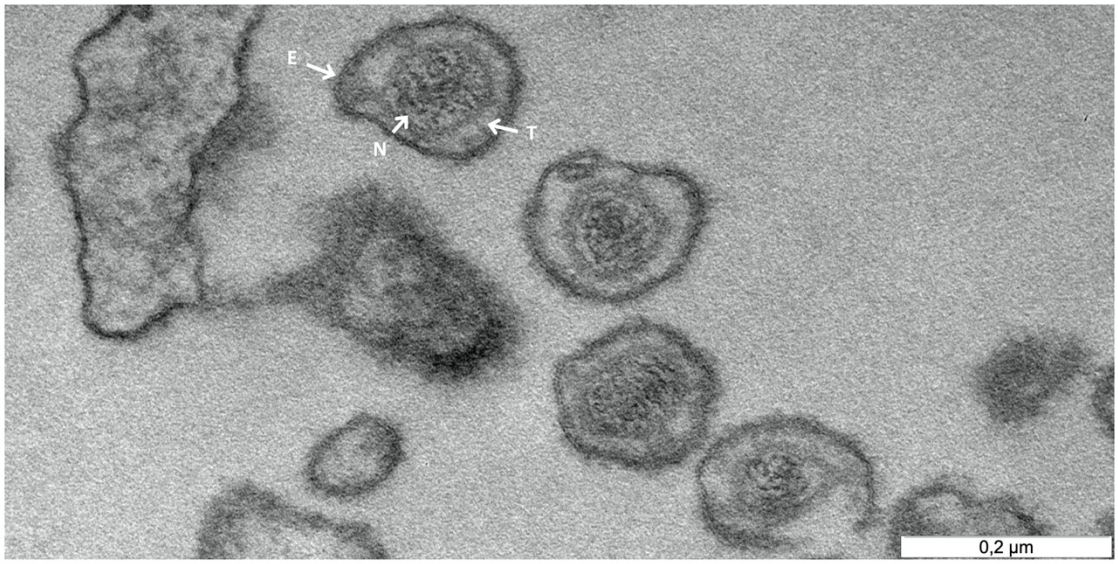

Figure 35: Viral particles of T-VEC. T-VEC virions with a size up to 200 nm in diameter consisting of a DNA containing nucleocapsid (N), tegument protein (T) and an envelope (E) with glycoprotein spikes. Reproduced from [1].

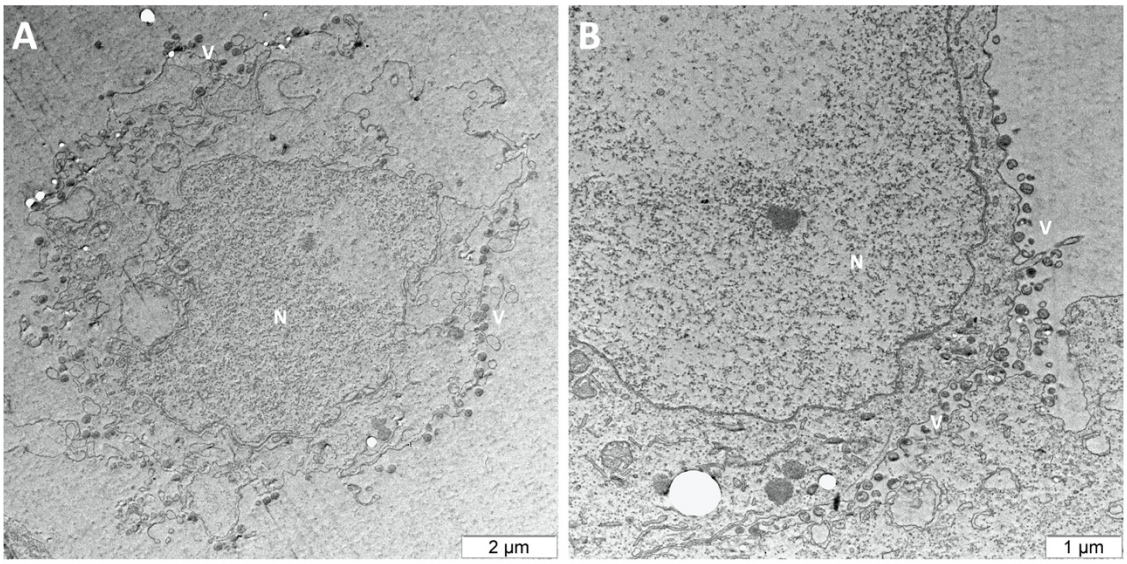

Figure 36: QGP-1 cells 96 hpi with T-VEC. (A) Lysed tumor cell due to T-VEC mediated cytotoxicity. Viral progeny (V) is visible at the cell membrane. Reproduced from [1]. **(B)** The tumor cell‘s synthesis mechanisms have been occupied by T-VEC; the cell membrane is completely covered with freshly produced virions (V).

NET cells displayed diverse morphological changes 96 hpi. A dense edge could be observed on the rim of the nucleus were virus assembly takes place, being a sign of massive virus synthesis (Fig 37, A and B). Further, some cells showed the formation of tubular mitochondrial networks after virus infection (Fig. 37 C and D). This is a cellular

response to metabolic stress to prevent autophagy of the mitochondria, ensuring cellular energy supply.

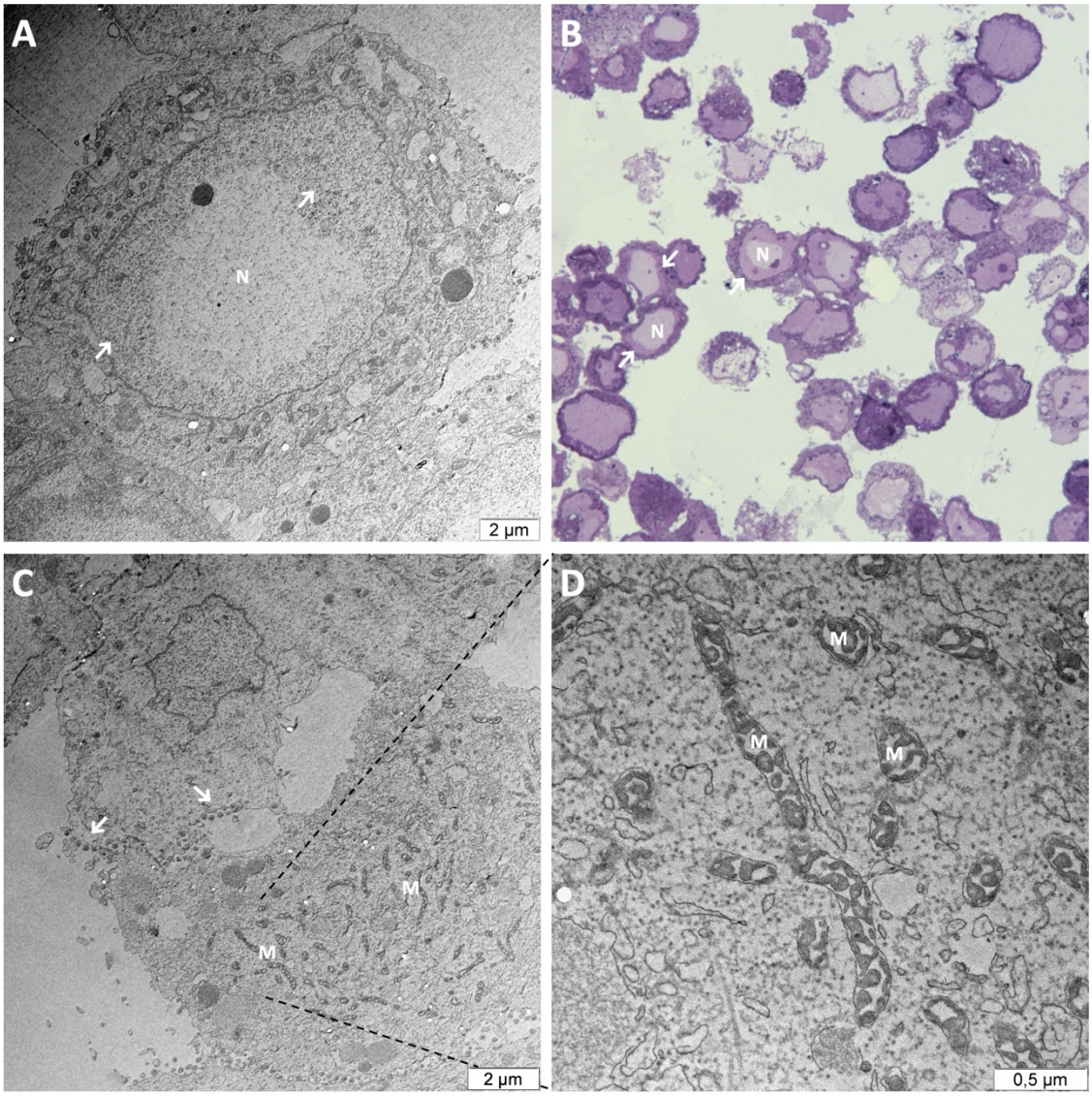

Figure 37: Morphological changes after T-VEC infection. (A) Cells 96 hpi. T-VEC infection induces a dense edge (arrows) at the rim of the enlarged nucleus (N), containing viral materials like DNA or capsid and tegument proteins. **(B)** This edge is also visible in light microscopic pictures of stained infected tumor cells. **(C)** QGP-1 cells at 72 hpi. Formation of elongated, tubular mitochondria (M) as a cellular response to virus infection. Viral particles (arrows) are visible in the extracellular space. **(D)** Elongated mitochondria (M) are visible in this T-VEC infected tumor cell. Metabolic stress (e.g. virus infection), nutrient depletion and autophagy can induce the fusion of mitochondria and the formation of tubular mitochondrial networks. As a result, elongated mitochondria are protected from autophagosomal degradation to ensure cellular ATP supply [86].

CHAPTER 4: DISCUSSION

There is a big need for therapies promising a complete, durable oncological response in advanced NEN. Oncolytic virotherapy has been reported to be a candidate to keep this promise, demonstrating long term remissions in particular cases [87, 88]. OVs are designed to infect, replicate in and finally kill tumor cells, with leaving healthy tissue untouched. By producing viral progeny and infectiously spreading throughout the tumor, tumors can be oncolysed. Thereby causing an inflammatory environment and immunogenic cell death (ICD), OVs promote immune activation and immune cell infiltration into the tumor. At best, a systemic antitumor immune response followed by a long lasting, profound tumor regression is the result.

"Until now, immunotherapy has not played a significant role in neuroendocrine cancer. There were approaches using dendritic cell vaccination [89] and a clinical phase I trial with an immune checkpoint inhibitor [90, 91], but results were not really encouraging. Recent studies show that only a small part of NETs and NECs show PD-L1 expression, which is the most encouraging target for immunotherapy so far [92]. But PD-L1 expression in metastatic NETs was found to be associated with higher WHO classification and worse overall survival [93]. The second well-established parameter for a response to immunotherapy is the tumor mutational burden, which is also relatively low in NETs [94]. Regarding the success of immune checkpoint inhibitors in non-SCLC and Merkel-cell carcinoma, these agents could possibly be efficient in similar tumors with a high tumor mutational burden like NECs [95]. Currently, clinical phase II/III studies investigating checkpoint inhibitors for treatment of NEN are ongoing and are described in detail by Weber and Fottner [91]. Trials employing virotherapeutics, in particular adenoviral agents and SVV, have been described above (Introduction, section 4). *In this context, oncolytic virotherapy might be a new way for immunotherapy to enter the field of neuroendocrine cancer."* **- [1]**

Several studies showed that virotherapy is capable of elevating the overall response rate to ICIs significantly [37]. OVs can turn a cold, immunosuppressive tumor environment into a hot, highly immunogenic one. This might be the necessary impulse to make NENs susceptible to immunotherapy.

This study aimed to lay the preclinical foundation for two well-established virotherapeutics in therapy of NEN. Both viral agents have been under extensive preclinical and clinical evaluation previously, but none of them has been tested for its efficacy in NEN before.

Two separate ways of treatment are strived with both OVs. GLV-1h68 can be delivered intravenously, which makes it easily applicable in combination with surgery or as a monotherapy. T-VEC has to be injected intralesionally, requiring endoscopic procedures for NEN. Further, both agents can be applied in the resection cavities of surgically removed tumors or possibly delivered through the hepatic artery.

Virotherapy alone shows superior results to Everolimus, favoring the OV T-VEC

In this study, monotherapy was first evaluated using the SRB viability assay, which has been used by the US National Cancer Institute (NCI) for screening of all kind of cytotoxic substances for many years [80]. Everolimus, GLV-1h68 and T-VEC were screened for their cytotoxicity in six NET and NEC cell lines originating from pancreas, lung and intestine.

At first, Everolimus monotherapy was evaluated to be compared and combined with virotherapy. The nature of the effect of Everolimus on BON-1 pNET cells was studied previously, showing a similar response pattern in viability assay like in this study. Further, antiproliferative effects like induction of cell cycle arrest as well as an hyperactivation of Akt could be shown [96]. Interestingly, the hyperactivation of Akt, which was also found in pNET cells could be favorable for T-VEC infection, as Akt activity seems to be important for HSV cell entry [66]. Results could be confirmed in this study, where also rather antiproliferative than cytoreductive effects of Everolimus monotherapy were shown (Results, section 1). For Everolimus monotherapy, very similar response patterns could be detected for all NET/NEC cell lines, therefore Everolimus can be assumed to have antiproliferative effects on all cell lines tested (Results section 1.1). The response pattern indicates a saturation of the effect of Everolimus. 1 to 10 nM was sufficient to exhibit the maximal mTOR inhibiting effect in most NET/NEC cell lines, higher

concentrations did not relevantly further decrease cell viability compared to mock treatment.

The antiproliferative effect could be confirmed using real-time cell monitoring of the lung NET cell line H727 (Results, section 1.2). Therefore, the electrical impedance of the cell layer was measured continuously over 120 hours. The Cell index calculated from impedance was earlier shown to correlate with cell viability, but also with cell morphology and attachment quality [97, 98]). In a synopsis with the results from SRB viability assay, the Cell index can be primarily seen as a measure for cell viability in this setting. Viability curves with higher Everolimus concentrations showed a lower gradient and hence a slower cell proliferation indicating cytostatic effects. Nevertheless, despite exhibiting antiproliferative effects, no cytoreductive effects or complete reductions of tumor cell counts could be observed, even when employing very high concentrations of Everolimus.

T-VEC was found to exhibit the highest cytotoxicity in all NET/NEC cell lines, requiring extremely low MOIs to kill these cell lines (Results, section 3.1.1). This could also be confirmed with microscopic pictures of the T-VEC infected cell layers (Results, section 3.1.5). GLV-1h68 was also able to reduce remaining tumor cell counts in all cell lines in a dose dependent manner, thereby requiring higher MOIs (Results, section 2.1.1).

Comparing the results from SRB viability assays to studies described previously, pretty similar cytotoxicity could be detected using GLV-1h68 in a panel of head and neck squamous cell carcinoma (HNSCC) cell lines. In four out of six HNSCC cell lines, a nearly complete cytoreduction was detected with MOI 1 after 96 h ([99], Figure 3). Here, a complete cytoreduction was detected in three out of six cell lines under the same conditions for NEN. In seven cell lines originating from pleural mesothelioma, only one cell line reached a complete cytoreduction after 96 h with GLV-1h68 at MOI 1 ([100], Figure 1.). For both, HNSCC and pleural mesothelioma, clinical trials using GLV-1h68 have been initiated following these preclinical results [55](NCT01766739).

"Interestingly, the cytotoxicity of T-VEC was found to be higher [in NEN] *than in melanoma cell lines in a previous work [33]. In this paper, a MOI of 0.1 did not lead to a complete reduction of tumor cells after 72 h, in contrast to the results with most of the*

cell lines employed in this work. This capability was shown to be stable throughout cells derived from lung and pNETs and intestinal NECs." - **[1]**

Based on the results in SRB assay, three arbitrary response categories were classified for each agent. Table 2 shows an overview of the response categories; however, the categories are not sufficient to compare different agents but are valuable to provide an overview of the therapeutic spectrum of either agent.

The two lung NET cell lines are shown on top, both pNET cell lines in the middle and the two NEC cell lines on the bottom of Table 2. Accordingly, GLV-1h68 antitumor activity seems to be independent from anatomical origin and grading of NEN. T-VEC might be particularly effective for well-differentiated NEN, whereas a resistant NEC cell line could be detected. In summary, all NET/NEC cell lines could be proved susceptible to infection and cytotoxicity of GLV-1h68 and T-VEC, indicating a generally broad spectrum of both OVs in NEN.

Cell line	Everolimus	GLV-1h68	T-VEC
NCI-H727	++	++	++
UMC-11	++	+	++
BON-1	+	++	++
QGP-1	+	+	+
HROC-57	+	++	++
NEC-DUE1	++	+	-

Table 2: Treatment susceptibility of NET/ NEC cell lines. Summary of the arbitrary response categories from SRB viability assays. (++) indicates highly permissive, (+) indicates permissive and (-) indicates resistant to the respective treatment. Both lung NET cell lines were shown to be highly permissive for T-VEC treatment, whereas pNET cells were suitable for both OVs.

Comparing virotherapy to Everolimus in this setting, virotherapy could be proved to be way more effective and exhibited not only antiproliferative but also cytoreductive effects. Considering that peak Everolimus concentrations in blood samples of patients reach up to 100 nM and mean Everolimus concentrations over 24 h are around 20 nM [101], higher reductions of tumor cell masses can definitely be achieved with both GLV-1h68 and T-VEC employing realistic MOIs (Results, sections 1.1, 2.1.1 and 3.1.1).

Using real-time cell monitoring, both OVs were proved to exhibit significant cytotoxic effects. Viability curves of cells infected with GLV-1h68 peaked at 28 hpi (MOI 0.1) and 36 hpi (MOI 0.25), respectively (Results, section 2.1.2). Viability curves of T-VEC

infected cells peaked at 24 hpi (MOI 0.001) and 40 hpi (MOI 0.0001) (Results, section 3.1.2). Concludingly, higher MOIs led to an earlier peak and earlier subsequent reduction of cell viability. As more cells can be initially infected with a higher MOI, viral progeny can be produced faster and therefore a faster viral spread through the cell layer mediating a cytotoxic effect is facilitated, resulting in an earlier peak and drop of the Cell Index. However, the first effects of viral infections on the curve are not necessarily connected to cell death. Also, a change in cell morphology or attachment quality as a response to early viral infection could slightly alter cellular impedance [97]. Anyway, the subsequent significant decrease of the Cell index can definitely be attributed to a significant loss of cell viability. Taken together, cytoreductive effects could be proved for both OVs. The viability curves of T-VEC infected cells showed a faster and deeper drop after their peak, indicating a quick loss of cell viability (Results, section 3.1.2). This points out the strong cytotoxicity mediated by T-VEC.

Next, viral replication in tumor cells was assessed. A sufficient viral replication is a crucial factor for OVs to disseminate in the tumor tissue, infect further tumor cells and induce ICD. High virus titers were observed in NET and NEC cells for both OVs (Results, sections 2.1.3 and 3.1.3). GLV-1h68 reached a titer of 10^7 PFU/ml 72 hpi in both cell lines tested, T-VEC also achieved titers that high in H727 and QGP-1 cells, whereas it took 96 h for it in NEC-DUE1 cells to surpass 10^7 PFU/ml. With highly permissive and permissive cell lines (H727 and BON-1 for GLV-1h68, H727 and QGP-1 for T-VEC), virus titers decreased again between 72 and 96 h, what can be attributed to the progression of viral oncolysis of host cells being necessary for virus replication. In “resistant” NEC-DUE1 cells, T-VEC replication was found to be slower, yet reaching high titers after a longer infection period. In summary, efficient and strong virus replication could be proved for both OVs, being the basis for successful virotherapy of NEN.

Viral transgene expression is an indicator for viral infection and replication. GLV-1h68 only carries transgenes for monitoring viral infection, whereas T-VEC holds a therapeutic transgene. The GM-CSF transgene is essential for the induction of an antitumor immunity after viral infection of the tumor. First thought to be important as a hematopoietic growth factor, GM-CSF was found to play a fundamental role in tissue inflammation and crosstalk between T cells and myeloid cells like macrophages, granulocytes and dendritic

cells [102]. The GM-CSF transgene is unquestionably a significant factor in the clinical success of T-VEC.

Accordingly, the transgene expression of both OVs was measured. Via fluorescence microscopy, a strong expression of the GLV-1h68 encoded GFP transgene, being MOI and time dependent, could be visualized in all NET/NEC cell lines (Results, section 2.1.4). For the T-VEC encoded GM-CSF transgene, two cell lines were picked, and an ELISA was carried out. High GM-CSF concentrations correlating with viral replication were detected, pointing out that the transgene is continuously expressed during virus replication in NET/NEC cells (Results, section 3.1.4).

Although the secondary antitumor immune response could not be modeled in this study, several key points indicate an immune activation after virotherapy of NEN. The demonstrated high cytotoxicity is crucial for the initiation of an immune activation, as a release of tumor neo-antigens, PAMPs and DAMPs is facilitated with cell death. Further, both viruses were shown previously to induce ICD in tumor cells, being a strong stimulus for the immune system [28, 103]. Additionally, the high GM-CSF concentrations detected after T-VEC infection are able to activate myeloid cells and induce a significant tissue inflammation, followed by the influx of immune cells.

For T-VEC monotherapy, TEM pictures were taken to visualize T-VEC replicating in pNET cells (Results, section 4).

"Both the viral egress and envelopment processes of T-VEC were visualized for the first time. The T-VEC virion has been observed under the TEM previously when it was investigated for its physical stability [104]. In this work, T-VEC capsid formation in the nucleus, budding at the IM, viral particles in the space between inner and OM, and the transport for exocytosis were demonstrated in pNET cells (Results, section 4.2). *The three possible pathways of alphaherpesvirus envelopment have been described in detail earlier [84, 105, 106]. Whether deenvelopment at the OM and subsequent secondary envelopment at cytosolic compartments plays a role in T- VEC envelopment remains unclear. Morphological changes of the pNET cells were also detected. The massive formation of euchromatin shortly after virus infection indicates a lytic rather than a latent virus infection [107]. In summary, the efficient production and release of viral progeny*

could be observed, consistent with the fact of rapidly increasing virus titers in the other experiment (Results, section 3.1.3)." **- [1]**

Moreover, autophagy could be detected as a special cellular response to ICP 34.5 deleted HSVs such as T-VEC (Fig. 31).

Taken together, virotherapy showed highly promising results when employed in NET/NEC cell lines. In particular T-VEC required extremely low concentrations to infect, replicate in and kill cells derived from NEN. Both OV appeared to be superior to the clinically approved mTOR inhibitor Everolimus.

Combinatorial therapy with Everolimus is not inferior to monotherapy

There is substantial evidence for synergistic effects by combining both virotherapeutics with an mTOR inhibitor such as Everolimus.

"Of note, previous studies regarding the combinatorial therapy of VACVs with the mTOR inhibitor rapamycin had resulted in the detection of synergistic effects. Both, everolimus and rapamycin target and inhibit mTORC1. The synergistic effects were explained by the effect of mTORC1 inhibition on antiviral immunity. It was found that mTORC1 downstream signaling via p70S6K/4E-BP1 influences cellular type I IFN response. Therefore, mTORC1 inhibition can make tumor cells more susceptible to VACV infection. In vivo, antiviral T-cell responses can be reduced by mTOR inhibitors, which also makes viral infections more effective [69, 108, 109]. These studies were conducted with malignant glioma models." **- [2]**

For T-VEC, beneficial effects of this combination could also be presumed from previous studies as outlined in the Introduction, section 6.

The additional effects of Everolimus observed in this study were small. In viability assays carried out 96 hpi, the addition of Everolimus to virotherapy could barely reduce tumor cell viability. The strongest effect observed was with GLV-1h68. By adding OV to Everolimus alone, a further reduction of 17 % of the remaining tumor cells could be achieved using NEC-DUE1 cells (Results, section 2.2.1). Effects observed with

GLV-1h68 in H727 cells or T-VEC treatment of both cell lines tested (H727 and NEC-DUE1) were smaller. By adding T-VEC to Everolimus alone, additional 11 % of tumor cells were killed (Results, section 3.2.1). When employing real-time cell monitoring, it became visible that bigger differences in cell viability between combinatorial therapy and virotherapy alone occurred earlier than 96 hpi. With GLV-1h68, a gap between the curves could be observed between 24 and 72 hpi, which was getting smaller between 72 and 96 hpi because of a significant drop of cell viability with GLV-1h68 alone (Results, section 2.2.2). The same phenomenon could be observed with T-VEC between 48 and 72 hpi (Results, 3.2.2). During this gap, cell viability was significantly smaller with the combinatorial treatment in both cases. But finally, the cell indices reached 96 hpi were similar with combinatorial therapy and virotherapy alone. This resembles the results observed with SRB viability assays, where the difference measured at 96 hpi was also quite small. In a last experiment, Everolimus was not found to have any particular impact on virus replication with both OVs (Results, sections 2.2.3 and 3.2.3). It is difficult to tell whether or not the difference in cell viability during the treatment period is clinically relevant, even though the outcome measures at 96 hpi were quite similar.

Briefly summing up, it was not possible to replicate the promising results reported in literature for this combination. Minor additional effects could be found combining Everolimus and both OVs. Everolimus did also not have a negative impact on viral replication and efficacy, making a combinatorial treatment yet feasible. Still, combinatorial therapy was found to be statistically significant more effective than monotherapy in most cases (GLV-1h68 both cell lines, T-VEC one cell line). Best results with the combination could be achieved with GLV-1h68 in NEC cells. It is also conceivable that Everolimus, known as an immunosuppressive agent, could limit the secondary antitumor immune response and could therefore be an unfavorable combination partner for virotherapy. Future research should focus on this combination in immune mimicking in vitro models or immunocompetent animal models to fully investigate the interaction between both and to deliver a final statement about the usefulness of this combinatorial regimen in NEN.

An alternative combinatorial partner for virotherapy of NEN would be the multikinase inhibitor sunitinib. Through VEGFR inhibition, it has anti angiogenic effects, which were

previously shown to be augmented by an oncolytic VACV [110]. Besides, it was shown to reduce immunosuppressive cell populations like Tregs or MDSC. This makes it suitable for a combination with OVs by enhancing the secondary antitumor immune response [111]. Recently, it could be shown that both effects play a role when the effects of an oncolytic VACV were augmented with sunitinib [112]. Further combinatorial approaches employing virotherapy and sunitinib are described [113].

T-VEC attenuation with GCV is effective

The virostatic GCV is a derivate of ACV, having an additional hydroxymethyl side chain. This makes it a suitable product for the human CMV encoded UL97 kinase, functioning similar to the HSV-TK. The viral UL97 kinase performs the first phosphorylation, whereas a second and third one is conducted by cellular kinases, activating GCV to its active metabolite GCV-triphosphate [114]. GCV thus only gets activated in virus infected cells to inhibit DNA synthesis there. Hence, GCV is broadly used to treat CMV infections in immune compromised patients and in transplantation medicine. For HSVs, GCV antiviral activity is similar to the state-of the-art treatment ACV, thereby exhibiting more adverse effects such as myelotoxicity [115].

Since the aim of this study was not only to discover a drug with a virostatic potential, but also assessing potential beneficial combination partners for virotherapy, GCV was employed. As outlined in the Introduction section 7, GCV promised both, a virostatic and an enhancing effect when it was combined with T-VEC.

GCV administered intravenously in a dose of 5 mg/kg/day is known to reach blood concentrations of 40 µM in peak and around 5 µM over 24 h [116, 117]. Accordingly, three concentrations of GCV being 1, 10 and 50 µM were employed here.

GCV could effectively prevent viral cell killing when added at an early point of virus infection (1 hpi), while exhibiting no relevant inherent cytotoxicity. Thereby, the whole cell population could be saved using realistically reachable concentrations of GCV (Results, section 3.3.1). This proved the efficacy of GCV as an antiviral drug for T-VEC.

By adding GCV at 72 hpi, the underlying approach had the intention to enhance cytotoxicity of the treatment regimen. T-VEC infected tumor cells where infection but no

cell killing had been accomplished express high amounts of HSV-TK at this point of time, possibly being sensitive to additional GCV treatment. When GCV was administered as late as 72 hpi, no additional but lower cytotoxicity could be detected employing 1 and 10 µM GCV. Concludingly, viral cell killing was prevented with lower GCV concentrations (1 and 10 µM), even when it was added 72 hpi. However, the limiting effect on viral cytotoxicity was smaller compared to GCV addition 1 hpi, as most tumor cells had already been killed 72 hpi.

By adding 50 µM GCV 72 hpi, the remaining cell mass became as low as with T-VEC without GCV again (Results, section 3.3.1). This reversal effect could be either due to the inherent GCV mediated cytotoxicity, or because of tumor cell killing with activated GCV through the HSV-TK suicide gene system. However, the effect with higher GCV concentrations only canceled out its virostatic effect in this setting, resulting in no additional benefit compared to T-VEC alone. Therefore, the main function of GCV in this setting was considered to be virostatic, being an effective inhibitor of viral cell killing in the case of an uncontrolled, overshooting virus replication.

Next, the restrictive effect on virus replication was also proved. GCV applied in realistic concentrations effectively limited T-VEC replication in all three cell lines tested (Results, section 3.3.2).

"Regarding this, the experiments demonstrate that GCV is an applicable virostatic drug also in NET/NEC cells to ensure safety of T-VEC virotherapy in cases of any overwhelming virus replication scenarios which otherwise are unstoppable." **- [1]**

As ACV is known to have similar virostatic effects on HSVs like GCV, it would also be a considerable option for safety of T-VEC treatment due to its favorable side effect profile.

For GLV-1h68, antiviral drugs targeting VACV such as cidofovir or vaccinia immune globulin (VIG) are available [118]. VIG has been used to treat adverse events occurring after the smallpox vaccine with VACVs [119].

Study limitations

"Despite great research efforts, there is still only a single US FDA/EMA oncolytic virus available for clinical use. One reason for that is the gap between promising preclinical data and limited clinical success. Since oncolytic viruses are biological agents, they might require more realistic in vitro tumor models than common monolayer tumor cell cultures to provide meaningful predictive preclinical evaluation results. For more realistic in vitro tumor models, three-dimensional tumor cell-culture systems can be employed in preclinical virotherapy research." - **[3]**

Further details on three-dimensional cell cultures in virotherapy are outlined in this review [3].

The major limitations of this study are associated with the limitations of monolayer cell culture, as this is the preclinical tumor model employed. Traditional monolayer cell culture is the most acknowledged and used preclinical tumor model. Anyway, it only contains one population of cells (i.e. tumor cells) and simplifies the actual tumor micro-environment with its three-dimensional architecture, various cell types, extracellular matrix and different metabolic areas.

Monolayer cell culture does also not reflect the influence of the immune system on the process of oncolysis. Therefore, the crucial secondary antitumor immune response could not be observed in this setting.

As described above, *"this effect directly depends on the primary virus mediated oncolysis/cytotoxicity, which was presented here in a very convincing manner. In addition, high concentrations of the immunostimulatory GM-CSF transgene were detected* [after T-VEC treatment], *predicting a further increase in efficacy by immune effects in animal models and first human trials."* - **[1]**

Further, every cell, also in monolayer cell culture, features inherent key mechanisms to initiate the innate immunity, e.g. the type I IFN response or STING expression.

Usually, studies employing virotherapeutics for the first time need to prove a relative specificity to cancer cells and attenuation in healthy human cells. Since both OVs used in

this study have already been tested in several human trials and demonstrated excellent safety profiles, a safety control with “healthy” cells was omitted here.

Conclusions

The aim of this study was to evaluate two OVs for their efficacy in neuroendocrine neoplasms (NEN). Moreover, combinatorial treatment regimens using virotherapy together with Everolimus or GCV were studied for their effects on cell lines derived from NEN.

T-VEC was shown to exhibit highly cytotoxic effects, requiring strikingly low virus concentrations. It was proven that T-VEC infects and replicates in NEN cells derived from several anatomical origins. Further, plausible evidence could be provided that T-VEC is able to generate an immune response against NEN.

Similar evidence could be provided for GLV-1h68. However, it took higher concentrations of GLV-1h68 to achieve comparable effects like with T-VEC.

For T-VEC, slightly stronger efficacy could be found in lung NETs and pNETs compared to NECs, whereas GLV-1h68 was found to be most efficient in pNETs and NECs.

The combinatorial regimen using Everolimus was not remarkably superior to each OV alone. Nevertheless, it was also not found to be worse, requiring more research employing immune competent animals to further elucidate the interactions between both.

GCV was proved to be an efficient virostatic agent, significantly limiting T-VEC replication and cytotoxicity.

In consequence of this study, our group started first experiments for the evaluation of T-VEC efficacy in murine NET models, further pursuing the preclinical and clinical development of T-VEC for treatment of NEN. Beyond that, an off-lable use of T-VEC for virotherapeutic treatment of NEN patients could become an option in the near future.

SUMMARY

Metastatic neuroendocrine neoplasms, including neuroendocrine tumors and neuroendocrine carcinomas, are still a fatal disease and are in desperate need for novel promising therapy options.

For oncolytic virotherapy, viruses are genetically engineered or selected to specifically replicate in tumor cells. By infecting, replicating and releasing viral progeny, oncolytic viruses spread infectiously through the tumor tissue and lyse tumor cells. Simultaneously, an inflammatory environment is created within the tumor, attracting immune cells and mobilizing the patient's immune system to perform a widespread systemic antitumor immune response.

This study aimed to evaluate oncolytic virotherapy for neuroendocrine neoplasms. Two oncolytic viruses, which have both already been administered to patients in clinical trials, were selected to be studied for their activity in six cell lines derived from neuroendocrine neoplasms. GLV-1h68 is an oncolytic vaccinia virus currently being tested in clinical phase I/II trials for several other cancer entities. The second virus is the herpes simplex virus T-VEC, being already clinically approved for treatment of advanced melanoma.

Six cell lines, two of them originating from pancreatic neuroendocrine tumors, two derived from neuroendocrine tumors of the lung and two originating from neuroendocrine carcinomas were employed in this study. The impact of both viruses on cell viability was measured using SRB viability assays and the development of cell viability over time was studied using real-time cell monitoring. Further, virus replication was quantified, microscopic pictures of the infected cell layer were taken and transgene expression of both viruses was assessed. Additionally, transmission electron microscopic pictures were taken to visualize T-VEC envelopment and cell egress. For both viruses, a combinatorial regimen using Everolimus, a state-of-the-art treatment for neuroendocrine tumors, was evaluated employing the same methods. Moreover, the effect of Ganciclovir on T-VEC treatment of cells from neuroendocrine neoplasms was studied.

Both viruses were shown to infect, replicate in and kill tumor cells in a time and dose dependent manner. T-VEC required outstandingly low concentrations, thereby character-

izing itself as a particularly promising drug candidate for neuroendocrine neoplasms. Via electron microscopy, the T-VEC virions as well as the cellular responses of neuroendocrine tumor cells to virus infection could be visualized. Transgene expression was found to be strong with both viral agents. The combinatorial treatment with Everolimus was only found to be slightly superior to monotherapy. The potency of Ganciclovir as a virostatic drug for T-VEC could be proven, efficiently limiting T-VEC replication.

In summary, oncolytic virotherapy was found to be a promising therapy for neuroendocrine neoplasms in vitro. Both, GLV-1h68 and T-VEC, were shown to have high oncolytic activity in a broad spectrum of cell lines originating from neuroendocrine neoplasms. T-VEC especially demands for further preclinical and clinical development, only requiring strikingly low concentrations to replicate in and kill tumor cells. The future role of a combinatorial treatment with Everolimus remains unclear, yet still being a considerable treatment option. Ganciclovir was shown to be an important safety feature in T-VEC mediated virotherapy, preventing safety concerns using a replication competent viral vector.

List of Abbreviations

4EBP1:	Eukaryotic translation initiation factor 4E-binding protein 1
ACV:	Acyclovir
AL:	Autolysosome
AP:	Autophagosome
Approx.:	Approximately
ATCC:	American Type Culture Collection
ATP:	Adenosine triphosphate
AV:	Autophagic vacuole
BiTE:	Bispecific T-cell engager
CD:	Cluster of differentiation
CM:	Cell membrane
CMC:	Carboxymethylcellulose
CMV:	Cytomegalovirus
CTLA-4:	Cytotoxic T-lymphocyte-associated antigen 4
DAMP:	Damage associated molecular pattern
DEPTOR:	DEP domain-containing mTOR-interacting protein
DMEM:	Dulbecco's modified eagle's medium
DNA:	Deoxyribonucleic acid
E:	Envelope
E1A:	Adenovirus early region 1A
EC:	Euchromatin
ECHO:	Enteric cytopathic human orphan
EEV:	Extracellular enveloped virion
ELISA:	Enzyme-linked immunosorbent assay
EMA:	European Medicines Agency
ER:	Endoplasmatic reticulum
FCS:	Fetal calf serum
FDA:	Food and Drug Administration
Fig.:	Figure
GCV:	Ganciclovir
GEP-NET:	Gastroenteropancreatic neuroendocrine tumor
GFP:	Green fluorescent protein
GM-CSF:	Granulocyte-macrophage colony-stimulating factor
gNET:	Gastric neuroendocrine tumor
h:	Hours
HC:	Heterochromatin
HNSCC:	Head and neck squamous cell carcinoma
hpi:	Hours post infection
HSV:	Herpes simplex virus
i.v.:	Intravenous
ICD:	Immunogenic cell death
ICI:	Immune checkpoint inhibitor
ICP:	Infected cell protein
IEV:	Intracellular enveloped virion
IFN:	Interferon
IL:	Interleukin
IM:	Inner nuclear membrane
IMV:	Intracellular mature virion
IRS:	Insulin receptor substrate
JCRB:	Japanese Collection of Research Bioresources Cell Bank
M:	Mitochondrion

MDSC:	Myeloid derived suppressor cell
mLST8:	Mammalian lethal with SEC13 protein 8
MOI:	Multiplicity of Infection
MTC:	Medullary thyroid carcinoma
mTOR:	Mechanistic target of rapamycin
mTORC1/2:	Mechanistic target of rapamycin complex 1/2
MTT:	Molecular targeted therapy
N:	Nucleus/Nucleocapsid
NCI:	National Cancer Institute
NCT:	National clinical trial
NEC:	Neuroendocrine carcinoma
NEN:	Neuroendocrine neoplasia
NET:	Neuroendocrine tumor
NK-cell:	Natural killer cell
NM:	Nuclear membrane
Nn:	Nucleolus
NP:	Nuclear pore
OM:	Outer nuclear membrane
OV:	Oncolytic virus
PAMP:	Pathogen associated molecular pattern
Parag:	Paraganglioma
PBS:	Phosphate buffered saline
PD-1:	Programmed death 1
Pen/Strep:	Penicillin-Streptomycin
Pexa-VEC:	Pexastimogene Devacirepvec
PFS:	Progression free survival
PFU:	Plaque forming units
Pheo:	Pheochromocytoma
PI3K:	Phosphatidylinositol-3-kinase
PIP_2:	Phosphatidylinositol-4,5-bisphosphate
PIP_3:	Phosphatidylinositol-3,4,5-trisphosphate
pNET:	Pancreatic neuroendocrine tumor
PRRT:	Peptide receptor radionuclide therapy
PS:	Perinuclear space
PTEN:	Phosphatase and tensin homolog
RTCA:	Real Time Cell Analyzer
RPM:	Rounds per minute
RPMI:	Cell culture medium developed at the Roswell Park Memorial Institute
RUC-GFP:	Renilla luciferase-Aequorea green fluorescent protein
SCLC:	Small cell lung cancer
SD:	Standard deviation
SEER:	Surveillance, Epidemiology, and End Results
siNET:	Small intestinal neuroendocrine tumor
SRB:	Sulforhodamine B
SSA:	Somatostatin analogue
SSV-1:	Seneca Valley Virus 1
STING:	Stimulator of interferon genes
SV:	Secretory vesicle
T-VEC:	Talimogene Laherparepvec
T:	Tegument protein
TCS:	Trichloroacetic acid
TEM:	Transmission electron microscopy
TK:	Thymidine kinase
TMP:	Thymidine monophosphate
T_{reg}:	Regulatory T-cell

TRIS:	Tris(hydroxymehtyl)-amino-methane
TSC1/2:	Tuberous sclerosis protein 1/2
TTP:	Thymidine triphosphate
TV:	Transport vacuole
US:	United States (of America)
V:	Viral progeny
VACV:	Vaccinia virus
VEGFR:	Vascular endothelial growth factor receptor
VIG:	Vaccinia immune globulin

LIST OF FIGURES

LIST OF TABLES

REFERENCES

[1] Kloker LD, Berchtold S, Smirnow I, Schaller M, Fehrenbacher B, Krieg A, Sipos B and Lauer UM. *The Oncolytic Herpes Simplex Virus Talimogene Laherparepvec Shows Promising Efficacy in Neuroendocrine Cancer Cell Lines.* Neuroendocrinology, 2019.

[2] Kloker LD, Berchtold S, Smirnow I, Beil J, Krieg A, Sipos B and Lauer UM. *Oncolytic vaccinia virus GLV-1h68 exhibits profound antitumoral activities in cell lines originating from neuroendocrine neoplasms.* BMC Cancer, 2020. **20**(1): p. 628.

[3] Kloker LD, Yurttas C and Lauer UM. *Three-dimensional tumor cell cultures employed in virotherapy research.* Oncolytic Virother, 2018. **7**: p. 79-93.

[4] Scholzen T and Gerdes J. *The Ki-67 protein: from the known and the unknown.* J Cell Physiol, 2000. **182**(3): p. 311-22.

[5] Velayoudom-Cephise FL, Duvillard P, Foucan L, Hadoux J, Chougnet CN, Leboulleux S, Malka D, Guigay J, Goere D, Debaere T, et al. *Are G3 ENETS neuroendocrine neoplasms heterogeneous?* Endocr Relat Cancer, 2013. **20**(5): p. 649-57.

[6] Perren A, Couvelard A, Scoazec JY, Costa F, Borbath I, Delle Fave G, Gorbounova V, Gross D, Grossma A, Jense RT, et al. *ENETS Consensus Guidelines for the Standards of Care in Neuroendocrine Tumors: Pathology: Diagnosis and Prognostic Stratification.* Neuroendocrinology, 2017. **105**(3): p. 196-200.

[7] O'Dorisio TM VA, Ruggle T. *What is neuroendocrine cancer?* Uihc.org. University of Iowa [Web] [cited 2020, 18 Feb]; Available from: https://uihc.org/health-topics/what-neuroendocrine-cancer.

[8] Huguet I, Grossman AB and O'Toole D. *Changes in the Epidemiology of Neuroendocrine Tumours.* Neuroendocrinology, 2017. **104**(2): p. 105-111.

[9] Yao JC, Hassan M, Phan A, Dagohoy C, Leary C, Mares JE, Abdalla EK, Fleming JB, Vauthey JN, Rashid A, et al. *One hundred years after "carcinoid": epidemiology of and prognostic factors for neuroendocrine tumors in 35,825 cases in the United States.* J Clin Oncol, 2008. **26**(18): p. 3063-72.

[10] Pavel M, Valle JW, Eriksson B, Rinke A, Caplin M, Chen J, Costa F, Falkerby J, Fazio N, Gorbounova V, et al. *ENETS Consensus Guidelines for the Standards of Care in Neuroendocrine Neoplasms: Systemic Therapy - Biotherapy and Novel Targeted Agents.* Neuroendocrinology, 2017. **105**(3): p. 266-280.

[11] Hicks RJ, Kwekkeboom DJ, Krenning E, Bodei L, Grozinsky-Glasberg S, Arnold R, Borbath I, Cwikla J, Toumpanakis C, Kaltsas G, et al. *ENETS Consensus Guidelines for the Standards of Care in Neuroendocrine Neoplasia: Peptide Receptor Radionuclide Therapy with Radiolabeled Somatostatin Analogues.* Neuroendocrinology, 2017. **105**(3): p. 295-309.

[12] Garcia-Carbonero R, Rinke A, Valle JW, Fazio N, Caplin M, Gorbounova V, J OC, Eriksson B, Sorbye H, Kulke M, et al. *ENETS Consensus Guidelines for the Standards of Care in Neuroendocrine Neoplasms. Systemic Therapy 2: Chemotherapy.* Neuroendocrinology, 2017. **105**(3): p. 281-294.

[13] Garcia-Carbonero R, Sorbye H, Baudin E, Raymond E, Wiedenmann B, Niederle B, Sedlackova E, Toumpanakis C, Anlauf M, Cwikla JB, et al. *ENETS Consensus Guidelines for High-Grade Gastroenteropancreatic Neuroendocrine Tumors and Neuroendocrine Carcinomas.* Neuroendocrinology, 2016. **103**(2): p. 186-94.

[14] Yu JS and Cui W. *Proliferation, survival and metabolism: the role of PI3K/AKT/mTOR signalling in pluripotency and cell fate determination.* Development, 2016. **143**(17): p. 3050-60.

[15] Laplante M and Sabatini DM. *mTOR signaling in growth control and disease.* Cell, 2012. **149**(2): p. 274-93.

[16] Thorpe LM, Yuzugullu H and Zhao JJ. *PI3K in cancer: divergent roles of isoforms, modes of activation and therapeutic targeting.* Nat Rev Cancer, 2015. **15**(1): p. 7-24.

[17] Jiao Y, Shi C, Edil BH, de Wilde RF, Klimstra DS, Maitra A, Schulick RD, Tang LH, Wolfgang CL, Choti MA, et al. *DAXX/ATRX, MEN1, and mTOR pathway genes are frequently altered in pancreatic neuroendocrine tumors.* Science, 2011. **331**(6021): p. 1199-203.

[18] Missiaglia E, Dalai I, Barbi S, Beghelli S, Falconi M, della Peruta M, Piemonti L, Capurso G, Di Florio A, delle Fave G, et al. *Pancreatic endocrine tumors: expression profiling evidences a role for AKT-mTOR pathway.* J Clin Oncol, 2010. **28**(2): p. 245-55.

[19] Sankhala K, Mita A, Kelly K, Mahalingam D, Giles F and Mita M. *The emerging safety profile of mTOR inhibitors, a novel class of anticancer agents.* Target Oncol, 2009. **4**(2): p. 135-42.

[20] Hasskarl J. *Everolimus.* Recent Results Cancer Res, 2018. **211**: p. 101-123.

[21] Yao JC, Shah MH, Ito T, Bohas CL, Wolin EM, Van Cutsem E, Hobday TJ, Okusaka T, Capdevila J, de Vries EG, et al. *Everolimus for advanced pancreatic neuroendocrine tumors.* N Engl J Med, 2011. **364**(6): p. 514-23.

[22] Yao JC, Fazio N, Singh S, Buzzoni R, Carnaghi C, Wolin E, Tomasek J, Raderer M, Lahner H, Voi M, et al. *Everolimus for the treatment of advanced, non-functional neuroendocrine tumours of the lung or gastrointestinal tract (RADIANT-4): a randomised, placebo-controlled, phase 3 study.* Lancet, 2016. **387**(10022): p. 968-977.

[23] Pavel M, O'Toole D, Costa F, Capdevila J, Gross D, Kianmanesh R, Krenning E, Knigge U, Salazar R, Pape UF, et al. *ENETS Consensus Guidelines Update for the Management of Distant Metastatic Disease of Intestinal, Pancreatic, Bronchial Neuroendocrine Neoplasms (NEN) and NEN of Unknown Primary Site.* Neuroendocrinology, 2016. **103**(2): p. 172-85.

[24] Chan DL, Segelov E and Singh S. *Everolimus in the management of metastatic neuroendocrine tumours.* Therap Adv Gastroenterol, 2017. **10**(1): p. 132-141.

[25] Hanahan D and Weinberg RA. *Hallmarks of cancer: the next generation.* Cell, 2011. **144**(5): p. 646-74.

[26] Lemos de Matos A, Franco LS and McFadden G. *Oncolytic Viruses and the Immune System: The Dynamic Duo.* Mol Ther Methods Clin Dev, 2020. **17**: p. 349-358.

[27] Choi AH, O'Leary MP, Fong Y and Chen NG. *From Benchtop to Bedside: A Review of Oncolytic Virotherapy.* Biomedicines, 2016. **4**(3).

[28] Bommareddy PK, Zloza A, Rabkin SD and Kaufman HL. *Oncolytic virus immunotherapy induces immunogenic cell death and overcomes STING deficiency in melanoma.* Oncoimmunology, 2019. **8**(7): p. 1591875.

[29] Yu D, Leja-Jarblad J, Loskog A, Hellman P, Giandomenico V, Oberg K and Essand M. *Preclinical Evaluation of AdVince, an Oncolytic Adenovirus Adapted for Treatment of Liver Metastases from Neuroendocrine Cancer.* Neuroendocrinology, 2017. **105**(1): p. 54-66.

[30] Gupta V, Wang W, Sosnowski BA, Hofman FM and Chen TC. *Fibroblast growth factor-2-retargeted adenoviral vector for selective transduction of primary glioblastoma multiforme endothelial cells.* Neurosurg Focus, 2006. **20**(4): p. E26.

[31] Yurttas C, Berchtold S, Malek NP, Bitzer M and Lauer UM. *Pulsed versus continuous application of the prodrug 5-fluorocytosine to enhance the oncolytic effectiveness of a measles vaccine virus armed with a suicide gene.* Hum Gene Ther Clin Dev, 2014. **25**(2): p. 85-96.

[32] Mastrangelo MJ, Maguire HC, Jr., Eisenlohr LC, Laughlin CE, Monken CE, McCue PA, Kovatich AJ and Lattime EC. *Intratumoral recombinant GM-CSF-encoding virus as gene therapy in patients with cutaneous melanoma.* Cancer Gene Ther, 1999. **6**(5): p. 409-22.

[33] Liu BL, Robinson M, Han ZQ, Branston RH, English C, Reay P, McGrath Y, Thomas SK, Thornton M, Bullock P, et al. *ICP34.5 deleted herpes simplex virus with enhanced oncolytic, immune stimulating, and anti-tumour properties.* Gene Ther, 2003. **10**(4): p. 292-303.

[34] Moesta AK, Cooke K, Piasecki J, Mitchell P, Rottman JB, Fitzgerald K, Zhan J, Yang B, Le T, Belmontes B, et al. *Local Delivery of OncoVEX(mGM-CSF) Generates Systemic Antitumor Immune Responses Enhanced by Cytotoxic T-Lymphocyte-Associated Protein Blockade.* Clin Cancer Res, 2017. **23**(20): p. 6190-6202.

[35] Yu F, Wang X, Guo ZS, Bartlett DL, Gottschalk SM and Song XT. *T-cell engager-armed oncolytic vaccinia virus significantly enhances antitumor therapy.* Mol Ther, 2014. **22**(1): p. 102-11.

[36] Puzanov I, Milhem MM, Minor D, Hamid O, Li A, Chen L, Chastain M, Gorski KS, Anderson A, Chou J, et al. *Talimogene Laherparepvec in Combination With Ipilimumab in Previously Untreated, Unresectable Stage IIIB-IV Melanoma.* J Clin Oncol, 2016. **34**(22): p. 2619-26.

[37] Ribas A, Dummer R, Puzanov I, VanderWalde A, Andtbacka RHI, Michielin O, Olszanski AJ, Malvehy J, Cebon J, Fernandez E, et al. *Oncolytic Virotherapy Promotes Intratumoral T Cell Infiltration and Improves Anti-PD-1 Immunotherapy.* Cell, 2017. **170**(6): p. 1109-1119 e10.

[38] Ylosmaki E and Cerullo V. *Design and application of oncolytic viruses for cancer immunotherapy.* Curr Opin Biotechnol, 2019. **65**: p. 25-36.

[39] Francini N, Cochrane D, Illingworth S, Purdie L, Mantovani G, Fisher K, Seymour LW, Spain SG and Alexander C. *Polyvalent Diazonium Polymers Provide Efficient Protection of Oncolytic Adenovirus Enadenotucirev from Neutralizing Antibodies while Maintaining Biological Activity In Vitro and In Vivo.* Bioconjug Chem, 2019. **30**(4): p. 1244-1257.

[40] Garofalo M, Saari H, Somersalo P, Crescenti D, Kuryk L, Aksela L, Capasso C, Madetoja M, Koskinen K, Oksanen T, et al. *Antitumor effect of oncolytic virus and paclitaxel encapsulated in extracellular vesicles for lung cancer treatment.* J Control Release, 2018. **283**: p. 223-234.

[41] Ferguson MS, Chard Dunmall LS, Gangeswaran R, Marelli G, Tysome JR, Burns E, Whitehead MA, Aksoy E, Alusi G, Hiley C, et al. *Transient Inhibition of PI3Kdelta Enhances the Therapeutic Effect of Intravenous Delivery of Oncolytic Vaccinia Virus.* Mol Ther, 2020. **28**(5): p. 1263-1275.

[42] Evgin L, Acuna SA, Tanese de Souza C, Marguerie M, Lemay CG, Ilkow CS, Findlay CS, Falls T, Parato KA, Hanwell D, et al. *Complement inhibition prevents oncolytic vaccinia virus neutralization in immune humans and cynomolgus macaques.* Mol Ther, 2015. **23**(6): p. 1066-1076.

[43] Kim J, Hall RR, Lesniak MS and Ahmed AU. *Stem Cell-Based Cell Carrier for Targeted Oncolytic Virotherapy: Translational Opportunity and Open Questions.* Viruses, 2015. **7**(12): p. 6200-17.

[44] Greig SL. *Talimogene Laherparepvec: First Global Approval.* Drugs, 2016. **76**(1): p. 147-54.

[45] Rudin CM, Poirier JT, Senzer NN, Stephenson J, Jr., Loesch D, Burroughs KD, Reddy PS, Hann CL and Hallenbeck PL. *Phase I clinical study of Seneca Valley Virus (SVV-001), a replication-competent picornavirus, in advanced solid tumors with neuroendocrine features.* Clin Cancer Res, 2011. **17**(4): p. 888-95.

[46] Yamamoto Y, Nagasato M, Rin Y, Henmi M, Ino Y, Yachida S, Ohki R, Hiraoka N, Tagawa M and Aoki K. *Strong antitumor efficacy of a pancreatic tumor-targeting oncolytic adenovirus for neuroendocrine tumors.* Cancer Med, 2017. **6**(10): p. 2385-2397.

[47] Zhang Q, Yu YA, Wang E, Chen N, Danner RL, Munson PJ, Marincola FM and Szalay AA. *Eradication of solid human breast tumors in nude mice with an intravenously injected light-emitting oncolytic vaccinia virus.* Cancer Res, 2007. **67**(20): p. 10038-46.

[48] Zhang Q, Liang C, Yu YA, Chen N, Dandekar T and Szalay AA. *The highly attenuated oncolytic recombinant vaccinia virus GLV-1h68: comparative genomic features and the contribution of F14.5L inactivation.* Mol Genet Genomics, 2009. **282**(4): p. 417-35.

[49] Lauer UM, Schell M, Beil J, Berchtold S, Koppenhofer U, Glatzle J, Konigsrainer A, Mohle R, Nann D, Fend F, et al. *Phase I study of oncolytic vaccinia virus GL-ONC1 in patients with peritoneal carcinomatosis.* Clin Cancer Res, 2018.

[50] Mayer N. *Difficult to treat cancer entities such as sarcomas and peritoneal carcinosis challenged by suicide gene- armed virotherapeutic vector systems MeV and VACV.* **p51 Figure 26.** 2014. Diss. Faculty of Medicine, University of Tübingen. Published in: TOBIAS-lib.

[51] Vanderplasschen A, Mathew E, Hollinshead M, Sim RB and Smith GL. *Extracellular enveloped vaccinia virus is resistant to complement because of incorporation of host complement control proteins into its envelope.* Proc Natl Acad Sci U S A, 1998. **95**(13): p. 7544-9.

[52] Ichihashi Y. *Extracellular enveloped vaccinia virus escapes neutralization.* Virology, 1996. **217**(2): p. 478-85.

[53] Smith GL, Vanderplasschen A and Law M. *The formation and function of extracellular enveloped vaccinia virus.* J Gen Virol, 2002. **83**(Pt 12): p. 2915-2931.

[54] Roberts KL and Smith GL. *Vaccinia virus morphogenesis and dissemination.* Trends Microbiol, 2008. **16**(10): p. 472-9.

[55] Mell LK, Brumund KT, Daniels GA, Advani SJ, Zakeri K, Wright ME, Onyeama SJ, Weisman RA, Sanghvi PR, Martin PJ, et al. *Phase I Trial of Intravenous Oncolytic Vaccinia Virus (GL-ONC1) with Cisplatin and Radiotherapy in Patients with Locoregionally Advanced Head and Neck Carcinoma.* Clin Cancer Res, 2017. **23**(19): p. 5696-5702.

[56] Lin SF, Price DL, Chen CH, Brader P, Li S, Gonzalez L, Zhang Q, Yu YA, Chen N, Szalay AA, et al. *Oncolytic vaccinia virotherapy of anaplastic thyroid cancer in vivo.* J Clin Endocrinol Metab, 2008. **93**(11): p. 4403-7.

[57] Hofmann E, Weibel S and Szalay AA. *Combination treatment with oncolytic Vaccinia virus and cyclophosphamide results in synergistic antitumor effects in human lung adenocarcinoma bearing mice.* J Transl Med, 2014. **12**: p. 197.

[58] Wilkinson MJ, Smith HG, Pencavel TD, Mansfield DC, Kyula-Currie J, Khan AA, McEntee G, Roulstone V, Hayes AJ and Harrington KJ. *Isolated limb perfusion with biochemotherapy and oncolytic virotherapy combines with radiotherapy and surgery to overcome treatment resistance in an animal model of extremity soft tissue sarcoma.* Int J Cancer, 2016. **139**(6): p. 1414-22.

[59] Binz E, Berchtold S, Beil J, Schell M, Geisler C, Smirnow I and Lauer UM. *Chemovirotherapy of Pancreatic Adenocarcinoma by Combining Oncolytic Vaccinia Virus GLV-1h68 with nab-Paclitaxel Plus Gemcitabine.* Mol Ther Oncolytics, 2017. **6**: p. 10-21.

[60] Advani SJ, Buckel L, Chen NG, Scanderbeg DJ, Geissinger U, Zhang Q, Yu YA, Aguilar RJ, Mundt AJ and Szalay AA. *Preferential replication of systemically delivered oncolytic vaccinia virus in focally irradiated glioma xenografts.* Clin Cancer Res, 2012. **18**(9): p. 2579-90.

[61] Kyula JN, Khan AA, Mansfield D, Karapanagiotou EM, McLaughlin M, Roulstone V, Zaidi S, Pencavel T, Touchefeu Y, Seth R, et al. *Synergistic cytotoxicity of radiation and oncolytic Lister strain vaccinia in (V600D/E)BRAF mutant melanoma depends on JNK and TNF-alpha signaling.* Oncogene, 2014. **33**(13): p. 1700-12.

[62] Mohr I, Sternberg D, Ward S, Leib D, Mulvey M and Gluzman Y. *A herpes simplex virus type 1 gamma34.5 second-site suppressor mutant that exhibits enhanced growth in cultured glioblastoma cells is severely attenuated in animals.* J Virol, 2001. **75**(11): p. 5189-96.

[63] Hughes T, Coffin RS, Lilley CE, Ponce R and Kaufman HL. *Critical analysis of an oncolytic herpesvirus encoding granulocyte-macrophage colony stimulating factor for the treatment of malignant melanoma.* Oncolytic Virother, 2014. **3**: p. 11-20.

[64] Hu JC, Coffin RS, Davis CJ, Graham NJ, Groves N, Guest PJ, Harrington KJ, James ND, Love CA, McNeish I, et al. *A phase I study of OncoVEXGM-CSF, a second-generation oncolytic herpes simplex virus expressing granulocyte macrophage colony-stimulating factor.* Clin Cancer Res, 2006. **12**(22): p. 6737-47.

[65] Kaufman HL, Kim DW, DeRaffele G, Mitcham J, Coffin RS and Kim-Schulze S. *Local and distant immunity induced by intralesional vaccination with an oncolytic herpes virus encoding GM-CSF in patients with stage IIIc and IV melanoma.* Ann Surg Oncol, 2010. **17**(3): p. 718-30.

[66] Cheshenko N, Trepanier JB, Stefanidou M, Buckley N, Gonzalez P, Jacobs W and Herold BC. *HSV activates Akt to trigger calcium release and promote viral entry: novel candidate target for treatment and suppression.* FASEB J, 2013. **27**(7): p. 2584-99.

[67] Fu X, Tao L, Rivera A and Zhang X. *Rapamycin enhances the activity of oncolytic herpes simplex virus against tumor cells that are resistant to virus replication.* Int J Cancer, 2011. **129**(6): p. 1503-10.

[68] Costa-Mattioli M and Sonenberg N. *RAPping production of type I interferon in pDCs through mTOR.* Nat Immunol, 2008. **9**(10): p. 1097-9.

[69] Lun XQ, Jang JH, Tang N, Deng H, Head R, Bell JC, Stojdl DF, Nutt CL, Senger DL, Forsyth PA, et al. *Efficacy of systemically administered oncolytic vaccinia virotherapy for malignant gliomas is enhanced by combination therapy with rapamycin or cyclophosphamide.* Clin Cancer Res, 2009. **15**(8): p. 2777-88.

[70] Suzutani T, Koyano S, Takada M, Yoshida I and Azuma M. *Analysis of the relationship between cellular thymidine kinase activity and virulence of thymidine kinase-negative herpes simplex virus types 1 and 2.* Microbiol Immunol, 1995. **39**(10): p. 787-94.

[71] Xie Y, Wu L, Wang M, Cheng A, Yang Q, Wu Y, Jia R, Zhu D, Zhao X, Chen S, et al. *Alpha-Herpesvirus Thymidine Kinase Genes Mediate Viral Virulence and Are Potential Therapeutic Targets.* Front Microbiol, 2019. **10**: p. 941.

[72] Hamel W, Magnelli L, Chiarugi VP and Israel MA. *Herpes simplex virus thymidine kinase/ganciclovir-mediated apoptotic death of bystander cells.* Cancer Res, 1996. **56**(12): p. 2697-702.

[73] Fischer U, Steffens S, Frank S, Rainov NG, Schulze-Osthoff K and Kramm CM. *Mechanisms of thymidine kinase/ganciclovir and cytosine deaminase/ 5-fluorocytosine suicide gene therapy-induced cell death in glioma cells.* Oncogene, 2005. **24**(7): p. 1231-43.

[74] Takahashi T, Nau MM, Chiba I, Birrer MJ, Rosenberg RK, Vinocour M, Levitt M, Pass H, Gazdar AF and Minna JD. *p53: a frequent target for genetic abnormalities in lung cancer.* Science, 1989. **246**(4929): p. 491-4.

[75] Giaccone G, Battey J, Gazdar AF, Oie H, Draoui M and Moody TW. *Neuromedin B is present in lung cancer cell lines.* Cancer Res, 1992. **52**(9 Suppl): p. 2732s-2736s.

[76] Evers BM, Ishizuka J, Townsend CM, Jr. and Thompson JC. *The human carcinoid cell line, BON. A model system for the study of carcinoid tumors.* Ann N Y Acad Sci, 1994. **733**: p. 393-406.

[77] Kaku M, Nishiyama T, Yagawa K and Abe M. *Establishment of a carcinoembryonic antigen-producing cell line from human pancreatic carcinoma.* Gan, 1980. **71**(5): p. 596-601.

[78] Gock M, Mullins CS, Harnack C, Prall F, Ramer R, Goder A, Kramer OH, Klar E and Linnebacher M. *Establishment, functional and genetic characterization of a colon derived large cell neuroendocrine carcinoma cell line.* World J Gastroenterol, 2018. **24**(33): p. 3749-3759.

[79] Krieg A, Mersch S, Boeck I, Dizdar L, Weihe E, Hilal Z, Krausch M, Mohlendick B, Topp SA, Piekorz RP, et al. *New model for gastroenteropancreatic large-cell neuroendocrine carcinoma: establishment of two clinically relevant cell lines.* PLoS One, 2014. **9**(2): p. e88713.

[80] Skehan P, Storeng R, Scudiero D, Monks A, McMahon J, Vistica D, Warren JT, Bokesch H, Kenney S and Boyd MR. *New colorimetric cytotoxicity assay for anticancer-drug screening.* J Natl Cancer Inst, 1990. **82**(13): p. 1107-12.

[81] Cavignac Y and Esclatine A. *Herpesviruses and autophagy: catch me if you can!* Viruses, 2010. **2**(1): p. 314-33.

[82] Cole NL and Grose C. *Membrane fusion mediated by herpesvirus glycoproteins: the paradigm of varicella-zoster virus.* Rev Med Virol, 2003. **13**(4): p. 207-22.

[83] Talloczy Z, Virgin HWt and Levine B. *PKR-dependent autophagic degradation of herpes simplex virus type 1.* Autophagy, 2006. **2**(1): p. 24-9.

[84] Leuzinger H, Ziegler U, Schraner EM, Fraefel C, Glauser DL, Heid I, Ackermann M, Mueller M and Wild P. *Herpes simplex virus 1 envelopment follows two diverse pathways.* J Virol, 2005. **79**(20): p. 13047-59.

[85] Johnson DC and Baines JD. *Herpesviruses remodel host membranes for virus egress.* Nat Rev Microbiol, 2011. **9**(5): p. 382-94.

[86] Rambold AS, Kostelecky B, Elia N and Lippincott-Schwartz J. *Tubular network formation protects mitochondria from autophagosomal degradation during nutrient starvation.* Proc Natl Acad Sci U S A, 2011. **108**(25): p. 10190-5.

[87] Schirrmacher V, Bihari AS, Stucker W and Sprenger T. *Long-term remission of prostate cancer with extensive bone metastases upon immuno- and virotherapy: A case report.* Oncol Lett, 2014. **8**(6): p. 2403-2406.

[88] Dispenzieri A, Tong C, LaPlant B, Lacy MQ, Laumann K, Dingli D, Zhou Y, Federspiel MJ, Gertz MA, Hayman S, et al. *Phase I trial of systemic administration of Edmonston strain of measles virus genetically engineered to express the sodium iodide symporter in patients with recurrent or refractory multiple myeloma.* Leukemia, 2017. **31**(12): p. 2791-2798.

[89] Papewalis C, Wuttke M, Seissler J, Meyer Y, Kessler C, Jacobs B, Ullrich E, Willenberg HS, Schinner S, Baehring T, et al. *Dendritic cell vaccination with xenogenic polypeptide hormone induces tumor rejection in neuroendocrine cancer.* Clin Cancer Res, 2008. **14**(13): p. 4298-305.

[90] Patnaik A, Kang SP, Rasco D, Papadopoulos KP, Elassaiss-Schaap J, Beeram M, Drengler R, Chen C, Smith L, Espino G, et al. *Phase I Study of Pembrolizumab (MK-3475; Anti-PD-1 Monoclonal Antibody) in Patients with Advanced Solid Tumors.* Clin Cancer Res, 2015. **21**(19): p. 4286-93.

[91] Weber MM and Fottner C. *Immune Checkpoint Inhibitors in the Treatment of Patients with Neuroendocrine Neoplasia.* Oncol Res Treat, 2018. **41**(5): p. 306-312.

[92] Sampedro-Nunez M, Serrano-Somavilla A, Adrados M, Cameselle-Teijeiro JM, Blanco-Carrera C, Cabezas-Agricola JM, Martinez-Hernandez R, Martin-Perez E, Munoz de Nova JL, Diaz JA, et al. *Analysis of expression of the PD-1/PD-L1 immune checkpoint system and its prognostic impact in gastroenteropancreatic neuroendocrine tumors.* Sci Rep, 2018. **8**(1): p. 17812.

[93] Kim ST, Ha SY, Lee S, Ahn S, Lee J, Park SH, Park JO, Lim HY, Kang WK, Kim KM, et al. *The Impact of PD-L1 Expression in Patients with Metastatic GEP-NETs.* J Cancer, 2016. **7**(5): p. 484-9.

[94] Lawrence MS, Stojanov P, Polak P, Kryukov GV, Cibulskis K, Sivachenko A, Carter SL, Stewart C, Mermel CH, Roberts SA, et al. *Mutational heterogeneity in cancer and the search for new cancer-associated genes.* Nature, 2013. **499**(7457): p. 214-218.

[95] Pavel ME and Sers C. *WOMEN IN CANCER THEMATIC REVIEW: Systemic therapies in neuroendocrine tumors and novel approaches toward personalized medicine.* Endocr Relat Cancer, 2016. **23**(11): p. T135-T154.

[96] Zitzmann K, De Toni EN, Brand S, Goke B, Meinecke J, Spottl G, Meyer HH and Auernhammer CJ. *The novel mTOR inhibitor RAD001 (everolimus) induces antiproliferative effects in human pancreatic neuroendocrine tumor cells.* Neuroendocrinology, 2007. **85**(1): p. 54-60.

[97] Xing JZ, Zhu L, Jackson JA, Gabos S, Sun XJ, Wang XB and Xu X. *Dynamic monitoring of cytotoxicity on microelectronic sensors.* Chem Res Toxicol, 2005. **18**(2): p. 154-61.

[98] Teng Z, Kuang X, Wang J and Zhang X. *Real-time cell analysis--a new method for dynamic, quantitative measurement of infectious viruses and antiserum neutralizing activity.* J Virol Methods, 2013. **193**(2): p. 364-70.

[99] Yu Z, Li S, Brader P, Chen N, Yu YA, Zhang Q, Szalay AA, Fong Y and Wong RJ. *Oncolytic vaccinia therapy of squamous cell carcinoma.* Mol Cancer, 2009. **8**: p. 45.

[100] Kelly KJ, Woo Y, Brader P, Yu Z, Riedl C, Lin SF, Chen N, Yu YA, Rusch VW, Szalay AA, et al. *Novel oncolytic agent GLV-1h68 is effective against malignant pleural mesothelioma.* Hum Gene Ther, 2008. **19**(8): p. 774-82.

[101] de Wit D, Schneider TC, Moes DJ, Roozen CF, den Hartigh J, Gelderblom H, Guchelaar HJ, van der Hoeven JJ, Links TP, Kapiteijn E, et al. *Everolimus pharmacokinetics and its exposure-toxicity relationship in patients with thyroid cancer.* Cancer Chemother Pharmacol, 2016. **78**(1): p. 63-71.

[102] Becher B, Tugues S and Greter M. *GM-CSF: From Growth Factor to Central Mediator of Tissue Inflammation.* Immunity, 2016. **45**(5): p. 963-973.

[103] Smith HG, Mansfield D, Roulstone V, Kyula-Currie JN, McLaughlin M, Patel RR, Bergerhoff KF, Paget JT, Dillon MT, Khan A, et al. *PD-1 Blockade Following Isolated Limb Perfusion with Vaccinia Virus Prevents Local and Distant Relapse of Soft-tissue Sarcoma.* Clin Cancer Res, 2019. **25**(11): p. 3443-3454.

[104] Kumru OS, Joshi SB, Thapa P, Pheasey N, Bullock PS, Bashiri H, Siska CS, Kerwin BA, He F, Volkin DB, et al. *Characterization of an oncolytic herpes simplex virus drug candidate.* J Pharm Sci, 2015. **104**(2): p. 485-94.

[105] Roizman B KD, Whitley RJ. *Herpes simplex viruses.* In: Knipe DM, Howley PM, editors. Fields virology. Philadelphia: Lippincott Williams & Wilkins; , 2013: p. 1823-97.

[106] Owen DJ, Crump CM and Graham SC. *Tegument Assembly and Secondary Envelopment of Alphaherpesviruses.* Viruses, 2015. **7**(9): p. 5084-114.

[107] Knipe DM and Cliffe A. *Chromatin control of herpes simplex virus lytic and latent infection.* Nat Rev Microbiol, 2008. **6**(3): p. 211-21.

[108] Ma XM and Blenis J. *Molecular mechanisms of mTOR-mediated translational control.* Nat Rev Mol Cell Biol, 2009. **10**(5): p. 307-18.

[109] Lun X, Chan J, Zhou H, Sun B, Kelly JJ, Stechishin OO, Bell JC, Parato K, Hu K, Vaillant D, et al. *Efficacy and safety/toxicity study of recombinant vaccinia virus JX-594 in two immunocompetent animal models of glioma.* Mol Ther, 2010. **18**(11): p. 1927-36.

[110] Hou W, Chen H, Rojas J, Sampath P and Thorne SH. *Oncolytic vaccinia virus demonstrates antiangiogenic effects mediated by targeting of VEGF.* Int J Cancer, 2014. **135**(5): p. 1238-46.

[111] Finke JH, Rini B, Ireland J, Rayman P, Richmond A, Golshayan A, Wood L, Elson P, Garcia J, Dreicer R, et al. *Sunitinib reverses type-1 immune suppression and decreases T-regulatory cells in renal cell carcinoma patients.* Clin Cancer Res, 2008. **14**(20): p. 6674-82.

[112] Kim M, Nitschke M, Sennino B, Murer P, Schriver BJ, Bell A, Subramanian A, McDonald CE, Wang J, Cha H, et al. *Amplification of Oncolytic Vaccinia Virus Widespread Tumor Cell Killing by Sunitinib through Multiple Mechanisms.* Cancer Res, 2018. **78**(4): p. 922-937.

[113] Meyers DE, Wang AA, Thirukkumaran CM and Morris DG. *Current Immunotherapeutic Strategies to Enhance Oncolytic Virotherapy.* Front Oncol, 2017. **7**: p. 114.

[114] Littler E, Stuart AD and Chee MS. *Human cytomegalovirus UL97 open reading frame encodes a protein that phosphorylates the antiviral nucleoside analogue ganciclovir.* Nature, 1992. **358**(6382): p. 160-2.

[115] Kimberlin DW and Whitley RJ, *Antiviral therapy of HSV-1 and -2*, in *Human Herpesviruses: Biology, Therapy, and Immunoprophylaxis*, A. Arvin, et al., Editors. 2007: Cambridge.

[116] Lalezari JP, Friedberg DN, Bissett J, Giordano MF, Hardy WD, Drew WL, Hubbard LD, Buhles WC, Stempien MJ, Georgiou P, et al. *High dose oral ganciclovir treatment for cytomegalovirus retinitis.* J Clin Virol, 2002. **24**(1-2): p. 67-77.

[117] Fletcher C, Sawchuk R, Chinnock B, de Miranda P and Balfour HH, Jr. *Human pharmacokinetics of the antiviral drug DHPG.* Clin Pharmacol Ther, 1986. **40**(3): p. 281-6.

[118] Prichard MN and Kern ER. *Orthopoxvirus targets for the development of new antiviral agents.* Antiviral Res, 2012. **94**(2): p. 111-25.

[119] Bell E, Shamim M, Whitbeck JC, Sfyroera G, Lambris JD and Isaacs SN. *Antibodies against the extracellular enveloped virus B5R protein are mainly responsible for the EEV neutralizing capacity of vaccinia immune globulin.* Virology, 2004. **325**(2): p. 425-31.

APPENDIX

1. Zusammenfassung

Metastasierte neuroendokrine Neoplasien, worunter neuroendokrine Tumore und neuroendokrine Karzinome zählen, sind immer noch tödliche Erkrankungen und erfordern dringend neuartige erfolgversprechende Therapiemöglichkeiten.

Zur onkolytischen Virotherapie werden Viren so selektiert oder genetisch verändert, dass sie spezifisch in Tumorzellen replizieren. Durch Infektion, Replikation und Freisetzung von neuen Viren breiten sich onkolytische Viren im Tumorgewebe aus und lysieren die Zellen des Tumors. Dabei erzeugen sie ein entzündliches Milieu im Tumor, welches Immunzellen anlockt und das Immunsystem des Patienten zur systemischen Tumorbekämpfung anregt.

Das Ziel dieser Dissertation war es, den Einsatz der onkolytischen Virotherapie für neuroendokrine Neoplasien zu evaluieren. Zwei onkolytische Viren, welche beide bereits in klinischen Studien im Patienten eingesetzt wurden, wurden zur weiteren Erprobung in Zelllinien neuroendokriner Neoplasien eingesetzt. Bei GLV-1h68 handelt es sich um ein onkolytisches Vaccinia Virus, das aktuell in klinischen Phase I/II Studien zur Therapie anderer Tumorentitäten getestet wird. Das zweite onkolytische Virus T-VEC gehört der Klasse der Herpes Simplex Viren an und ist bereits für die Therapie des fortgeschrittenen Melanoms klinisch zugelassen.

Sechs Zelllinien wurden in dieser Studie untersucht. Davon stammen je zwei aus neuroendokrinen Tumoren des Pankreas, zwei aus neuroendokrinen Tumoren der Lunge und zwei aus neuroendokrinen Karzinomen. Der Einfluss beider Viren auf die Zellviabilität wurde mittels SRB Viabilitätsassay bestimmt und die Veränderung dieser über die Zeit wurde durch Echtzeit Zellanalyseverfahren untersucht. Im Weiteren wurden die Virusreplikation quantifiziert, mikroskopische Bilder der infizierten Zellen angefertigt sowie die zelluläre Transgenexpression beider Viren gemessen. Darüber hinaus wurden durch elektronenmikroskopische Bilder der Prozess der Virusumhüllung sowie der Zellaustritt von T-VEC visualisiert. Zusätzlich wurde mit denselben Methoden eine Kombinations-

therapie mit dem für diese Indikation eingesetzten Medikament Everolimus und beiden onkolytischen Viren evaluiert. Außerdem wurde die Wirkung von Ganciclovir auf die T-VEC Behandlung von neuroendokrinen Tumorzellen beurteilt.

Es konnte gezeigt werden, dass beide Viren Tumorzellen infizieren, darin replizieren und diese Zeit- und Dosisabhängig zerstören. Hierbei wurden nur sehr niedrige Konzentrationen von T-VEC benötigt, welches sich hierdurch als besonders vielversprechende zukünftige Therapie für neuroendokrine Neoplasien auszeichnete. Mittels Transmissionselektronenmikroskopie konnten das T-VEC Virion sowie die zellulären Veränderungen von neuroendokrinen Tumorzellen nach Infektion mit T-VEC visualisiert werden. Darüber hinaus konnte eine starke Transgenexpression beider Viren nachgewiesen werden. Die Kombinationstherapie beider Viren mit Everolimus erwies sich nur als minimal der Monotherapie überlegen. Ganciclovir zeigte sich als potentes Virostatikum, indem es effektiv die Replikation von T-VEC einschränkte.

Zusammenfassend konnte in vitro gezeigt werden, dass die onkolytische Virotherapie eine vielversprechende Therapiemöglichkeit für neuroendokrine Neoplasien darstellt. Sowohl GLV-1h68 als auch T-VEC demonstrierten hohe onkolytische Aktivität in Zelllinien eines breiten Spektrums neuroendokriner Neoplasien. Insbesondere T-VEC empfiehlt sich für eine weitere präklinische und klinische Entwicklung, da bemerkenswert niedrige Viruskonzentrationen für eine effektive Replikation und Toxizität in Tumorzellen ausreichten. Die Bedeutung der Kombinationstherapie mit Everolimus bleibt unklar. Ganciclovir konnte als wichtiges Virostatikum für T-VEC etabliert werden, um Sicherheitsbedenken bei der Therapie mit diesem replikationskompetenten Virus zu vermeiden.

2. Veröffentlichungen

2.1. Publikationen

- Kloker LD, Yurttas C and Lauer UM. *Three-dimensional tumor cell cultures employed in virotherapy research.* Oncolytic Virotherapy, 2018. **7**: p. 79-93.

- Kloker LD, Berchtold S, Smirnow I, Schaller M, Fehrenbacher B, Krieg A, Sipos B and Lauer UM. *The Oncolytic Herpes Simplex Virus Talimogene Laherparepvec Shows Promising Efficacy in Neuroendocrine Cancer Cell Lines.* Neuroendocrinology, 2019. **109:** p. 346.

- Kloker LD, Berchtold S, Smirnow I, Beil J, Krieg A, Sipos B and Lauer UM. *Oncolytic vaccinia virus GLV-1h68 exhibits profound antitumoral activities in cell lines originating from neuroendocrine neoplasms*. BMC Cancer, 2020. **20(1)**: p. 628.

2.2. Posterpräsentationen

- Forschungkolloquium der Medizinschen Fakultät der Universität Tübingen: *Kloker LD, Berchtold S, Lauer UM. Virotherapie Neuroendokriner Tumoren.* Januar 2019.

- 20th International AEK Cancer Congress, Heidelberg: *Kloker LD, Berchtold S, Lauer UM. Virotherapy of Neuoendocrine Neoplasia.* Februar 2019.

3. Erklärung zum Eigenanteil

Die Arbeit wurde in der Medizinischen Universitätsklinik Tübingen in der Abteilung VIII für Medizinische Onkologie und Pneumologie unter Betreuung von Herrn Prof. Dr. med. Ulrich M. Lauer durchgeführt.

Die Konzeption der Studie erfolgte durch Herrn Prof. Dr. med. Ulrich M. Lauer (Leiter der Arbeitsgruppe Virotherapie) in Zusammenarbeit Dr. med. Susanne Berchtold (Laborleiterin) und mich selbst. Sämtliche Versuche wurden nach Einarbeitung durch Irina Smirnow (MTA), Dr. med. Susanne Berchtold und Andrea Schenk (MTA) vollständig eigenständig von mir durchgeführt. Ausnahmen hiervon sind die Versuche mit der Methode zum Real-time Cell Monitoring (Ergebnisse 1.2, 2.1.2, 2.2.2, 3.1.2, 3.2.2.) sowie die SRB Assays zur Kombination beider Virotherapeutika mit Everolimus (Ergebnisse 2.2.1 und 3.2.1), bei denen einige Versuchsdurchläufe auch von Irinia Smirnow und Dr. med. Susanne Berchtold durchgeführt wurden. Die elektronenmikroskopischen Bilder (Ergebnisse 4.) wurden nach Vorbereitung der Proben durch mich von Prof. Martin Schaller (Universitätshautklinik Tübingen) und Birgit Fehrenbacher (MTA, Universitätshautklinik Tübingen) aufgenommen.

Die Datenanalyse und statistische Auswertung erfolgten durch mich. Ich versichere, das Manuskript selbständig unter Anleitung und Korrektur durch Prof. Dr. Ulrich M. Lauer und Dr. med. Susanne Berchtold verfasst zu haben und keine weiteren als die von mir angegebenen Quellen verwendet zu haben.

Die aus den Originalpublikationen wörtlich übernommenen Textpassagen wurden von mir selbst verfasst und sämtliche übernommene oder modifizierte Abbildungen wurden auch ursprünglich von mir selbst unter Aufsicht von Prof. Dr. Ulrich M. Lauer und Dr. med. Susanne Berchtold entworfen. Weitere Informationen zum Anteil der Autoren an den Originalpublikationen finden sich in den „Author Contributions“ Abschnitten der jeweiligen Originalpublikation [1,2]. Die aus dem Literaturreview [3] übernommene Textpassage im Abschnitt „Study Limitations“ der Diskussion habe ich vollständig selbst verfasst.

Tübingen, den 11.01.2021

4. Danksagung

Ich möchte mich an dieser Stelle sehr herzlich bei allen bedanken, die zum guten Gelingen dieser Arbeit beigetragen haben.

Mein erster Dank geht an meinen Doktorvater Prof. Ulrich Lauer, der mich von Anfang an in jeder Lage unterstützt hat und auch mal zu unmöglichen Uhrzeiten eine E-Mail beantwortet hat. Sein großes Interesse an meiner Arbeit und seine konstruktive Arbeitsweise haben entscheidend zu dieser Dissertation beigetragen und eine meiner Ansicht nach perfekte Betreuung ermöglicht.

Insbesondere gilt mein Dank auch Dr. Susanne Berchtold, die mir als meine direkte Betreuerin und Nebensitzerin im Labor bei allen Unwägbarkeiten zur Seite stand und sicher dutzende Seiten an Manuskript akribisch gegengelesen hat. Im Weiteren möchte ich mich bei Irina Smirnow bedanken, welche mir und vielen anderen planlosen Medizinstudenten vor mir mit viel Geduld die ersten und wichtigsten Handgriffe im Labor beigebracht hat. Bei Andrea Schenk, Dr. Julia Beil, Prof. Sascha Venturelli, Dr. Markus Burkhard und Christian Leischner möchte ich mich für die freundliche Aufnahme in die Arbeitsgruppe und die vielen lustigen Kaffeerunden bedanken.

Außerdem möchte ich mich bei Brigit Fehrenbacher und Prof. Martin Schaller der Universitätshautklinik Tübingen bedanken, die durch die Ermöglichung elektronen-mikroskopischer Bilder diese Arbeit noch anschaulicher gemacht haben. Des Weiteren bedanke ich mich bei Prof. Bence Sipos (Universität Tübingen) und Prof. Andreas Krieg (Heinrich-Heine-Universität Düsseldorf) für die Hilfe bei der Akquirierung der neuroendokrinen Tumorzelllinien.

Ohne die Hilfe und Unterstützung durch das von Prof. Marlies Knipper und Dr. Inka Montero geleitete IZKF Promotionskolleg wäre diese Arbeit nicht in diesem Umfang möglich gewesen. Außerdem möchte ich mich bei der Universität Tübingen für die finanzielle Unterstützung durch das Deutschlandstipendium bedanken.

Zu guter Letzt möchte ich auch PD Corina Schneidawind (Universität Tübingen) und Prof. Susanne Bailer (Universität Stuttgart) für die Begutachtung meiner Arbeit danken.